FATIGUE LOADING OF REINFORCED CONCRETE MEMBERS STRENGTHENED USING CARBON FIBER REINFORCED POLYMER COMPOSITES

by

MICHAËL A. BENOUAICH

Submitted to the Department of Civil Engineering

in Partial Fulfillment of the Requirements

for the Degree of

INGÉNIEUR CIVIL DIPLOMÉ

ÉCOLE POLYTECHNIQUE FÉDÉRALE DE LAUSANNE

March 2000

FATIGUE LOADING OF REINFORCED CONCRETE MEMBERS STRENGTHENED USING CARBON FIBER REINFORCED POLYMER COMPOSITES

by

MICHAËL A. BENOUAICH

Author

March 2000

Approved by

Marc Badoux

Thesis supervisor, École Polytechnique Fédérale de Lausanne

Michael E. Kreger

Thesis supervisor, University of Texas at Austin

Certified by

Service Académique, École Polytechnique Fédérale de Lausanne

A mes parents et à mon frère David, pour leur dévotion et leur amour.

This thesis was typed by the author.

ACKNOWLEDGEMENTS

The experimental study reported herein was performed as part of a research venture between The University of Texas at Austin, USA, and the Swiss Federal Institute of Technology, in Lausanne, Switzerland. Funding was provided by the Texas Department of Transportation under project No. 0-1776, "Development of Methods to Strengthen Existing Structures with Composites".

I would like to express my sincere gratitude to my supervisor Dr. Marc Badoux, from the Swiss Federal Institute of Technology in Lausanne, who entrusted me and granted me the great opportunity to conduct my graduate thesis at the University of Texas at Austin.

I wish to thank sincerely Dr. Michael E. Kreger, and Dr. Sharon L. Wood, from the University of Texas at Austin, whose invaluable guidance, critiques, availability, and patience throughout my stay in Austin were highly appreciated. They both, in different ways, contributed considerably to the overall learning experience.

I greatly appreciated the dedication of Sergio F. Breña, whose continuing assistance, enthusiasm, and friendship enabled the completion of this thesis. I feel very fortunate to have work with him. I extend my gratitude to the personnel of the Phil M. Ferguson Structural Engineering Laboratory, especially to the technicians for their help during the testing.

I also wish to address special thanks to Professor Urs Meier, from the Swiss Federal Laboratories for Materials Testing and Research at Duebendorf, whose help for the literature review was greatly appreciated.

Finally, deepest gratitude goes to my family whose consistent and unfailing support, help, and encouragements were instrumental to completion of this thesis.

NOTICE

The United States Government, the State of Texas, and the author do not endorse products or manufacturers. Trade or manufacturers' names appear herein solely because they are considered essential to the object of this report.

FATIGUE LOADING OF REINFORCED CONCRETE MEMBERS STRENGTHENED USING CARBON FIBER REINFORCED POLYMER COMPOSITES

ABSTRACT

The present thesis reports testing involving the static and fatigue performance of rectangular reinforced concrete (R/C) beams strengthened using epoxy bonded Carbon Fiber Reinforced Polymer (CFRP) composite materials. The overall objective was to establish the influence of fatigue loading on flexural behavior of strengthened R/C members.

Six specimens, strengthened using different configurations of CFRP flexible sheets and pultruded plates, were subjected to fatigue loading under various stress ranges representative of service-load conditions and potential overloading. Monotonic static tests to failure were conducted on five of these specimens after they had undergone a repeated loading sequence to a maximum number of 1,000,000 cycles.

Beams were extensively instrumented to monitor load, deflections, strains, and acoustic emissions over the entire spectrum of loading to failure. The post-cyclic static response is reported. Structural ductility and energy ductility indices are computed to describe the overall structural behavior.

Test results showed no evidence of damage propagation at the concrete-composite interface when beams were subjected to service-load cycling. Monotonic tests demonstrated no influence of the fatigue loading on the ultimate static capacity. However, post-cyclic ultimate deformations and structural ductility

were reduced after cyclic loading. Fatigue performance under high stress range appeared to be governed by debonding at the concrete-adhesive interface. One specimen failed under fatigue loading. Test results are also compared with previous research found in the literature in the form of an S-N curve.

TABLE OF CONTENTS

LIST OF FIGURES

List of Tables

Chapter 1 Introduction

1.1 General

A deficient or obsolete infrastructure may have a severe impact on the social and economic activities in a nation. In North America, as well as in Europe, a significant portion of aging civil structures needs to be either retrofitted or demolished. Demolition is often not an available option, as some structures have historical significance or are part of the architectural heritage. Moreover, consequences of traffic interruptions and delays may be unbearable on a local scale. On the other hand, rehabilitation or strengthening provides a better use of resources and is competitive today with the bridge replacement alternative.

Rehabilitation of existing structures may be required as a consequence of time-dependent damage such as reinforcement corrosion and freeze-thaw action, or accidental actions such as over-loading, earthquake, explosion or fire. Thus, the primary aim of rehabilitation is to restore the initial strength and function of the damaged members. The reasons for strengthening include change in design codes as a result of new safety requirements, increase in traffic load, road widening, change in structural system, and poor initial design or deficient construction.

Numerous retrofitting methods have been used in the past: cross-section enlargement, external prestressing, and bonding of steel plates, among others. Originally invented in France by L'Hermite and Bresson [32], then developed in Switzerland and Germany in the 1960s, the application of bonded steel plates by means of a two-component epoxy adhesive on the tensile face of concrete members has been proven to be an effective retrofitting method. It has been demonstrated to

both increase the flexural capacity and decrease cracking due to live loads [33-35]. The low cost of the materials and increasing number of uses of the technique since the early 1980s make this an attractive system.

However, due to the heavy weight of steel, the plates are difficult to handle on the construction site. The delivery length of the plates is therefore limited introducing complicated joints. Such inconveniences result in high scaffolding and labor costs. Furthermore, extensive long-term studies conducted at the Swiss Federal Laboratories for Materials Testing and Research (EMPA), at Duebendorf, Switzerland, have highlighted the susceptibility of the steel plates to corrosion, especially at the joint between the steel and the adhesive, leading to the potential failure of the strengthening system [38].

Compared to steel, fibrous composite materials, such as aramid, glass, or carbon fibers, present a large number of advantages. They offer low density along with very high stiffness and strength, resistance to corrosive and electromagnetic environments, and outstanding long-term and fatigue behavior, resulting in low-installation and maintenance costs. In addition, the manufacturing processes allow endless laminates, so joints are no longer needed.

Fiber Reinforced Polymer (FRP) materials are approximately ten times more expensive than steel. However, the amount of FRP material required for a retrofitting project is approximately 10% of the equivalent quantity of steel that would be necessary to develop the same resistance. On the other hand, the usual cost of materials constitutes approximately 20% of the total cost of a rehabilitation or strengthening project. Thus, the remaining 80% associated with labor costs can be reduced considerably due to the ease of handling [40].

Carbon Fiber Reinforced Polymer (CFRP) laminates have been tested in the laboratory for strengthening reinforced concrete (RC) members in flexure and shear

since the mid-1980s [36] and have been applied on site since 1986 (*The Kattenbusch Bridge, Germany*). In subsequent years, the technique was successfully used to strengthen concrete and wooden bridges (*The Ibach Bridge near Lucern, Switzerland, The historic covered wooden bridge, Sins, Switzerland*) commercial office buildings, parking garages, and chimneys of nuclear plants (*Leibstadt, Switzerland*), among others [37, 38].

Today the static behavior of structures strengthened using externally bonded CFRP materials is described exhaustively in the literature, but there still remains a gap in knowledge regarding the long-term behavior, especially under repeated loading.

1.2 Background

A recent survey on the condition of existing bridges throughout the United States conducted by the Federal Highway Administration (FHWA) in 1998 concluded that 30% of the total number of bridges were structurally deficient or functionally obsolete (Table 1.1). In the State of Texas in particular, the FHWA has listed 3,812 bridges out of a total number of 47,173 as being structurally deficient [57], (Table 1.2).

Since 1995, the FHWA has promoted rehabilitation and strengthening of existing bridges as an alternative to replacement [19]. Furthermore, as part of the strategic goals for 1999, the FHWA encouraged each State Department of Transportation to reach "4.6% reduction [per year] in the number of deficient bridges over the next 8 years," which implies approximately 20 bridges that need to be strengthened per year in Texas [57].

To meet this goal, the Texas Department of Transportation (TxDOT) is conducting an ongoing research program of bridge strengthening for structures that

do not reach current rating standards. The criterion adopted by the TxDOT is to upgrade existing bridges that are not deemed sufficient to carry an HS-20 design truck as specified in the AASHTO Standard Specifications for Highway Bridges [49], (Figure 1.1).

Most bridges that fall into this category in Texas are simply supported, short-span bridges, designed in the 1940s for either H-10 or H-15 AASHTO truck loading (Figure 1.1), such as pan-joist bridges and flat slab bridges usually used in off-system roads. Strengthening of these bridges may be necessary for two main reasons. First, to allow the economical growth of local areas, some bridges on heavily traveled routes need to be upgrade to the HS-20 AASHTO standard. Second, to widen existing bridges for a larger traffic volume, bridges must attain an operating rate of at least an HS-20 truck. About 33% of the total number of pan-joist bridges and 20% of the flat slab bridges are currently deficient according to the HS-20 standard.

Thus, TxDOT has funded a research project at the Phil M. Ferguson Structural Engineering Laboratory at the University of Texas at Austin, to develop methods to strengthen existing RC bridges using FRP composite materials that are readily available in the construction industry. Overall, the main objective of this research is to provide economical, efficient methods to increase the capacity of pan-joist and flat slab bridges as an alternative to bridge replacement.

The first phase of the research project included testing twenty-two RC beams externally reinforced for flexure using CFRP composites from four different manufacturers to define the optimal arrangement of sheets and strips. All the specimens were loaded statically to failure. Two specimens were subjected to wet-dry cycles to assess the effect of environmental exposure on ultimate strength [11, 12].

The second phase involves testing of four large-scale specimens corresponding to actual deficient bridge cross-sections [12].

Finally, the third phase involves fatigue testing six rectangular RC beams strengthened using the CFRP configuration that produced the most reliable results during the first phase in terms of load increase, modes of failure and deflections. The present thesis reports the results for the third phase of the research program.

Table 1.1: Number of deficient and obsolete bridges in the United States in 1992, 1995 and 1998.

Source: U.S. Department of Transportation, Federal Highway Administration [57].

YEAR	TOTAL NUMBER OF BRIDGES	STRUCTURALLY DEFICIENT		FUNCTIONALLY OBSOLETE		TOTAL OF BOTH	
		Number	Percentage	Number	Percentage	Number	Percentage
1992	572,453	118,575	21%	80,462	14%	199,037	35%
1995	577,919	103,636	18%	80,217	14%	183,853	32%
1998	583,414	93,119	16%	79,576	14%	172,695	30%

Table 1.2: Number of deficient and obsolete bridges in the State of Texas in 1992, 1995 and 1998.

Source: U.S. Department of Transportation, Federal Highway Administration [57].

YEAR	TOTAL NUMBER OF BRIDGES	STRUCTURALLY DEFICIENT		FUNCTIONALLY OBSOLETE		TOTAL OF BOTH	
		Number	Percentage	Number	Percentage	Number	Percentage
1992	46,667	5,837	13%	6,273	13%	12,110	26%
1995	47,115	4,686	10%	6,707	14%	11,393	24%
1998	47,173	3,812	8%	6,780	14%	10,592	23%

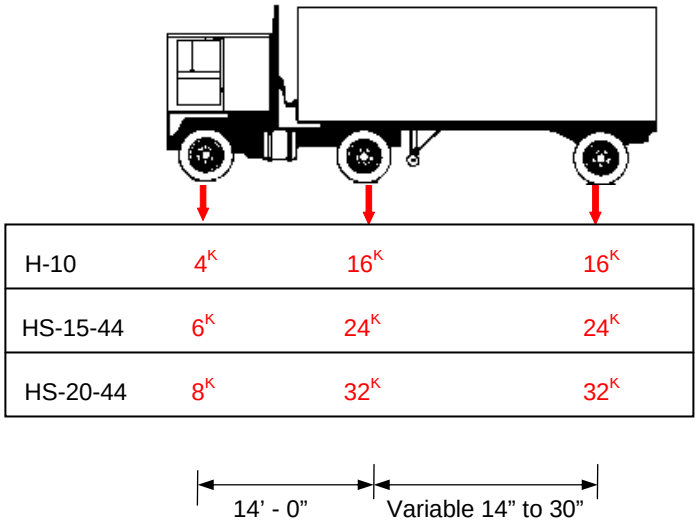

Figure 1.1: AASHTO design loading truck, Imperial units.
Adapted from [49].

1.3 Research objectives and scope

The present experimental study aims to identify the influence of repeated loading on the serviceability and ultimate behavior of RC beams strengthened with different types of CFRP sheets and plates under realistic loading conditions.

Static tests carried out during the past 18 months in the Phil M. Ferguson Structural Engineering Laboratory at the University of Texas at Austin, have demonstrated that particular arrangements of carbon fiber sheets and laminates can provide the desired level of flexural strength increase [11, 12]. In particular, research results demonstrate that anchorage of the CFRP flexural reinforcement using CFRP flexible straps significantly improves the ultimate strength and deformation capacity. Two types of strengthening configurations were found suitable to upgrade bridges to the HS-20 standard and have been selected for the repeated loading tests. This former study also highlighted that the ultimate static

strength of the strengthened beams is primarily governed either by debonding or rupture of the longitudinal CFRP laminate providing the flexural reinforcement.

The repeated loading test program thus focuses on the behavior of RC beams strengthened using externally bonded CFRP sheets and plates along with transverse straps to anchor the longitudinal sheets or plates. Cumulative damage in RC members resulting from fatigue loading could affect the concrete-epoxy interface, the fibers, the composite matrix, or the fiber-matrix bond leading to a reduction in the efficiency of the CFRP reinforcement. The behavior of RC elements externally reinforced using the CFRP configuration developed under repeated loading is therefore required.

Five specimens were loaded monotonically to failure after being subjected to a program of fatigue loading. The behavior of specimens after different numbers of load cycles is reported herein. The post-cyclic static performances of strengthened beams were compared with both strengthened and unstrengthened companion RC beams tested statically to failure. This comparison was made on the basis of ultimate strength, mode of failure, deformations, and structural ductility.

Furthermore, the results are compared qualitatively with the behavior of RC beams subjected to repeated loading as described in the literature in order to highlight the benefit of the external reinforcement under repeated loading conditions.

The primary goal was not to reach the fatigue limit of the strengthened members. However, in light of the first set of test results, the research program was modified from the original plan. The last beam was subjected to a fatigue test, with peak load above the yield level of the steel reinforcement, in order to gain insight into the fatigue failure mechanism for the strengthened member.

1.4 Thesis outline

The present report is organized in six chapters.

Chapter 2 presents the results of a brief literature review performed prior to testing. The purpose of this review was not to expose detailed design procedures for fatigue or strengthening but to provide comprehensive information on both the properties of the strengthening materials and the behavior of the reinforced members under static and repeated loading conditions, and to identify areas that need further investigation. The following topics are reviewed: FRP materials, manufacturing and application process, flexural behavior of reinforced concrete, fatigue properties unidirectional composite materials, and flexural behavior of RC members strengthened with advanced composite materials under static and repeated loading regimes.

C*hapter 3* presents a methodology for the design of RC beams strengthened with FRP composites. The main assumptions and the design philosophy are presented. An upper limit for the amount of FRP materials that should be used for preliminary design is proposed. Finally, a method to compute the ultimate flexural capacity, the cracking and yield moments of the strengthened section is described.

The experimental program is presented in *Chapter 4*. Details of the test specimens, materials properties, instrumentation, and test set-up for the repeated loading system are presented. The choice of the different loading parameters is explained and justified.

Test results and observations are discussed in C*hapter 5*. The previous static loading tests and the repeated loading tests are compared on the basis of ultimate strength, mode of failure, mid-span deflection, stiffness, curvature, strains across the section, and structural ductility. Two different energy approaches are used to evaluate the structural ductility. A comparison between these two definitions is

made based on the test results. The behavior of the strengthened members is qualitatively compared to the one of RC members subjected to repeated loading as described in the literature. Results of fatigue tests are compared with previous research reviewed in Chapter 2.

Finally, *Chapter 6* summarizes the main findings of the experimental study and highlights conclusions regarding the flexural and the fatigue behavior of RC members reinforced with CFRP materials.

The A*ppendices* present select results in more detail, and hand computations necessary to this work. Tables for conversion between Imperial and SI units are also presented.

Chapter 2 Literature review

2.1 Fiber Reinforced Polymers strengthening materials

Fiber Reinforced Polymer (FRP) materials in the form of sheets or plates used in the rehabilitation and strengthening of civil structures are presented in this section. Other materials, such as cables, reinforcing bars, or molded materials, also fabricated with FRP are not included.

2.1.1 Fiber Reinforced Polymer materials

Advanced fibrous composite materials are built up two separate materials acting together, namely, the fibers and the matrix, as shown in the microscopic view of the FRP material in Figure 2.1. The fibers have a diameter of about 7 μm (2¾ mils). They are oriented in a specific direction, have a specified volume fraction, and are embedded in the matrix. The purpose of such a combination is to achieve outstanding physical and mechanical properties that the individual cannot attain alone.

The fibers can be made of glass, aramid (Kevlar), or carbon, and their function is to provide stiffness and tensile strength to the composite. The matrix is usually made using either a polyester, vinylester or epoxy resin. Its function is to transfer the forces to the fibers, thereby compensating for inevitable flaws in the fibers, and providing compressive strength and chemical protection [20].

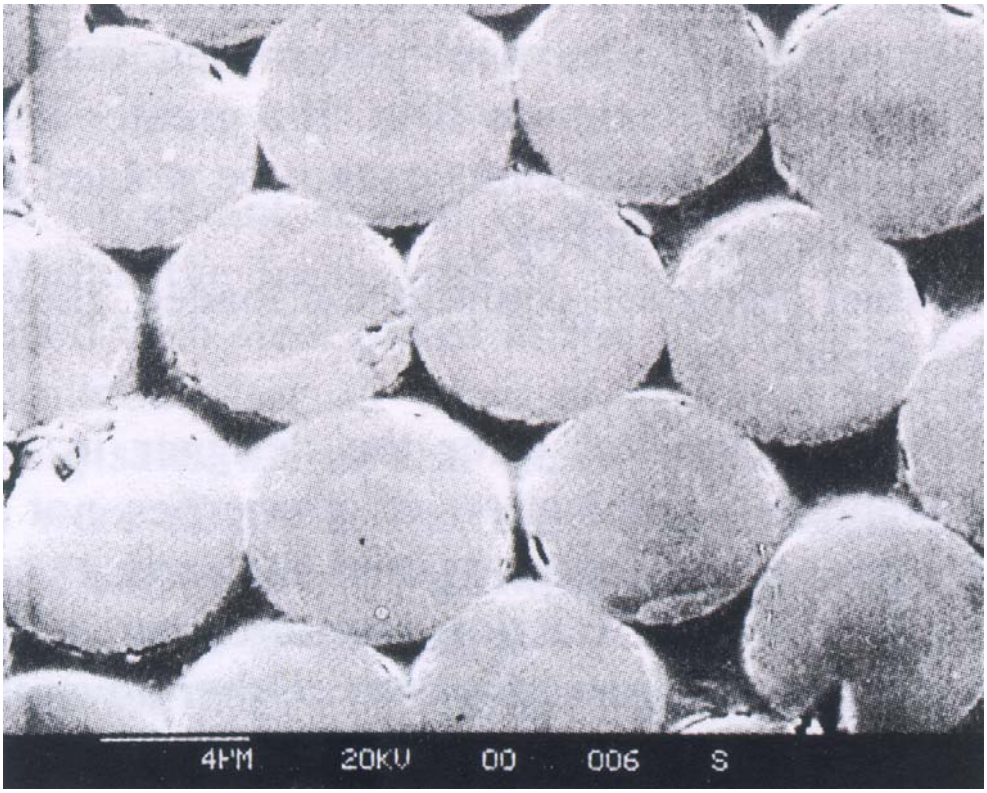

Figure 2.1: Scanning electron micrograph (SEM) of a CFRP plate.

Source: Meier [37].

Two main types of composite materials are available for use in the construction industry for strengthening or rehabilitation purposes [20, 26]:

Continuous unidirectional fiber composites are made up one or several unidirectional layers (laminates) that can be bonded together with an adhesive and oriented in pre-defined directions. The interlaminate strength, provided by the resin, is rather low, so laminates may separate from each other (delamination).

Woven multi-directional fabric composites were derived directly from textile technology. Individual yarns are woven into a fabric resulting in diverse cross-

pattern fiber layouts. These fabrics form a single layer, so delamination is not possible. However, the woven fibers are not straight and the cross-pattern of the fibers impedes resin impregnation of the fibers resulting in lower tensile properties.

Width and length of these products are only limited by the dimensions of the manufacturing facilities and machines. Their light weight and flexibility allow them to be delivered by rolls of indefinite length.

2.1.2 Adhesives

Bonding techniques were made possible by the development of appropriate adhesives since the 1940s [26]. The purpose of the adhesive is to provide continuous bond between the surface of the member to be strengthened and the FRP laminate to ensure that full composite action can be developed by the transfer of shear stress across the adhesive layer.

Two-component, cold-curing epoxy adhesives constitute a large part of the adhesives in use in the construction industry. They present several advantages over other polymer adhesives: high cured cohesive strength, high adhesive strength, high resistance to chemicals, inertness, low shrinkage, and low water absorption. An extensive description of adhesive properties can be found in Reference [26].

They are typically suitable for a service operating temperature in the range of -60°C to +60°C (-76°F to 140°F). However, at the time of application, the viscosity of the adhesive can vary markedly with temperature, affecting workability and application.

2.1.3 Manufacturing and application processes

FRP materials are manufactured and placed mainly through three different processes: the filament winding process, wet lay-up process, and pultrusion system [20, 26].

In the *filament winding process*, continuous unidirectional fibers are successively coated with resin and wound automatically around the element to be strengthened. The process can be used conveniently to retrofit circular or rectangular elements such as bridge piers, building columns, and chimneys. It provides additional confinement to concrete and has been successfully used as an earthquake-retrofitting method, particularly in California.

The *wet lay-up process* consists of flexible dry fiber sheets or fabrics impregnated with a resin at the time of bonding (Figure 2.2.a and 2.3). The sheets come in the form of rolls of dry fibers (tow-sheets), which can easily be cut to the desired dimensions. Several layers of fibers can be applied successively after applying a layer of resin between them. In this case, the resin acts simultaneously as the bonding agent and the composite matrix.

The *pultrusion process* is shown schematically in Figure 2.5. Continuous unidirectional fibers are pulled through a resin bath, preformed and cut to the required length. The process allows shaping of the basic structural cross-sections. The resulting products provide a constant-section profile and a high quality due to the good quality control during the manufacturing process. The composite pultruded strips used for strengthening typically exhibit approximately 65% volume fraction of fibers (V_f , defined as the ratio of the volume of fibers to the total volume). The plates are directly bonded to the prepared concrete surface using an adhesive resin (Figure 2.2.b, and 2.4).

Other processes are also available such as pre-cured pre-impregnated (prepreg) plates, or prepreg sheets or tapes cold-laminated in place.

The materials used in this study fall into the categories of a wet lay-up system, commercialized by Master Builders [35], and a pultruded plate system, manufactured by Sika Corporation [47] (Sections 4.1.3 and 4.1.4). The complete bonding procedure is presented in Section 4.2.2.

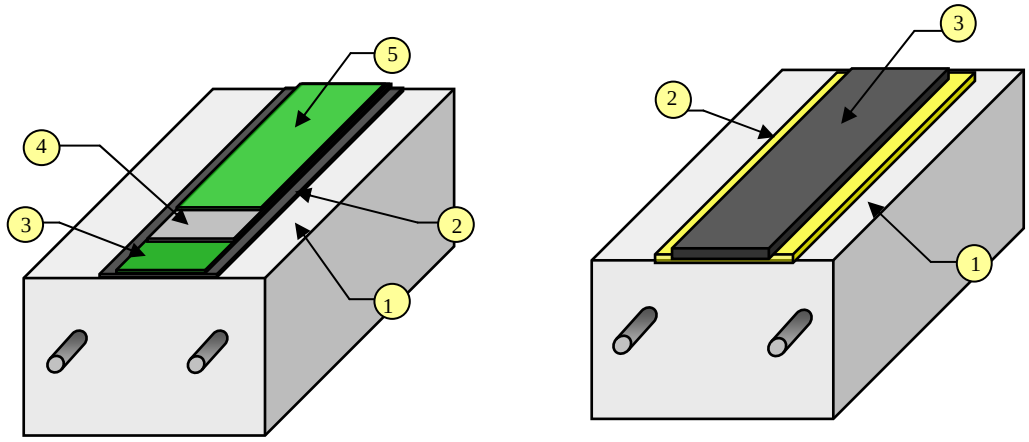

Wet lay-up composite system

1. Prepared concrete surface
2. Primer: surface sealant
3. Epoxy: bonding agent
4. Unidirectional CFRP sheet
5. Epoxy: matrix of the composite

Pultruded plate system

1. Prepared concrete surface
2. Epoxy: bonding agent
3. CFRP pultruded plate

Figure 2.2: Schematic view of strengthening systems:

(a) Wet lay-up composite system (b) Pultruded plate system.

Figure 2.3.a: Slab flexural strengthening

Figure 2.3.b: Guider flexural and shear strengthening

Figure 2.3: Wet lay-up composite system applications [35]

Figure 2.4.a: Slab flexural strengthening

Figure 2.4.a: Guider flexural and shear strengthening

Figure 2.4: Pultruded plate system applications [47]

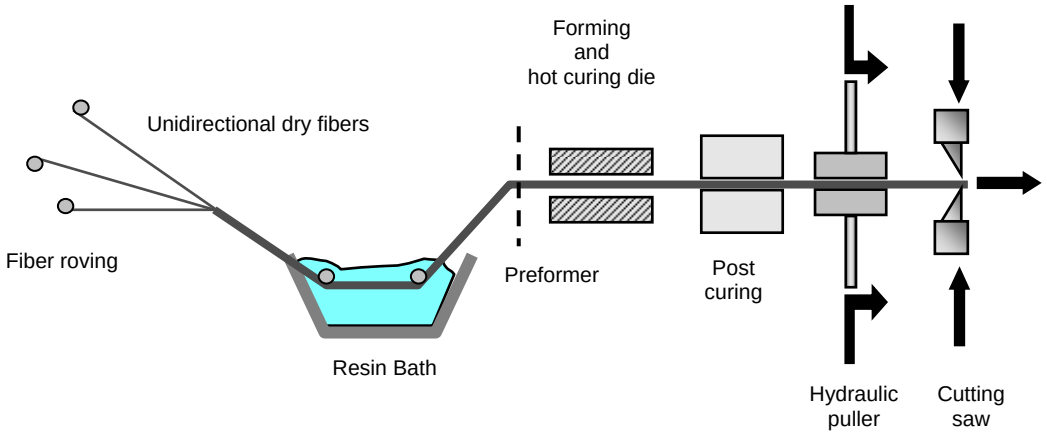

Figure 2.5: Pultrusion process.

Adapted from Hollaway and Leeming [26].

2.1.4 Mechanical properties

Composite materials exhibit a linear stress-strain response to failure without any plastic reserve (Figure 2.6). When subjected to tension, they fail in a brittle manner, with a large liberation of energy (Figure 2.7).

Table 2.1 compares the average properties of metallic and non-metallic construction materials. Fibers used for composite materials appear to have both higher tensile strength and tensile modulus along with lower density than steel. Two different types of carbon fibers are available: high strength or high modulus fibers. Moreover, a qualitative comparison between different types of FRP sheets designates carbon fibers as the most suitable material for strengthening or rehabilitation purposes (Table 2.2).

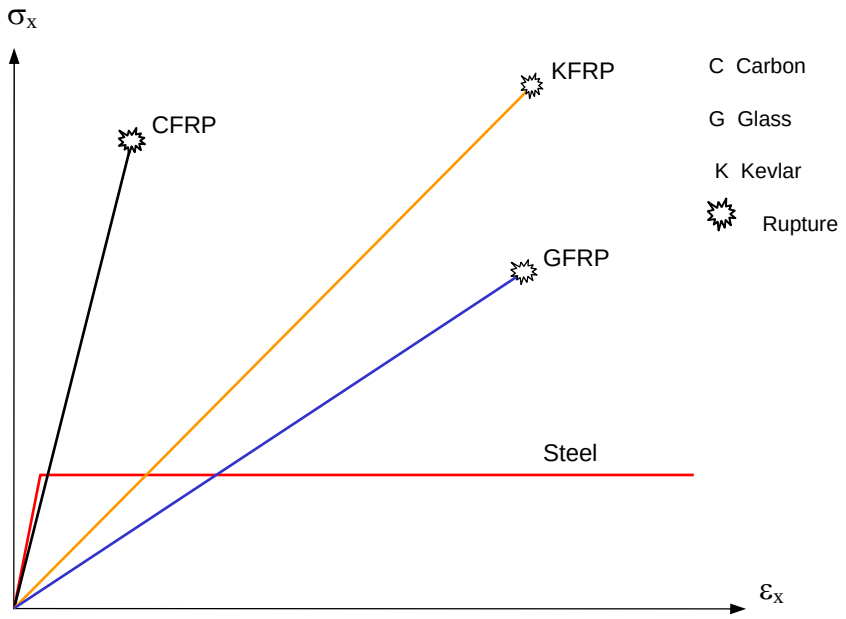

Figure 2.6: Typical stress-strain response of composite materials versus steel.

Source: Berset [9].

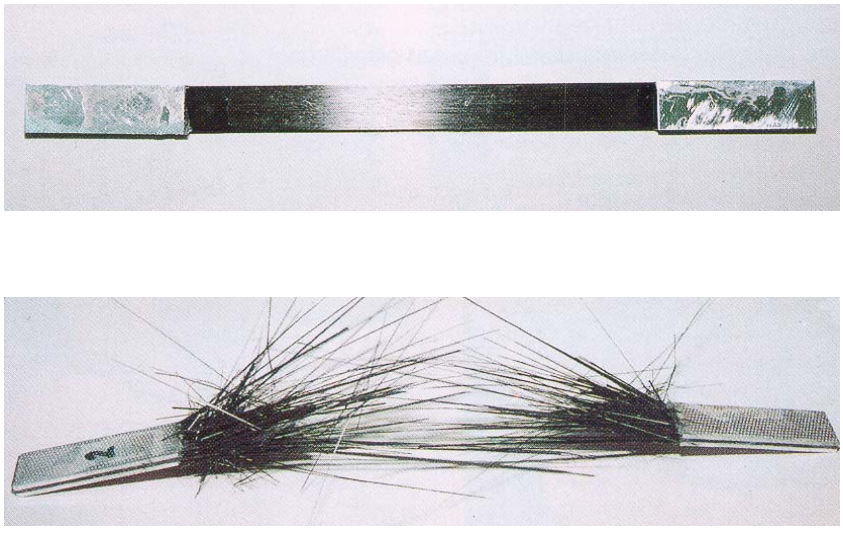

Figure 2.7: CFRP pultruded plate specimen before failure and after failure [47].

Table 2.1: Average properties of metallic and non-metallic construction materials. Values in SI units by Frey [20], approximate conversion.

	MATERIAL	TENSILE STRENGTH*		TENSILE MODULUS*		DENSITY	
		Gpa	Ksi	Gpa	Ksi	g/cm^3	lb/cu ft
Non-Metallic Fibers	Carbon HS+	2.5 - 7.0	365 - 1,015	220 - 400	31,900 - 58, 000	1.6 - 1.8	100 - 112
	Carbon HM++	1.6 - 3.0	230 - 435	500- 900	72,500 - 130,600	2.0 - 2.2	125 - 137
	Aramid (Kevlar 49)	3.6	520	120 - 130	17,400 - 18,900	1.4 - 1.5	87 - 94
	E-glass	3.2 - 3.5	465 - 510	73	10,600	2.6	162
Metals	Mild Steel	0.46	67	200	29,000	7.9	493
	Presstressing Steel	1.7 -2.0	250 - 290	196	28,500	7.9	493
	Aluminum	0.3	45	70	10,200	2.7	169

*In the direction of the fibers + HS: High Strength ++ HM: High Modulus

Table 2.2: Qualitative comparison of main properties of FRP sheets made of approximately 65% volume fraction of fibers. Source: Meier [38]

CHARACTERISTICS	TYPE OF FIBERS		
	E-GLASS	ARAMIDE	HS CARBON
Tensile strength	Very good	Very good	Very good
Compressive strength	Good	Poor	Good
Stiffness	Poor	Good	Very good
Cyclic fatigue	Fair	Good	Excellent
Density	Fair	Excellent	Good
Alkaline resistance	Poor	Good	Very good
Cost	Good	Fair	Sufficient
COMPARISON	FAIR	GOOD	VERY GOOD

This comparison applies for laminates used in rehabilitation and strengthening works.

2.2 Behavior of RC and FRP materials under repeated loading

2.2.1 Definitions

At this point, it is worthwhile to define several terms that are used throughout the report:

Static loading is a load maintained constant with time or applied slowly and monotonically with time. The ultimate corresponding strength is referred to as the *static strength*.

A *repeated loading* is a sequence of arbitrary repeated loads that may not necessarily cause failure.

A member or a material failing under a sequence of repeated loads, each smaller than the single static load that would cause failure, is said to have failed in *fatigue*. Fatigue is a process of progressive permanent internal damage in materials subjected to repeated loading.

A very high level of repeated loading, due to an earthquake for instance, may cause failure before 100 cycles [2]. These failures are referred to as *low-cycle fatigue*.

The *fatigue strength* is defined as a fraction of the static strength that a material can support repeatedly for a given number of cycles. It is influenced mainly by rate of loading, stress range, load history, material properties and environmental conditions [2]. The ratio of fatigue strength to static strength (S) versus the logarithm of the number of cycles to failure (N), commonly referred to as S-N curve (Figure 2.8), allows comparing the influence of diverse load ranges.

If the curve becomes asymptotic parallel to the horizontal axis (Figure 2.8), the corresponding stress level is called the *fatigue limit*. A stress applied below the fatigue limit corresponds to an infinite life of the material under repeated loading conditions.

The *endurance*, of *fatigue life*, corresponds to the number of cycles to failure.

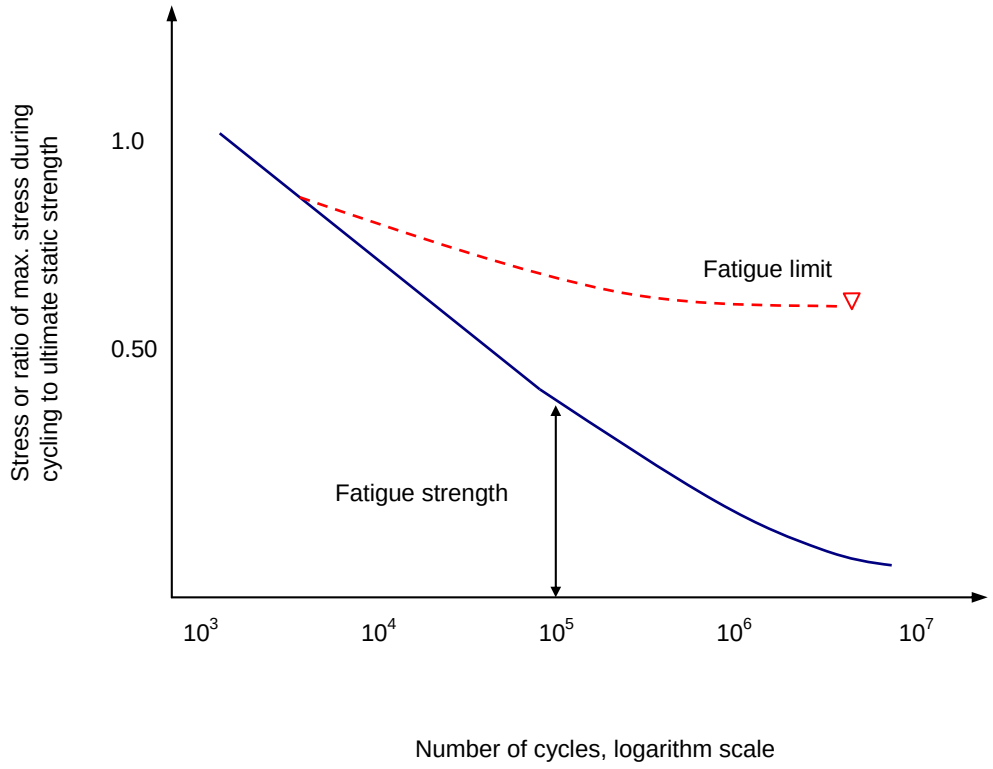

Figure 2.8: Typical SN curves.
Adapted from [43].

2.2.2 Reinforced concrete in flexure

The ACI Committee 215 has performed an extensive review of research on concrete structures subjected to fatigue loading. The papers reviewed – more than 100 – date back from 1898 to 1974 and are summarized in [1]. Most of the conclusions presented below are the result of the work reported by ACI Committee 215 [1, 2].

Both concrete and steel used in reinforced concrete (RC) possess the characteristic of failing by gradual fracture. Therefore, RC members subjected to fatigue experience failure of either the steel or concrete.

In plain concrete, cumulative damage results in progressive growth of cracks and complete fracture if the range of loading is sufficiently large. Fatigue fracture of concrete is characterized by considerably larger strain and microcracking as compared with static rupture. Failure at the bond between the aggregates and the cement paste is a predominant mode of rupture. For 10 million cycles in compression, tension, or flexure, the fatigue strength of plain concrete was found to be approximately 55% of the static strength. It was also concluded that it is affected by the minimum stress in the cycles, the stress range, and the stress gradient, but is not sensitive to stress concentration.

For design purposes, the modified Goodman diagram [2] (Figure 2.9) shows the influence of the range of loading and minimum stress level on the fatigue strength of plain concrete. Based on a series of experimental studies, this diagram presents a linear decrease of the stress range as the minimum stress level is increased. For instance, for a zero minimum stress level, the stress range the concrete can withstand without failure is taken conservatively as 50% of the static strength; for a 15% minimum stress level, the maximum stress the concrete can support without failure is about 57% of the static strength.

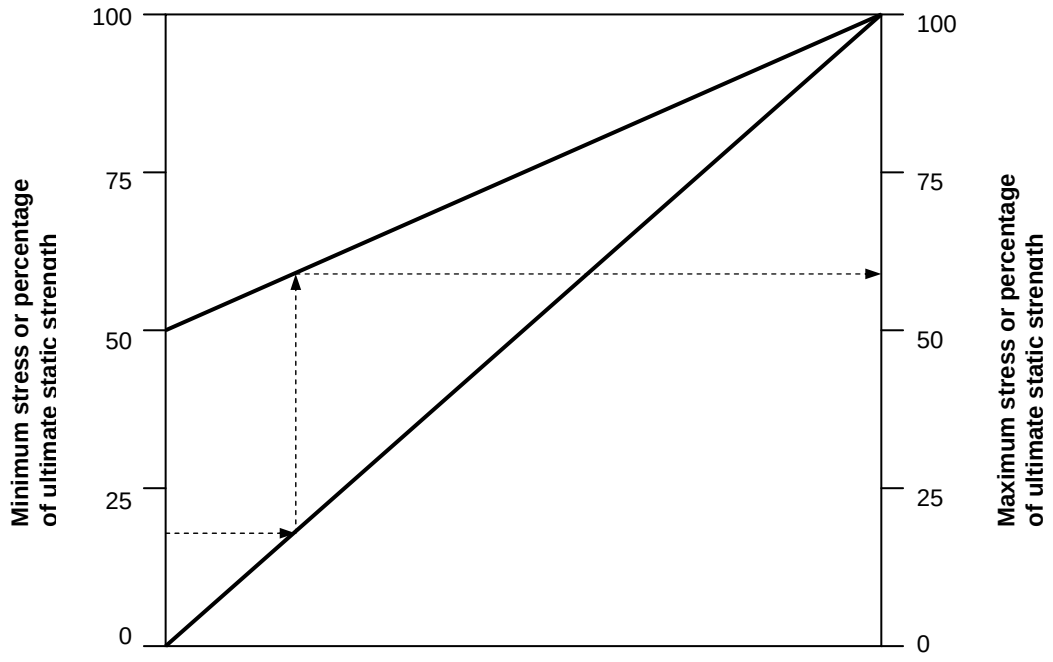

Figure 2.9: Modified Goodman diagram. Fatigue strength of plain concrete in tension, compression or flexure [2].

Most experimental work has demonstrated that fatigue flexural failure of RC members is due to fracture in the reinforcing steel related to severe cracking [1], [43]. A typical fatigue fracture in a reinforcement bar embedded in the tension zone of a concrete beam shows a smooth zone corresponding to the growth of the fatigue crack. The weakened bar thus presents a reduced section and subsequently fails in tension [1].

Helgason and Hanson [24] compared the fatigue strength of reinforcement bars using S-N curves (Figure 2.10). The fatigue strength of reinforcement bars was found to be essentially independent of the yield strength. It decreased as the stress range increased, and as the lower stress in the cycle decreased. They also noticed that the fatigue strength could be reduced by up to 50% by bends, tack welds or

notches, and is sensitive to stress concentration. For design, it is recommended that the stress range in bars of RC members subjected to 1 million cycles or more should not exceed 20 ksi (138 MPa) [33].

Contrary to concrete, steel exhibits a clear fatigue limit. The fatigue limit for straight ASTM A 615 bars, as well as for Grade 40 (yielding at 276 MPa) and Grade 60 (yielding at 413 MPa) bars, is about 24 ksi (165 MPa) [24].

Figure 2.10: Test data on fatigue of deformed bars from a single U.S. manufacturer [24].

Numerous researchers reported on the influence of repeated loading on the flexural behavior of RC beams (Berry 1909 [8], Batson and Hyde 1922 [7], Heim 1930 [23], Treiber 1934 [52, 53]). The tests carried out have demonstrated that, before reaching 1 million cycles, new cracks appeared, cracking progressed but without shifting the neutral axis, the stiffness of the beam decreased, but beam deflections stabilized as the number of cycles increased. The ultimate load capacity was not reduced by a repeated load sequence of 1 million cycles as long as the maximum load remained under the fatigue strength. The fatigue strength of a RC beam designed to fail in flexure was reported to be between 50% and 65% of the static strength [16, 23, 43]. On the other hand, deflections never stabilized in beams subjected to a maximum load above their fatigue strength, and deflection amplitudes increased until beam failure

A maximum test frequency of approximately 2 Hz is recommended [6] in order to allow the beam to recover fully from one load before the application of the next one.

The following design recommendations for RC elements subjected to fatigue loading were reported by ACI Fatigue Committee 215 [2] and ACI Bridge Committee 343 [3]:

- Compressive stress range, f_{cr}, should not exceed

$$f_{cr} = 0.4f'_c + 0.47f_{min} \quad [ksi] \qquad (2.1)$$

where f_{min} is the minimum compressive stress in the cycle (positive in compression), and f'_c is the nominal compressive strength of the concrete.

- For bars with normal lug geometry, the tension stress range should not exceed

$$f_r = 23.4 - 0.33 f_{min} \quad [ksi] \qquad (2.2)$$

where f_r is the algebraic difference between the maximum and the minimum stresses, and f_{min} is the minimum stress during the cycles.

2.2.3 Unidirectional fibrous composite materials in tension

Most studies on the fatigue properties of advanced composite materials are related to the aerospace industry, where composites have been in use since the early 1950s. Their excellent fatigue resistance has allowed them to be used in high demand applications, such as for helicopter rotor-blades.

Curtis [14] reviewed the fatigue properties of high performance continuous reinforced composite materials containing an organic matrix. In particular, the damage propagation process was presented for typical unidirectional materials, and the fatigue performances were compared for different types of materials. His parametric study included the type of fiber and matrix, stress level, and environmental exposure effects.

Typical peak tensile strength versus logarithm of the number of cycles (S-N curve) for unidirectional composite materials is shown in Figure 2.11. Glass fiber- and aramid fiber-epoxy composites exhibited a smaller ratio of fatigue stress at high life to static strength than carbon fiber reinforced materials. Furthermore, carbon fiber-epoxy composites showed no sign of degradation before 3 million cycles [14]. However, no clear evidence of a fatigue limit was identified [15].

The fatigue behavior might be expected to be essentially dependent on the performances of the fibers. However, experimental parametric studies (Curtis [14],

Talreja [50]) have demonstrated that the strain level in the matrix primarily determines the slope of the S-N curve (i.e. the speed of degradation of the material). On the other hand, the use of higher performance fibers in the same epoxy resin resulted in little improvement of the fatigue life.

The manufacturing process can also affect the fatigue properties. Compared with pultruded plates, fabric-based composite materials exhibit lower stresses at low number of cycles and additional degradation, due to the distortion of the fibers in the weave, resulting in a steeper S-N curve.

For unidirectional reinforced composites, cyclic loading under 10 Hz has no effect on fatigue life. This frequency limit encompasses most of the civil structures since bridges, for instance, are designed to accommodate a loading frequency of around 1 Hz [15].

For design purposes in civil engineering, Demers [15] defined, through statistical distributions, lower bounds for fatigue life of E-glass FRP and CFRP materials.

Compared with metals, fatigue damage propagation and failure modes of composite materials are essentially different. Under repeated loading, metals generally exhibit a progressive growth of a single localized defect. In contrast, composite materials develop complex, widespread damage zones, and no single flaw growth is observed [14]. Four basic fatigue failures were observed in FRP materials: matrix cracking, delamination, fiber failure, and fiber-resin debonding [25].

In conclusion, unidirectional carbon fiber-epoxy composites demonstrate outstanding fatigue properties in the range of stresses encountered in civil engineering, even higher than most of the more commonly used construction materials.

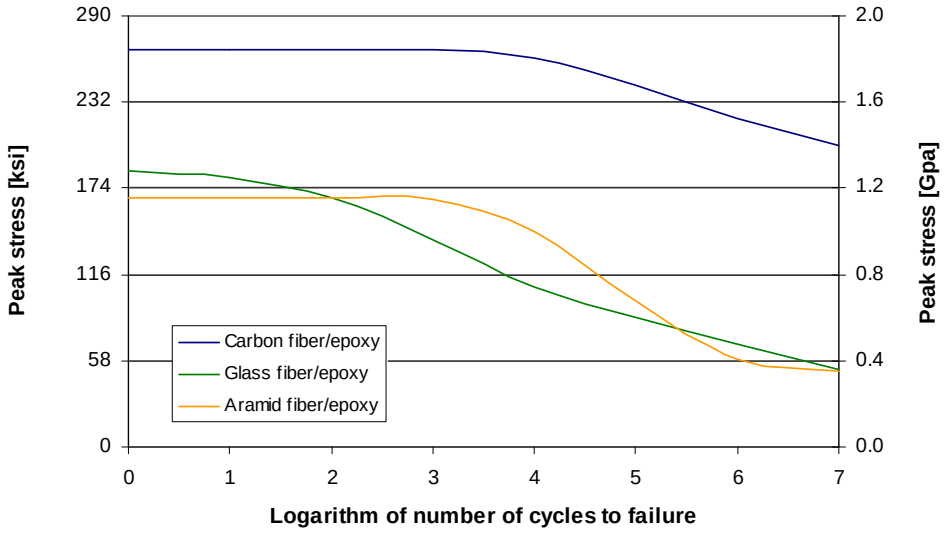

Figure 2.11: S-N fatigue data for unidirectional composite materials.

Values in SI units by Curtis [14].

2.3 Flexural strengthening of RC beams using externally bonded CFRP laminates

2.3.1 Static behavior

Investigations on the use of externally bonded FRP composites to strengthen RC structures as an alternative to steel plate bonding were pioneered at the Swiss Federal Laboratories for Materials Testing and Research (EMPA), at Duebendorf, Switzerland, in the mid-1980s [36]. The overall research program conducted at EMPA, including more than 90 strengthened beams with various cross-sectional shapes, demonstrated the validity of the strain compatibility method for RC members strengthened with CFRP materials. This implies that the traditional RC beam theory

can be applied safely when using advanced composite materials to strengthened beams in flexure [39].

Numerous authors have reported on the static behavior of RC members strengthened with CFRP materials (Meier 1987 [36-40], Kaiser 1989 [30], Spadea *et al.* 1998 [48], Hollaway and Leeming 1999 [26]). The general behavior reported is similar in every study. A substantial review of experimental investigations carried out in Europe and North America can be found in Reference [26], and in Reference [38] for Switzerland.

A typical load deflection response for a rectangular RC beam strengthened using CFRP laminates with a shear span/depth ratio of approximately 3.0 is shown in Figure 2.12 along with an unstrengthened control beam. Both beams demonstrate the same stiffness before cracking, because the laminate has relatively little influence on the second moment of inertia of the uncracked section The post-cracking stiffness of the strengthened beam is higher than that of the unstrengthened beam. The increase in stiffness and ultimate strength is largely dependent upon the properties of the FRP material and cross-sectional area of the laminate.

After the appearance of the first cracks in the concrete, the steel reinforcement and the CFRP laminate both contribute to the tensile force. The contribution of the CFRP laminate results in a decrease of the stress level in the reinforcing bars because the two materials have almost the same modulus of elasticity and are subjected to about the same strain level. As a result, the yield stress of the steel reinforcement is reached at a higher applied load in the strengthened beams.

As the steel bars reach yielding, only the CFRP laminate resists increases in the tension force, resulting in a reduction in stiffness of the element but far less than for the control beam. The ultimate flexural capacity can be increased by as much as

100% [40], but the deformation capacity of the element is reduced substantially. However the actual increase in load capacity is dependent upon the amount of steel reinforcement, the cross-sectional shape, and the quality of the materials used. Finally, the laminate ruptures or debonds in a brittle manner leading to collapse. FRP sheets applied to the side of the member result in a more ductile and progressive mode of rupture [11, 12].

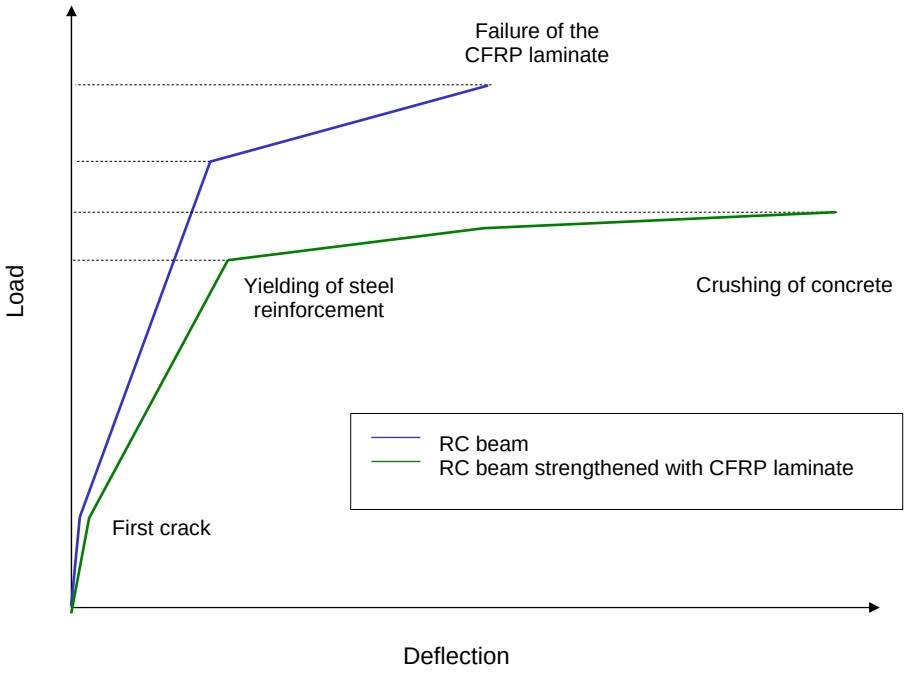

Figure 2.12: Typical load-deflection curves for unstrengthened RC beam and RC beam strengthened using CFRP materials with a shear span/depth ratio around 3.0.

The presence of the CFRP laminate also influences the crack pattern. Fewer and narrower cracks, and a more even distribution along the beam can be observed at the same load level as compared with the unstrengthened beam. Moreover, the beams that were pre-cracked before bonding of the CFRP materials exhibited the same performance as the beams that were not pre-cracked [26].

The use of CFRP sheets or strips without appropriate anchorage results in a severe decrease of the structural ductility and early debonding of the CFRP laminate [11, 12, 48]. In this case, the strengthened member cannot reach the theoretical ultimate strength calculated by assuming perfect bond of the laminate. With careful consideration to anchor the CFRP laminate, using bolts and steel plates for end anchorage, or steel or FRP straps along the beam, the composite action of the strengthened beam can be maintained up to its ultimate load [38], and the stiffness is increased after yielding [21]. Furthermore, the strengthened beam can regain a part of the structural ductility it had lost as compared with the unstrengthened beam [48].

Even if the structural benefit of anchorages is more sensitive under a low shear span/depth ratio (Figure 2.13), it is recommended to apply anchorages in any case, until long-term practical experience suggest otherwise [21]. The influence of the shear span/depth ratio on the failure mode and the efficiency of the anchorage are reviewed in Reference [26]. For a span/depth ratio greater than 4.0, the anchorage had no effect on the peeling-off of the laminate. For a span/depth ratio around 3.0, the anchorage delayed the debonding and considerably enhanced the ultimate capacity and member stiffness [11, 12, 22].

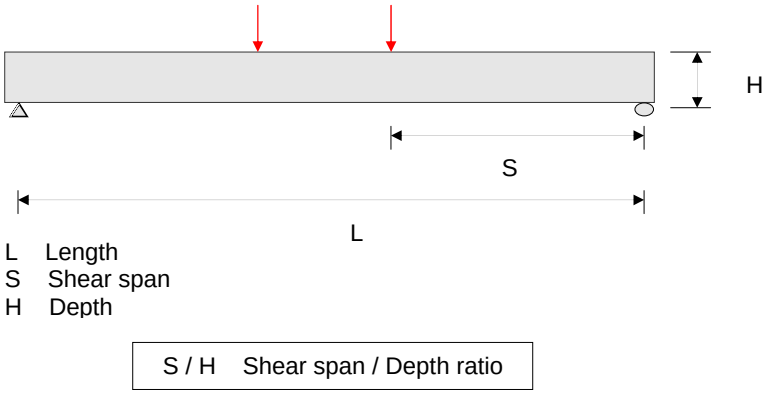

Figure 2.13: Definition of the shear span/depth ratio.

CFRP strips can also be prestressed. The higher stress level in the strips reduces the deformations at service load level and avoids the shearing off of the strip due to shear failure in the concrete [40]. However, pretensionned strips have not been commercialized yet. This case will not be discussed herein.

2.3.2 Failure modes

Nine failure modes are theoretically possible in a RC beam strengthened with CFRP materials [4, 10, 37], (Fig. 2.14):

1. Rupture of the CFRP laminate. Because CFRP materials have a linear behavior up to failure, this rupture is sudden and explosive. However, failure is preceded well in advance by cracking sounds.

2. Rupture of the steel reinforcement. This case may occur if the fatigue limit is reached.

3. Crushing of concrete in the compression zone.

4. Shear failure.

5. Failure cause by the debonding (peeling-off) of the laminate. Forces are transmitted to the laminate by shear between the concrete surface and the adhesive. Thus, shear stresses larger than the shear capacity of either the concrete surface or the adhesive lead to failure of the interface. Relative displacement of the edges of a crack due to shear (detail 5a) or uneven concrete bond surface (detail 5b) may cause stresses perpendicular to the surface that exceed the tensile strength of the materials, leading to debonding. Without anchorage, peeling-off can occur at any point along the laminate, due to the development of normal stresses (Section 2.3.3).

6. Rupture of the laminate-adhesive interface.

7. Rupture of the concrete-adhesive interface. This failure mode, as well as the previous one may be the consequence of improper surface preparation.

8. Cohesive failure within the adhesive. This could be the result of inadequate preparation of the adhesive material.

9. Interlaminate shear within the CFRP material (observed as a secondary failure). For CFRP flexible sheets, the resin is used as matrix and bonding agent, so failure may occur either in the matrix or in the adhesive (failure mode 8), leading to delamination.

Ninety percent of the total number of failures observed in RC members strengthened using externally bonded CFRP materials are due to the failure modes described in points five and seven above.

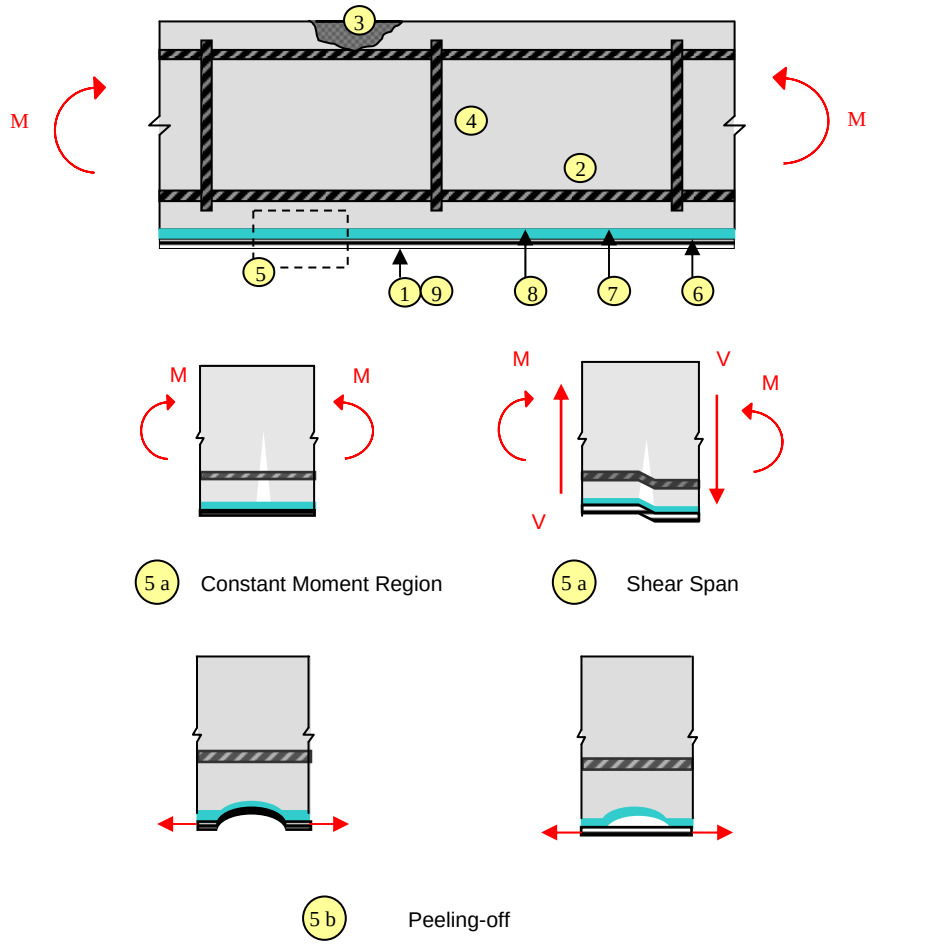

Figure 2.14: Failure modes in RC members strengthened using externally bonded FRP materials.

Adapted from Berset [9, 10].

2.3.3 Mechanical model for peeling-off

Peeling-off of CFRP plates or delamination between sheets cannot be explained by the plane stress condition usually used to describe the behavior of thin laminates. Indeed, at the free edge of laminated composite materials, stresses perpendicular to the laminate surface may appear, leading to delamination.

The simplified model presented in Figure 2.15 explains this phenomenon. This model involves two distinct layers: the epoxy resin and the carbon fibers. Because the Poisson coefficient of the epoxy resin is higher than that for the carbon fibers, tension applied in the longitudinal direction (x) in this model would result in different contractions for the two materials in the direction perpendicular to the normal stress (y).

Because the materials act together as a composite, the compatibility of deformations in both elements of the model must be preserved. Tension stresses in the x direction generate out-of-plane stresses (σ_z) due to deformation compatibility, and these could be higher than the tension strength of the epoxy, resulting in separation of the laminates [20].

The same mechanism explains peeling-off at the free edges of a CFRP sheet or plate bonded to the concrete surface. However, it is worthwhile to note that cracked concrete does not present a regular surface. For externally bonded laminates, the phenomenon described above is also accompanied by relative vertical displacements across shear cracks in concrete, leading to sudden peeling-off of the laminate, as described in Section 2.3.2.

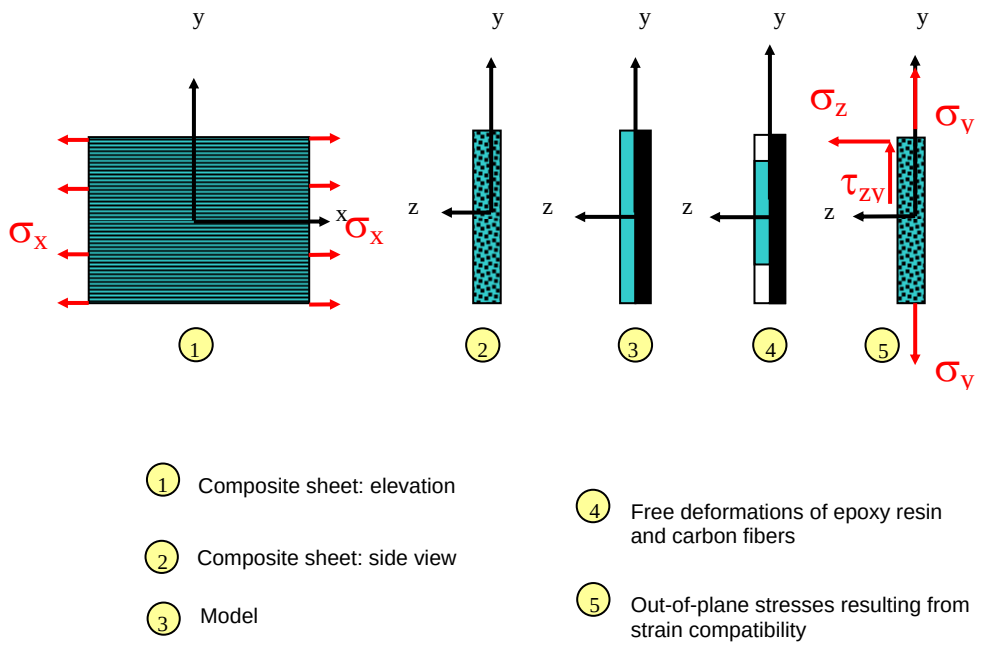

Figure 2.15 Simplified mechanical model for peeling-off of FRP laminates.

Adapted from Frey [20].

2.3.4 Behavior under repeated loading

The fatigue behavior of strengthened beam has received much less attention than the testing under static loading conditions. Recent research have reported on the behavior of RC beams strengthened with FRP materials under repeated loading (Kaiser 1989 [30], Shijie and Ruixian 1993 [46] Barnes and Mays 1999 [6], Shahawy and Beitelman 1999 [45]), and concluded the fatigue performance was noticeably improved as compared to the unstrengthened control beam. However, fatigue fracture of the internal reinforcement appeared to govern the failure of RC members strengthened in flexure with CFRP materials. It is therefore recommended [6] that the stress range in the rebars of the strengthened element should not exceed range permitted for conventional RC members.

Kaiser [30] conducted fatigue tests at EMPA on RC beams strengthened with a glass/carbon fiber hybrid composite. The cross-section of the RC beam was 300 mm (11.8 in) wide and 250 mm (9.8 in) deep, and the span was 2,000 mm (78.7 in). The conventional reinforcement consisted of two 8 mm (0.31 in) bars in the tension zone. The composite sheet had a 0.3 mm (11.8 mils) by 200 mm (7.9 in) cross-section and was bonded to the tensile face of the beam. It was subjected to two-point loading and cycled from 1 to 19 kN (0.2 to 4.3 kips) at a frequency of 4 Hz, corresponding to a stress range in the reinforcing bars of 386 N/mm^2 (56 ksi). The first fatigue damage to the rebars occurred after 480,000 cycles. The first damage in the composite appeared after 750,000 cycles in the form of fracture of individual fibers in the strips. The relatively sharp concrete at the edges of cracks rubbed against the strips at every cycle, and the composite finally failed after 805,000 cycles. This result clearly indicated that FRP laminates could sustain significant further loading after failure of the steel reinforcement.

Deuring performed further tests at EMPA [37] on beams with a T-shaped cross-section under more realistic loading conditions. The cross-section was 900 mm (35.4 in) wide and 500 mm (19.7 in) deep, and the span 6,000 mm (236 in). It was cycled from 126 to 283 kN (28.3 to 63.6 kips), representing 15% to 35% of its static ultimate capacity. The corresponding stress range in the rebars was 131 N/mm^2 (19.0 ksi). Crack development was noted after 2 million cycles. After 10.7 million cycles at room temperature, the test temperature was increased to 40°C (104°F) and the relative humidity to 95%. The first failure in the rebars occurred at 12 million cycles. After 14.09 million cycles the second bar failed and the CFRP strip sheared from the concrete surface.

A third fatigue test similar to that described above was conducted at EMPA with pretensioned strips, and 30 million load cycles were performed without any damage [40].

Fatigue tests by Shijie and Ruixian [46] showed that the fatigue lives of Glass FRP plated members could be up to three times longer than the lives of unstrengthened RC control specimen. Both the post-cyclic static strength and stiffness diminished with increasing number of cycles, but by a smaller magnitude than for the unstrengthened beam.

As part of the *ROBUST* project (st*R*engthening *O*f *B*ridges *U*sing polymeric compo*S*ite ma*T*erials) in England, Barnes and Mays [6] investigated the fatigue performance of RC beams strengthened using CFRP plates for design applications. A RC beam 2,300 mm (60.6 in) long, 130 mm (5.1 in) wide, and 230 mm (9.1 in) depth was selected for the study. Five specimens were tested, two unplated control beams, and three plated beams. The strengthening plates consisted of 68% volume fraction high-strength unidirectional carbon fibers (*Toray T300*) embedded in a vinylester resin, and bonded using a two-part cold-curing epoxy adhesive (*Sikadur 31 PBA*). Each specimen was subjected to two-point loading at a frequency of 1 Hz. Three loading options were tested: (1) apply the same load to both the plated and unplated beams, (2) apply loads to give the same stress range in the rebars in both the beams, and (3) apply the same percentage of ultimate static capacity to each specimen. S-N curves are displayed for the test results and compared with research carried out by Moss 1982 [41], Leeming 1989 [31], Mallet 1991 [33], and Meier *et al.* 1993 [37] for both plated and unplated beams. Even though the plated beams demonstrated a better stress endurance performance, the authors concluded that a criterion for design guidance would be to expect the same fatigue life for plated and unplated beams, with comparable values of stress range in the reinforcing steel.

Shahawy and Beitelman [45] performed fatigue tests on severely cracked RC beams post-strengthened using different arrangements of CFRP biaxial fabrics applied on the bottom face or fully wrapped on the stem. The objective of the test was to study the effect of strengthening on extension of fatigue life of severely

damaged members. They tested six beams with a T-shaped cross-section that was 584 mm (23.0 in) wide, 445 mm (17.5 in) high, with a 5,790 mm (228 in) span. They were loaded at two points. The load represented 25% to 50% of the ultimate capacity, the stress range in the rebars being about 103.4 MPa (15 ksi), or 0.25fy (Grade 60). At this level, the authors expected the steel to have a fatigue life of approximately 1 million cycles. The unstrengthened control specimen failed after 295,000 cycles. One unstrengthened specimen was previously subjected to fatigue loading for 150,000 cycles and then strengthened using 2 layers of CFRP biaxial fabric bonded on the full stem of the beam. This specimen failed after 2 million cycles following rupture of the fabric, after fatigue failure of the steel. After strengthening, the specimen demonstrated a slight increase of stiffness up to just before failure. Specimens wrapped with three layers of fabric survived up to 3 million cycles. The author concluded that the fatigue life of strengthened specimens was prolonged and that severely damaged members could be effectively rehabilitate using externally bonded CFRP materials.

An extensive review of research carried out in North America, Europe, and Japan, including both short-span and long-span beams, can be found in [26].

2.4 Summary

The literature review given in this chapter aims to present the behavior of RC members strengthened using CFRP material under both static and repeated loading conditions.

After a description of the Fiber Reinforced Polymer composite materials, the static and fatigue properties of the reinforced concrete and the composite materials have been reviewed. Fatigue failure in RC members is governed mainly by fracture

of the reinforcing bars when subjected repeatedly to stresses about to the fatigue limit of steel. Therefore, the stress range in the reinforcing bars is proposed as a criterion for design of RC members subjected to repeated loading. On the other hand, unidirectional carbon fiber-epoxy composites used for structural strengthening exhibit outstanding fatigue properties in addition to high strength/weight ratio and corrosion resistance.

The improvement of flexural static strength and stiffness brought by externally bonded CFRP materials has been demonstrated and the different failure modes exposed in detail. Several researches have confirmed that classical RC theory can be applied safely when using FRP composites to strengthened RC members in flexure. A design guideline in accordance with the flexural RC theory is thus proposed in Chapter 3 in order to asset the overall static behavior of rectangular beams strengthened using FRP laminates and predict the load-deflection and moment curvature responses.

Under fatigue loading, RC beams strengthened using CFRP laminates exhibit better stress-endurance performance than classical RC beams. However, fatigue failure of strengthened beams appears to be determined by fatigue fracture of the reinforcing bars. Consequently, for fatigue design, the stress range in existing steel should not exceed the limits stated for RC when the beam is strengthened using FRP materials. However, no conclusion has been found on the influence of a repeated sequence of loading neither on the ultimate static strength, on the post-cyclic static stiffness nor on the ultimate capacity of deformation of the strengthened member when using Carbon FRP materials.

Chapter 3 Flexural capacity of RC beams strengthened using FRP materials

3.1 Objective

The main purpose of this Chapter is to assess the overall response of rectangular RC beams strengthened using FRP materials by identifying three critical points on the moment-curvature curve, namely, the cracking moment, the yield moment, and the ultimate moment. The methodology proposed uses simplifying assumptions in order to lead to quick hand computations. However, this methodology is not a complete design guideline, and numerous other verifications should be done for design purpose.

3.2 Assumptions and design philosophy

As discussed in Section 2.3.1, the strain compatibility method can be used in the analysis of RC beams strengthened using externally bonded FRP materials. Thus, the basic assumptions used in flexural analysis of reinforced concrete sections can be applied:

1. Sections perpendicular to the axis of bending that are plane before bending remain plane after bending (Bernoulli assumption).

2. Strain in the reinforcement is equal to the strain in the concrete at the same level (perfect bond assumption).

3. Stresses in concrete and reinforcing steel can be computed from the strains using the corresponding stress-strain curves for each material.

4. Resistance of concrete in tension can be neglected after yielding of the steel reinforcement.

A conventional RC member is normally designed such that failure occurs when concrete in the extreme compression fiber reaches its ultimate strain (ε_{Cu}) after yielding of the internal reinforcement. Impending collapse is noticeable in advance by the presence of cracks in concrete and excessive deformations.

Ultimate strength of a RC element strengthened with FRP materials cannot be computed in the same manner because of the linear-elastic behavior of the composite materials up to failure. Thus, the flexural capacity is reached when failure of the external FRP reinforcement occurs following yielding of the internal steel but before concrete crushing occurs in the compressive zone, ensuring a ductile mode of failure. This implies that RC members with a reinforcement ratio close to the balanced reinforcement ratio should not be considered for strengthening.

Moreover, it is recommended that yielding of the reinforcing bars should not occur before reaching the permitted design load. As a consequence, reinforcement of a structure should not exceed 50% of its original capacity. Thus, if an accidental failure of the strengthening system occurs, a residual global safety factor of approximately 1.2 would remain, avoiding the collapse of the structure (EMPA, [38]).

Additional assumptions have to be made for the FRP material and the concrete-composite interface:

5. Stress-strain curve of FRP composite material is linear to failure (Figure 2.6).

6. Perfect bond exists between the concrete and the FRP laminate.

This last assumption, made to simplify the complex non-linear behavior of the concrete-adhesive interface, is reasonable because research results shown that the no-slip composite action of the strengthened beam can be extended up to almost the theoretical ultimate load if anchorage of the FRP laminate is provided [48]. A complete analysis of this behavior and analytical models to predict the ultimate shear stress before debonding occurs can be found in References [30, 32].

In addition, bond length of the laminate, forces in the anchorage, shear stresses at the concrete-adhesive interface, and structural ductility should also all be checked. These verifications are part of the design process for strengthening of RC structures using composite materials but do not constitute the main goal of this Chapter and therefore would not be discussed herein.

A typical moment-curvature curve presented in Figure 3.1 shows the three steps required for the practical calculation of RC members externally reinforced using FRP materials. The cracking moment, yield moment, and ultimate bending moment capacity computations are developed for rectangular RC beams in Section 3.2.

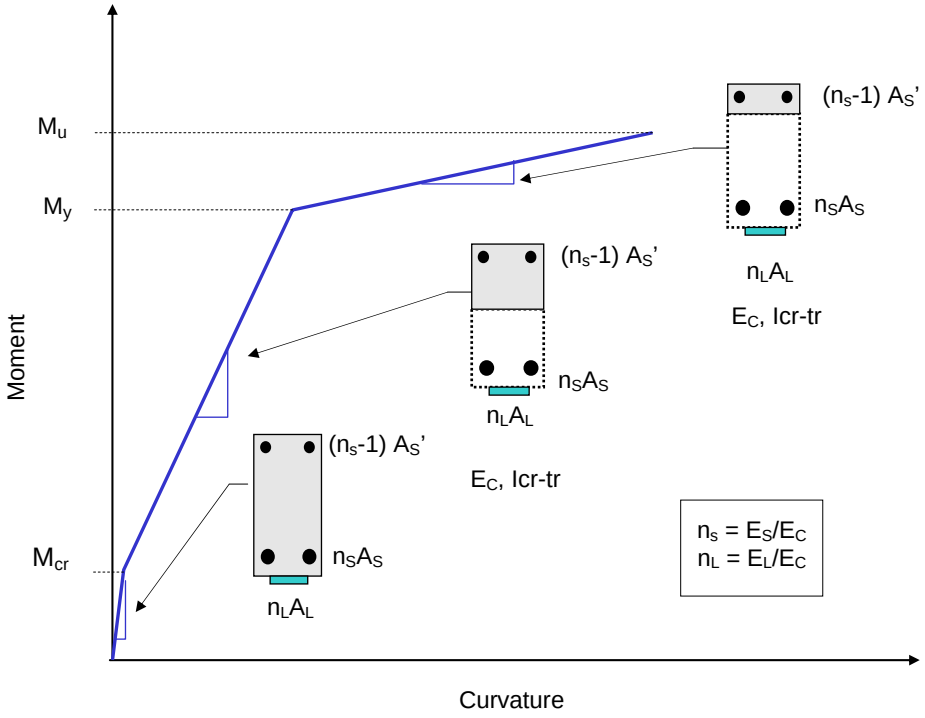

Figure 3.1: Typical moment-curvature curve for RC beam strengthened using externally bonded FRP materials with a shear span/depth ratio of 3.0.

3.3 Flexural capacity of RC beams strengthened using FRP materials

The methodology presented in this section is based on preventing undesirable failure modes such as crushing of concrete prior to FRP rupture or debonding. This philosophy is consistent with the current design for RC.

3.3.1 Preliminary design

The first step in the design process is to estimate the maximum thickness of the FRP laminate t_{Lmax} that can be used for a given width b_L (Figure 3.2.a). The quick approach for preliminary design proposed herein considers a failure mode

where the laminate fails at the same time that concrete reaches its maximum strain at the top fiber. For that ultimate state, all the parameters are known but the thickness of the laminate, which can thus be determined easily. The maximum thickness (t_{Lmax}) obtained in this way would trigger a brittle mode of failure and therefore should not be considered for design. Taking for instance 80% of t_{Lmax} allows a convenient determination of the ultimate bending moment as described in Section 3.2.2.

Figure 3.2 shows the strains, stresses, and internal forces for a rectangular cross-section.

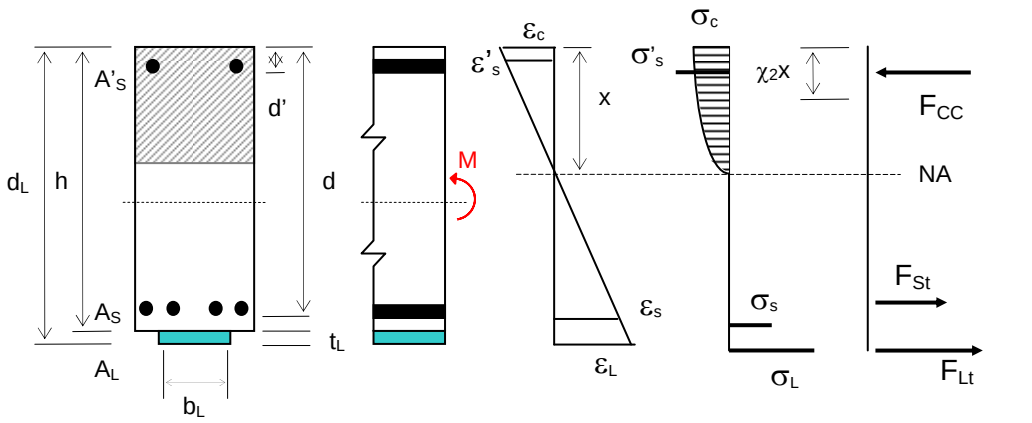

Figure 3.2: Cross-section, free body, strains, stresses, and internal forces diagrams, assuming a parabolic distribution of stresses in concrete.

At the ultimate state the stress block coefficient χ_2, defining the position of the compressive force, is equal to 0.8[1]. The condition of compatibility allows the direct computation of the neutral axis position, x:

$$x = \frac{\varepsilon_{Cu}}{\varepsilon_{Cu} + \varepsilon_{Lu}} d_L \qquad (3.1)$$

The equilibrium conditions are expressed as follows:

$$\Sigma F = 0 \quad \Leftrightarrow \quad F_{St} + F_{Lt} - F_{Cc} = 0 \qquad (3.2)$$

$$\Leftrightarrow \quad A_S f_y + A_L f_{Lu} - 0.8 x b f_C = 0 \qquad (3.3)$$

Thus, a first estimation of the maximum thickness $t_{L,\max}$ can be calculated by:

$$t_{L,\max} = \frac{A_L}{b_L} = \frac{0.8 x b f_C - A_S f_y}{f_{Lu} b_L} \qquad (3.4)$$

Finally, the design thickness can be estimated by:

$$t_L \cong 0.8 \times t_{L,\max} \qquad (3.5)$$

Note: Inversely, for a pultruded plate, the design thickness is generally given and the width of the plate is to be found in a similar way using Equation (3.4).

[1] The stress bloc coefficient χ_1 is equal to 0.8 according to the Swiss Codes [44], and to 0.85 according to the American Codes [13].

3.3.2 Ultimate flexural capacity

The design method presented below can be considered as part of the current state of practice for design of RC members strengthened using FRP composites (Kaiser 1989 [30], Berset 1995 [10]).

Figure 3.2 shows the strains, stresses, and internal forces for a rectangular cross-section. The equilibrium conditions can be expressed as follows:

$$\Sigma F = 0 \Leftrightarrow F_{St} + F_{Lt} - F_{Cc} = 0 \qquad (3.2)$$

and

$$\Sigma M = 0 \Leftrightarrow F_{St}\left(d - \chi_2 x\right) + F_{Lt}\left(d_L - \chi_2 x\right) - M = 0 \qquad (3.6)$$

On the basis of strain compatibility, the strains in the different materials are given by:

$$\varepsilon_C = \frac{\varepsilon_L}{d_L - x} x + \varepsilon_{C0} \qquad (3.7)$$

$$\varepsilon_S = \frac{\varepsilon_L}{d_L - x}\left(d - x\right) + \varepsilon_{S0} \qquad (3.8)$$

where ε_{C0} and ε_{S0} are initial strains respectively in the concrete and steel, related to the initial state of the beam before strengthening.

The compressive force in concrete can be computed using the stress block coefficient χ_1 defining the maximum compressive stress in the concrete:

$$F_{Cc} = \chi_1 b x f'_C \qquad (3.9)$$

Depending on the maximum strain in the concrete ε_C, the rectangular stress block coefficients χ_1 and χ_2, defining respectively the maximum compressive stress in the concrete and the position of the compressive force, are derived as follow [30]:

- If $0.002 \le \varepsilon_C \le 0.0035$

$$\chi_1 = \frac{3000\varepsilon_C - 2}{3000\varepsilon_C} \tag{3.10}$$

$$\chi_2 = \frac{1000\varepsilon_C(3000\varepsilon_C - 4) + 2}{2000\varepsilon_C(3000\varepsilon_C - 2)} \tag{3.11}$$

- If $\varepsilon_C \le 0.002$

$$\chi_1 = \frac{1000\varepsilon_C(6 - 1000\varepsilon_C)}{12} \tag{3.12}$$

$$\chi_2 = \frac{8 - 1000\varepsilon_C}{4(6 - 1000\varepsilon_C)} \tag{3.13}$$

Strains along a cracked element can vary considerably as illustrated in Figure 3.3. However, the strain distributions are computed on the basis of average deformation, while the FRP laminate and the reinforcing steel forces for equilibrium conditions correspond to the maximum strains. The ratios of average to maximum strains are described by the composite factors $\kappa_L (<1)$ for the laminate and $\kappa_S (\le 1)$ for the steel:

$$\varepsilon_{Lm} = \kappa_L \varepsilon_{L\max} \tag{3.14}$$

$$\varepsilon_{Sm} = \kappa_S \varepsilon_{S\max} \tag{3.15}$$

The coefficients κ_L and κ_S can be estimated by [30]:

$$\kappa_L = 0.65 \quad to \quad 0.8, \quad for \quad \sigma_{L\max} = \sigma_{Lu}$$

$$\kappa_S = 0.90 \quad to \quad 1.0, \quad for \quad \sigma_{S\max} \geq f_y$$

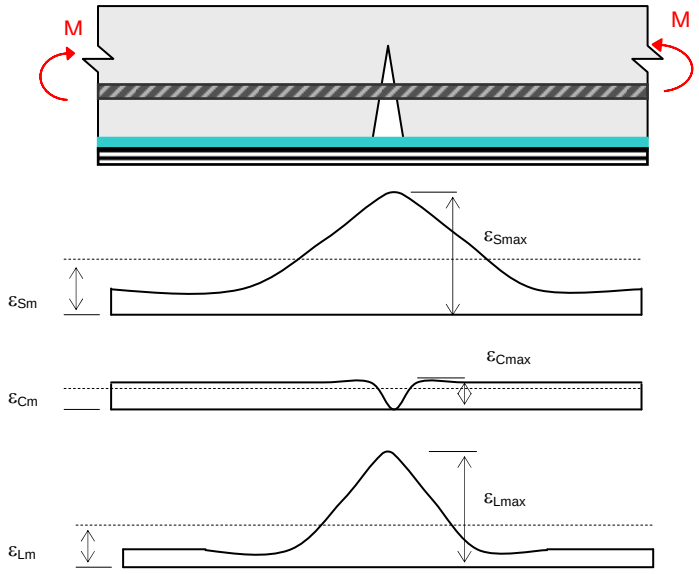

Figure 3.3: Strains along a cracked element.

Source: Berset [10].

At the ultimate state, introducing Equation (3.14) in Equation (3.7), the strain in the concrete can be expressed by:

$$\varepsilon_C = \frac{\kappa_L \varepsilon_{Lu}}{d_L - x} x + \varepsilon_{C0} \qquad (3.16)$$

Thus equation *(3.2)* can be written as:

$$A_S f_{yS} + A_L f_{Lu} - \chi_1 b x f_C = 0 \qquad (3.17)$$

The position of the neutral axis x is deduced using the following iterative process:

i. Estimate value of x

ii. Compute ε_C using equation *(3.16)*

iii. Introduce ε_C in equation *(3.10)* or *(3.12)* to compute χ_1

iv. Substitute $\chi_1$in equation *(3.17)* and compute a new value for x

v. Repeat steps (i) to (iv) until x converges.

Finally, the ultimate moment M_u is obtained by solving equation *(3.6)* that yielding the following:

$$M_u = A_S f_{yS}(d - \chi_2 x) + A_L f_{Lu}(d_L - \chi_2 x) \qquad (3.18)$$

At this stage, the following parameters must be checked:

$$\varepsilon_C < \varepsilon_{Cu} = 0.0035$$

$$\varepsilon_{L\max} = \varepsilon_{Lu}$$

$$\varepsilon_{Sy} \le \varepsilon_{S\max} = \frac{\varepsilon_S}{\kappa_S} \le \varepsilon_{Su}$$

If the ultimate bending moment obtained does not correspond to the desired strength, or if strain limits are not fulfilled, then the design thickness has to be adjusted. A numerical example is presented in Appendix B based on the test specimens.

Once the dimensions of the laminate cross-section have been determined, analysis of the static behavior requires the computation of the cracking moment, the yield moment and the corresponding deformations of the member.

3.3.3 Cracking moment

The cracking moment corresponds to the appearance of the first crack and can be computed using the transformed section of concrete defined by the appropriate modular ratios:

$$n_S = \frac{E_S}{E_C} \qquad and \qquad n_L = \frac{E_L}{E_C} \tag{3.19}$$

The stress repartition in concrete is assumed to vary linearly with depth (Figure 3.4). The position of the centroid of the uncracked transformed section is expressed as follow:

$$n_S A_S (\mathrm{x} - d) + n_L A_L (\mathrm{x} - d_L) - bh\left(\mathrm{x} - \frac{h}{2}\right) + (n_s - 1)A_s'(\mathrm{x} - d') = 0 \tag{3.20}$$

The equation is to solved for the position of the neutral axis, x:

$$\mathrm{x} = \frac{b\frac{h^2}{2} + (n_s - 1)A_s' d' + n_S A_S d + n_L A_L d_L}{bh + n_S A_S + (n_s - 1)A_s' + n_L A_L} \tag{3.21}$$

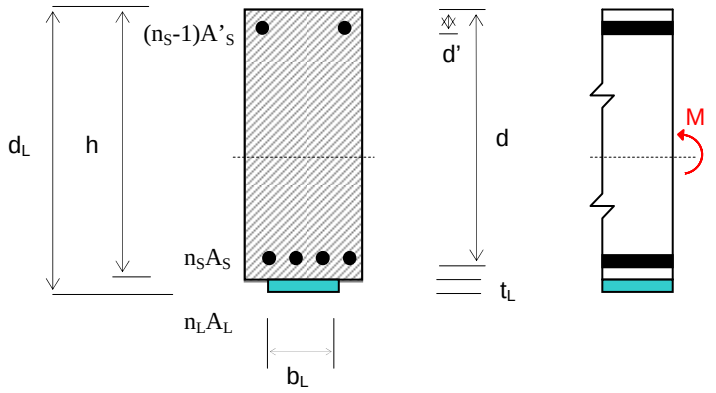

Figure 3.4: Cross-section and free body diagram of the uncracked transformed section.

The moment of inertia for the transformed uncracked section I_{tr}, is thus expressed by:

$$I_{tr} = bh\left(\frac{h}{2} - \mathrm{x}\right)^2 + n_S A_S (d - \mathrm{x})^2 + (n_s - 1)A_s'(\mathrm{x} - d')^2 + n_L A_L (d_L - \mathrm{x})^2 \qquad (3.22)$$

Note: the presence of the CFRP laminate at the bottom face has little influence on the moment of inertia of the uncracked section.

The cracking moment is reached when the stress at the bottom face attain the tensile limit of the concrete and is deduced using:

$$M_{cr} = \frac{f_{Ct} I_{cr}}{h - \mathrm{x}} \qquad (3.23)$$

3.3.4 Yield moment

The yield moment is attained when the internal reinforcement reaches its yield stress. The computation of the yield moment requires the description of the static and kinematic conditions, as well as the material laws (Figure 3.5). The contribution of the compression steel is neglected.

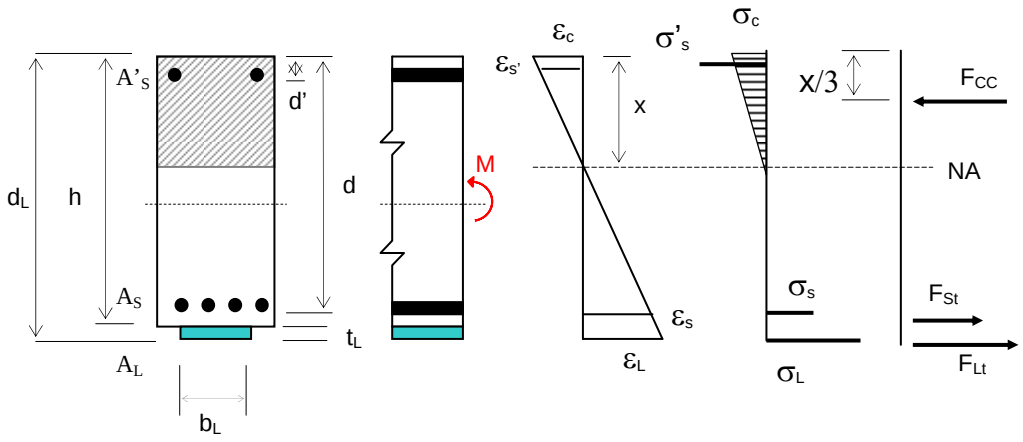

(a) Cross-section (b) Free body (c) Strains (d) Stresses (e) Internal forces

Figure 3.5: Cross-section, free body, strains, stresses, and internal forces diagrams, assuming a linear distribution of stresses in concrete.

The static condition is expressed by the equilibrium of the internal forces:

$$\Sigma F = 0 \Leftrightarrow F_{St} + F_{Lt} - F_{Cc} = 0 \qquad (3.2)$$

The kinematic condition is given by the strain compatibility:

$$\varepsilon_y = 0.02 \qquad (3.24)$$

$$\varepsilon_C = \frac{x}{d-x}\varepsilon_y + \varepsilon_{C0} \qquad (3.25)$$

$$\varepsilon'_S = \frac{(x-d')}{d-x}\varepsilon_y + \varepsilon'_{S0} \qquad (3.26)$$

$$\varepsilon_L = \frac{(d_L - x)}{d - x}\varepsilon_y \qquad (3.27)$$

Because the strains in concrete are rather low at yield, it can be assumed that the stresses in concrete vary linearly with depth. Thus, the stresses in materials are described as:

$$\sigma_C = E_C \varepsilon_C \qquad (3.28)$$

$$\sigma_L = E_L \varepsilon_L \qquad (3.29)$$

$$\sigma_S = f_y \qquad (3.30)$$

Using the Equations (3.2) and (3.28) to (3.30), the equilibrium can be expressed as follows:

$$E_C \frac{1}{2} \mathrm{x} b \varepsilon_C - A_S f_y - E_L A_L \varepsilon_L = 0 \qquad (3.31)$$

Introducing the condition (3.21) to (3.24), and after rearrangement:

$$\left[\frac{E_C b}{2}\right]\mathrm{x}^2 + \left[E_S A_S + E_L A_L\right]\mathrm{x} - \left[E_S A_S d + E_L A_L d_L\right] = 0 \qquad (3.32)$$

Defining:

$$\mathrm{x} = \zeta d\ ,\ \rho = \frac{A_S}{bd}\ ,\ \rho_L = \frac{A_L}{bd}\ ,\ n_S = \frac{E_S}{E_C}\text{, and } n_L = \frac{E_L}{E_C}$$

The equation can be expressed in function of ζ:

$$\frac{d}{2}\zeta^2 + \left[\left(n_S \rho_S + n_L \rho_L\right)d\right]\zeta - \left[n_S \rho_S d + n_L \rho_L h\right] = 0 \qquad (3.33)$$

Solving for ζ provides the position of the neutral axis, x.

The strain in the composite laminate is deduced using Equation (3.27). Finally, the yield moment is obtained using the following:

$$M_u = A_S f_{yS}\left(d - \frac{x}{3}\right) + A_L E_L \varepsilon_L \left(d_L - \frac{x}{3}\right) \qquad (3.34)$$

Chapter 4 Description of test program

The primary aim of the experimental study presented in this section is to investigate the influence of repeated loading on the serviceability and ultimate load behavior of RC beams strengthened using different types of CFRP sheets and plates under realistic loading conditions. The objectives and scope of the research are presented in Section 1.3.

4.1 Material properties

4.1.1 Concrete

All beams were fabricated using concrete with a nominal compressive strength equal to 5,000 psi (34.5 MPa). Slump of the concrete measured before placement was 3¾ in. (95 mm). Specimens were kept in the forms and covered with wet burlap and plastic sheets for 7 days to avoid shrinkage cracks.

Tests of standard concrete cylinders 12 in. long, 6 in. diameter (305 mm long, 153 mm diameter) were performed 3, 7, 21, 28, and 70 days after casting. Figure 4.1 shows the increase in compression strength with time. The measured compression strength of the concrete was 5,500 psi (38 MPa) at 28 days, and 5,667 psi (39 MPa) at 70 days.

The stress-strain response of concrete and the effective compression strength f_C' were determined after 70 days. Figure 4.2 shows the measured and theoretical stress-strain curves used to compute internal forces in the beam specimens. The peak and ultimate stresses were available only for one cylinder,

for which the maximum compressive strength reached 5,913 psi (40.8 MPa). The equation for the idealized stress-strain curve is given by Todeschini *et al.*[54], and was proposed originally by Hognestad:

$$\sigma_C = 0.94\, f_C' \left[\frac{2\varepsilon_C}{\varepsilon_0} - \left(\frac{\varepsilon_C}{\varepsilon_0} \right)^2 \right] \text{ for } \varepsilon_C \le \varepsilon_{Cu} = 0.0035 \qquad (4.1)$$

Note: the equation was adjusted with a coefficient 0.94 instead of 0.90 originally proposed by Todeschini *et al*. to match the test results.

In order to fully represent the behavior of the concrete during testing, a linear portion was added to take into account the resistance of concrete in tension:

$$\varepsilon_{Ct} = -0.000094\,, \quad f_{Ct} = -3.4\, psi \qquad (4.2)$$

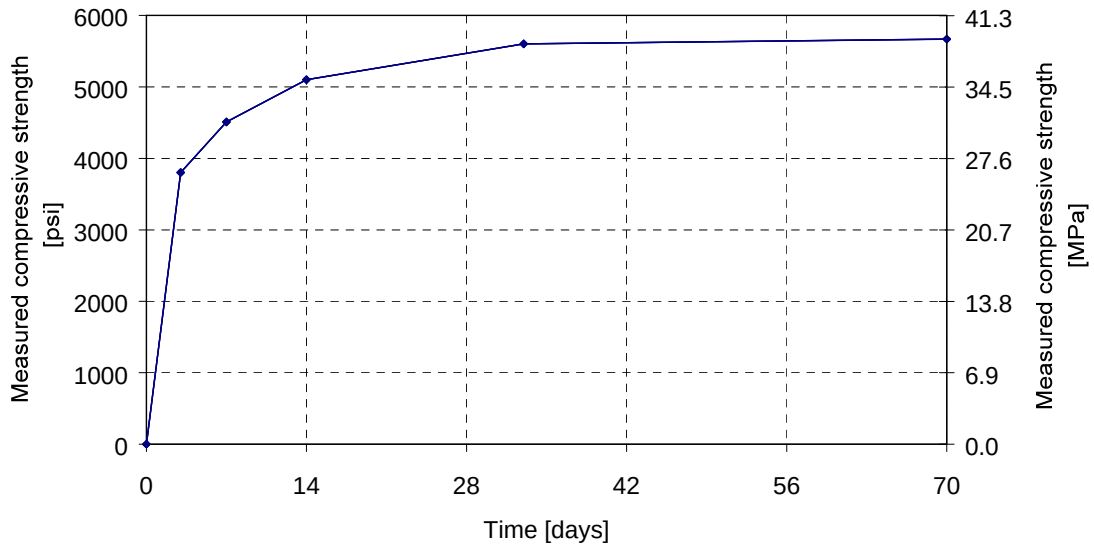

Figure 4.1 Evolution of concrete compressive strength. Each point was obtained by averaging the data from three cylinders.

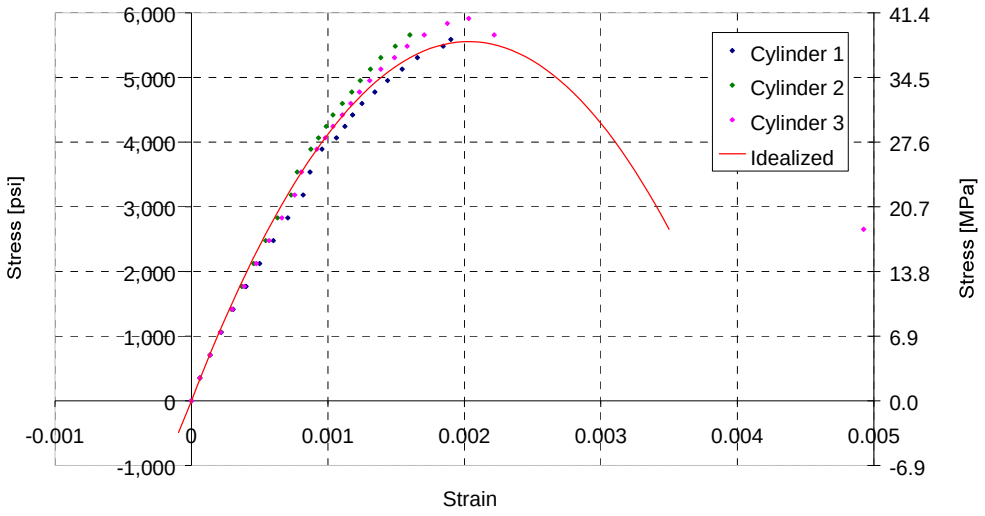

Figure 4.2: Concrete compressive strength at 70 days. The idealized curve corresponds to the Equation 4.1.

4.1.2 Internal steel reinforcement

Reinforcement consisted of 2#5 (2 x 0.31 sq.in., 2 x 200 mm^2) bars as main tension reinforcement and 2#3 (2 x 0.11 sq.in., 2 x 71 mm^2) bars in the compression zone. The reinforcing bars were tested in tension, and the resulting properties are listed in Table 4.1. Figure 4.3 shows the stress-strain curve for the #5 Grade 60 steel bars and the corresponding tri-linear idealized curve used in the computations. The idealized curve was discribed using the following equations:

1. $\sigma_S = E_S \varepsilon_S$ for $\varepsilon_S \le \varepsilon_{Sy} = 0.00217$ *(4.3)*

2. $\sigma_S = f_y$ for $\varepsilon_{Sy} \le \varepsilon_S \le \varepsilon_{Sh} = 0.00723$ *(4.4)*

3. $\sigma_S = f_y + E_{Sh}\left(\varepsilon_S - \varepsilon_{Sh}\right)$ for $\varepsilon_{Sh} \le \varepsilon_S \le \varepsilon_{Su} = 0.035$ *(4.5)*

Shear reinforcement was provided along the shear span using #2 (2×0.049 sq.in., 32 mm^2) stirrups to avoid shear failure. All reinforcing bars were tied together rather than welded to avoid premature fracture of the bars.

Table 4.1: Measured properties of tensile reinforcing bars (Grade 60).

STEEL PROPERTIES			
PROPERTIES	SYMBOL	IMPERIAL UNITS	SI UNITS
Modulus of elasticity	E_S	29,000 [ksi]	199,995 [MPa]
Strain hardening slope	E_{Sh}	1336 [ksi]	2,501 [MPa]
Yield stress	f_y	62 [ksi]	427 [MPa]
Yield strain	ε_{Sy}	0.00217 [-]	0.00217 [-]
Strain hardening strain	ε_{Sh}	0.00723 [-]	0.00723 [-]
Measured ultimate stress	$f_{Su,\ mes}$	105[ksi]	724 [MPa]
Assumed ultimate stress	f_{Su}	100[ksi]	689 [MPa]
Measured ultimate strain	$\varepsilon_{Su,mes}$	0.125 [-]	0.125 [-]
Assumed ultimate strain	ε_{Su}	0.035 [-]	0.035 [-]

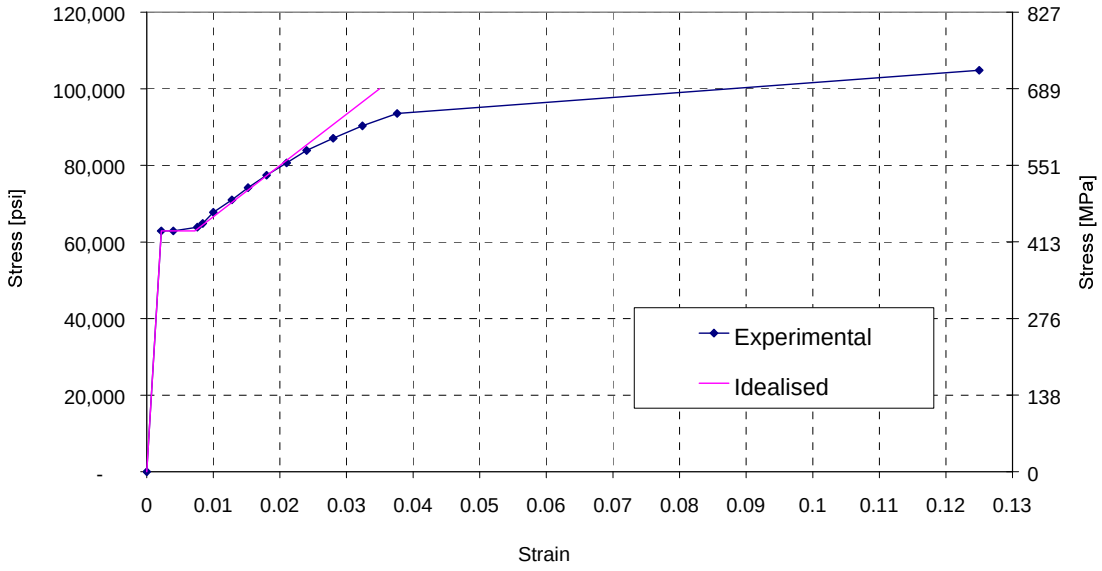

Figure 4.3: Stress-strain response of #5 Grade 60 reinforcing bars.

4.1.3 CFRP Materials

Two different systems were tested: a wet lay-up fiber composite system, distributed by Master Builders (*MB Brace FTS C-130*), and a pultruded composite plate system, manufactured by Sika Corporation (*Sika CarboDur S512*). Differences between these two systems were presented in Section 2.1.

The CFRP pultruded plates had a 68% volume fraction content of high strength carbon fibers embedded in an epoxy matrix. A wet lay-up fiber composite system provided the lateral anchorages for the Sika system (*SikaWrap Hex 103C*). The properties of the CFRP materials are listed in Table 4.2

Table 4.2: Properties of the CFRP materials published by suppliers [35, 47].

CARBON FIBER LAMINATES	DESIGN THICKNESS		TENSILE STRENGTH		TENSILE MODULUS		MAX TENSILE FORCE		ELONG. AT FAILURE
	[mil]	[mm]	[Ksi]	[Mpa]	[ksi]	[Gpa]	[kip/in.]	[kN/cm]	[%]
Sika CarboDur S512	47.2	1.20	348	2,400	22,500	155	16.4	28.8	1.9
SikaWrap Hex 103C+	40.0	1.02	139	958	10,600	73.1	5.56*	9.77*	1.3
MBrace FTS C1-30+	6.5	0.165	505	3,480	33,000	228	3.28*	5.74*	1.7

+ Design properties for cured laminate * Per ply 1 mil = 1/1000 inch

4.1.4 Adhesives

The adhesives used for both types of laminates were two-component cold-curing epoxies. For the wet lay-up system, the epoxy (*MBrace Saturant LTC*) is fluid and presents a blue or green color after mixing (about 3 minutes). It is used for both the sheet applied on the tensile face and the anchorages. Before application of the sheets, a primer, consisting of a fluid epoxy resin, is used to seal the concrete surface.

The epoxy used to bond the pultruded strips (*Sikadur 30*) is a viscous resin that acquires a uniform gray color after adequate mixing (about 5 minutes) of the two components. The epoxy used for the flexible sheets providing the anchorages (*Sikadur Hex 300/306*) is similar to the MB epoxy and is transparent.

Careful mixing is required to achieve the design strength of the adhesive. A seven-day curing period is necessary for the epoxy to develop its full strength. However, the epoxy is sensitive to temperature during the first 48 hours of curing (low temperature slows down the hardening process). Table 4.3 lists the properties of the epoxy provided by the manufacturers. The Sikadur 30 resin has

an elongation at failure (1%), which is less than the ultimate elongation of the CFRP plate material (1.9%). Therefore, the adhesive is a limitation of the pultruded plate system system.

Table 4.3: Properties of the epoxy resins published by suppliers [35, 47].

EPOXY ADHESIVES	TENSILE STRENGTH		TENSILE MODULUS		ELONG. AT FAILURE [%]	COMPRESSIVE STRENGTH		SHEAR STRENGTH	
	[ksi]	[Mpa]	[ksi]	[Gpa]		[ksi]	[Mpa]	[ksi]	[Mpa]
Sikadur 30	3.6	24.8	650	4.48	1.0	14.5	>100	3.55	24.8
Sikadur Hex 300/306	10.5	72.4	459	3.16	4.8	NA	NA	NA	NA
MBrace Saturant LTC	2.1	14.5	165	1.14	5.3	5.2	36	NA	NA

NA: non available

4.2 Specimen details

Six beams strengthened using externally bonded CFRP materials were subjected to fatigue loading. Two strengthened beams and two control-unstrengthened specimens were previously tested under static loading conditions.

4.2.1 Details of tested beams

Two beam sizes were selected for testing. The cross sections were 8 in. x 14 in. (203 x 356 mm^2) and 8 in. x 16 in. (203 x 406 mm^2), and the respective spans 114 in. (2900 mm) and 126 in. (3200 mm). Figures 4.4 and 4.5 show the dimensions, the internal reinforcement and the CFRP position for each

type of beam. The arrangement of CFRP materials used was dictated by previous static tests conducted by Breña and Bramblett [12, 11] at the Phil M. Ferguson Structural Engineering Laboratory at the University of Texas at Austin (see Section 4.4).

The wet lay-up composite system was used to strengthen the 8 in. x 14 in. beams (MB series). Two layers of 2 in. (51 mm)-wide carbon fibers were applied on the extreme tensile face for flexural strengthening, and one layer of transverse straps was applied to enhance anchorage. The calculated tensile strength in the laminate was 13.1 kips (58.3 kN).

The pultruded strips were used to strengthen the 8 in. x 16 in. beams (SK series). Two 2 in. (51 mm)-wide pultruded plates were applied on the sides of the beam. The calculated tensile strength in the laminate was 42.5 kips (189 kN). One layer of Sika flexible sheets was used for the transverse anchorage straps.

Two unstrengthened specimens (UN14 and UN16) were also tested as control beams for each of the beam sizes.

Figure 4.4: internal reinforcement

figure 4.5: CFRP arrangements

4.2.2 Bonding procedure

Strengthening of the beams was conducted according to the procedure described in Table 4.4. The complete bonding procedure for field applications can be found in [26], [35] and [47].

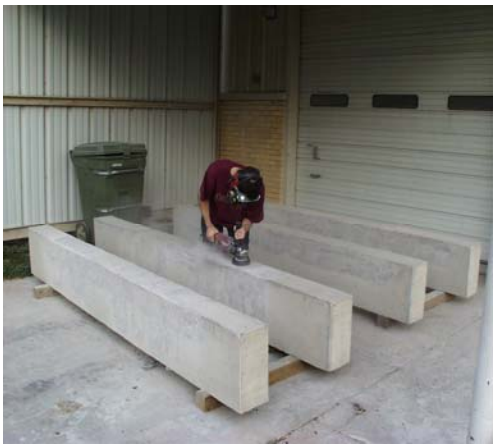

Figure 4.6.a: Beams are turned upside down to prepare the bonding surface.

Figure 4.6.b: Grinding of the concrete surface.

Figure 4.6: Surface preparation.

Table 4.4: Bonding procedure for CFRP flexible sheets and pultruded plates.

STEP	DESCRIPTION OF PROCEDURE	
	WET LAY-UP SYSTEM	PULTRUDED PLATE SYSTEM
1	Mark the intended locations of the CFRP laminates on the beam	
2	Grind the corresponding area to remove surface laitance, expose aggregates, and provide a smooth and uniform surface (Fig. 4.6.a and b)	
3	Blow away dust and particles using air hose	
4	Fill holes in concrete with epoxy mortar at CFRP location, and apply primer to seal surface	Fill holes in concrete with epoxy mortar at anchorage locations only (flexible sheets)
5	Cut carbon fibers (Fig. 4.8.a)	Cut carbon fibers for anchorages and saw pultruded plates (Fig. 4.8.a)
6	Carefully clean concrete surface with acetone to remove dust and grease	Carefully clean concrete surface and the CFRP plates with acetone to remove dust and grease (Fig. 4.8.b)
7	Mix the two components of the epoxy for 3 minutes	Mix the two components of the epoxy for 5 minutes
8	Apply mixed epoxy using a paint brush (Fig. 4.7.a)	Apply 1 mm (40 mil) of adhesive resin to plate using a spatula
9	Place CFRP sheet proceeding from one end of the beam to the other and apply slight pressure with a roller to impregnate fibers with epoxy (Fig. 4.7.b and c)	Place tape to limit the surface application of the adhesive and apply 1 mm (40 mil) of resin to concrete surface using a spatula (Fig. 4.8.c)
10	Let epoxy saturate fibers for 30 min and apply second coat of epoxy to complete saturation	Place plate on one end of beam and work along beam applying slight pressure (Fig. 4.8.d)
11	Repeat steps 8 through 9 for the second layer of carbon fibers	Increase hand pressure to squeeze out excess resin
12	Apply cover layer of epoxy on top of saturated fibers	Remove excess resin
13	Repeat steps 8 through 9, and 12 for lateral anchorages (Fig. 4.7.d)	Repeat steps 7 through 9, and 12 of the wet lay-up system for lateral anchorages (Fig. 4.8.e and f)
14	Allow 48 hours to cure at room temperature before removing specimens	
15	Allow 7 days for complete curing	

Figure 4.7.a: Apply epoxy resin.

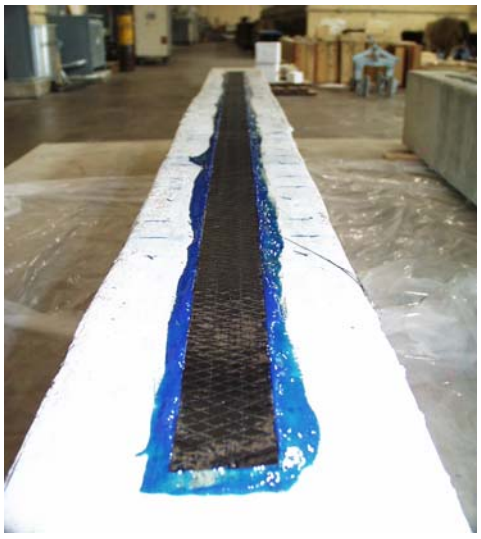

Figure 4.7.b: Apply CFRP unidirectional flexible sheet.

Figure 4.7.c: Apply slight pressure to impregnate the fibers.

Figure 4.7.d: Lateral anchorages.

Figure 4.7: Bonding procedure for the wet lay-up system.

Figure 4.8.a: Cut CFRP flexible sheets.

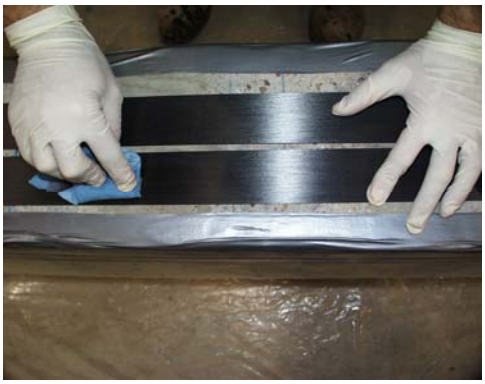

Figure 4.8.b: Clean CFRP pultruded plates.

Figure 4.8.c: Apply epoxy resin.

Figure 4.8.d: Place pultruded plate.

Figure 4.8.e: Apply epoxy resin for lateral anchorages.

Figure 4.8.f: Apply CFRP flexible sheets for lateral anchorages.

Figure 4.8: Bonding procedure for the pultruded plate system

4.3 Test setup and instrumentation

All specimens were simply supported using elastomeric bearing pads and were subjected to two-point loading as shown in Figures 4.9 and 4.10. The resulting shear span/depth ratio was 3.0.

Application of the repeated load was achieved by means of a closed-loop system programmed to deliver a sinusoidal load at a frequency of 2 Hz. The load span, load set point, frequency, and preset number of cycles were controlled by an electronic controller (MTS® 407 Controller). The sinusoidal waveform was checked using a conventional oscilloscope. Load was monitored using a fatigue-resistant load cell.

Deflections were measured at the supports, load points, and midspan using linear potentiometers (Figures 4.12.c and d). Two cross-sections, noted A-A and B-B in Figure 4.4, were instrumented using electrical-resistance strain gages. The locations of the strain gages are shown in Figure 4.11. Strains were monitored on the tension reinforcing bars (Figure 4.12.a), on the CFRP laminate(s), and on the concrete surface on both sides of each specimen at 1.5 in. (38.1 mm) from the extreme top fiber. Section A-A included a crack initiator (Figure 4.12.b) in order to measure the maximum strain in the reinforcing bars. In addition, acoustic emission sensors were used to monitor progressive damage in the composite materials and in the concrete. The results of this particular study are forthcoming in [5]. The cumulative energy of acoustic emission will be analyzed to relate damage in the concrete and composite materials with the load level, number of cycles, and visual crack patterns.

Figure 4.9: Test set-up, beam strengthened with the wet lay-up system.

Figure 4.10: Test set-up

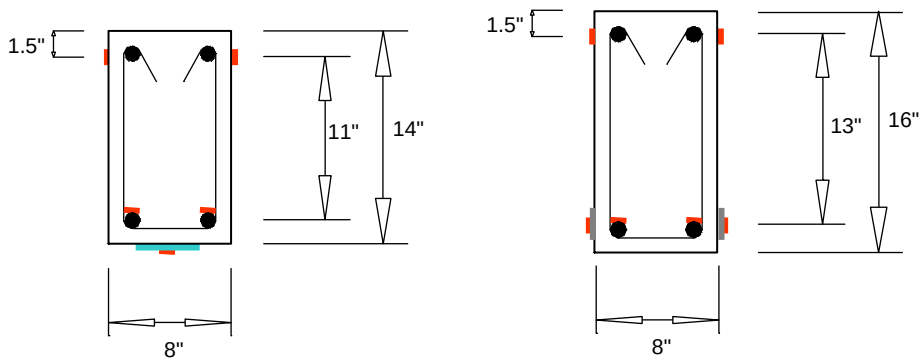

Figure 4.11: Electric-resistance strain gage locations

in the cross-sections A-A and B-B (see Figure 4.4).

Figure 4.12.a: Electric strain gages on #5 reinforcing bars.

Figure 4.12.b: Steel cages in the form. Strain gage protection and crack initiator.

Figure 4.12: Detail of the instrumentation.

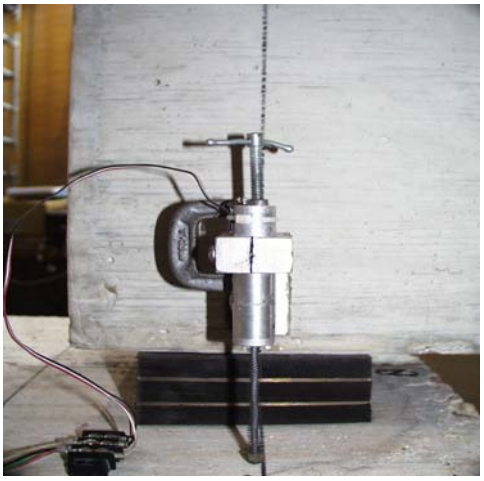

Figure 4.12.c: Linear potentiometer at support to measure deformation of elastomeric bearing pad.

Figure 4.12.d: Linear potentiometer at the bottom face of the beam and acoustic emission sensor.

Figure 4.12: Details of the instrumentation.

4.4 Previous static loading tests

The purpose of the static test program was to determine particular arrangements of carbon fiber laminates to provide the required level of flexural strength increase. The parametric study carried out at the Phil M. Ferguson Structural Engineering Laboratory at the University of Texas at Austin by Breña and Bramblett [12, 11] included the type of FRP materials, position of the FRP laminates, bond length, and influence of anchorages.

Three different types of Carbon FRP systems readily available in the construction industry were tested. Two wet lay-up systems, commercialized respectively by Master Builders and Mitshubishi, and a pultruded plate system, manufactured by Sika.

Two types of beams (8 in. x 14 in. and 8 in. x 16 in., or 203 x 356 mm^2 and 203 x 406 mm^2) were selected in order to adapt the specimens to the respective strength of each strengthening system.

The first objective was to investigate the behavior of the bond interface when CFRP laminates are placed on the tensile face of the beam. Therefore, all laminates were 2 in. (51 mm) wide, so the same shear strength was achieved for all cases. The increase in ultimate capacity was not relevant in this stage.

In the first series, the bond length was progressively increased until the optimal length was determined. The observed failure mode was premature debonding of the laminate, well before the ultimate elongation of the CFRP material could be reached.

In order to avoid, or at least delay debonding, the specimens were partially wrapped with CFRP flexible straps to enhance anchorage (Figure 4.7.d, and Figures 4.8.e and f). A significant increase in the flexural capacity was thus achieved and strains in the main laminate were close to ultimate. Rupture of the carbon fibers was achieved for the wet lay-up system.

On the other hand, pultruded plates placed on the bottom face of the beam appeared to be sensitive to the relative displacements of crack edges due to shear-flexure interaction (Figure 2.13, detail 5.a), leading to early peeling-off of the plate. The plates were thus applied on the side of the beams where this phenomenon has less influence. The ultimate strength was considerably enhanced, even more so in the presence of transverse anchorage straps.

The two CFRP schemes selected for the fatigue tests were those that performed the best under static loading conditions. The same details were also tested on the full-scale specimens. The complete description and analysis of the static tests are forthcoming in References [11] and [12].

4.5 Repeated loading tests

4.5.1 Number of cycles and frequency

As described in Section 2.2.2, fatigue fracture of reinforcing bars is assumed to govern the behavior of RC members strengthened using externally bonded CFRP materials under repeated loading. Therefore, the number of fatigue cycles was determined using the SN curve presented on Figure 2.10 appropriate for RC design. The resulting number of cycles for each specimen, with the exception of the last specimen, was chosen to avoid fatigue fracture in the rebars. The maximum number of cycles was chosen to be 1 million for two reasons. First, the fatigue strength of RC is often defined for 1 million cycles. Moreover, within the constraints of the experimental program, it was not possible to subject each beam to more than 1 million cycles.

The test frequency was fixed at 2 Hz for all tests, with the exception of the last fatigue test, which was carried out at ½ Hz, because of the capacity limitations of the closed-loop system. These frequency levels allowed the members to fully recover their initial position after each application of load.

4.5.2 Load determination

The maximum load applied to the rectangular specimens during fatigue loading was determined based on field loading conditions on the pan-joist bridge (Section 1.2). The flowchart (Figure 4.13) presents the approach used to compute the load. First, strains in the strengthened bridge under live load were computed for the CFPR material. The maximum load applied on the test specimens was computed to provide the very same strains in the composite material. The minimum stress in the CFRP laminate corresponds with the

unloaded state of the bridge, and so is close to zero (no consideration has been given to long-term effects in the laminate).

Stress levels obtained in the reinforcing bars and CFRP materials correspond to live loads on the actual bridge. The specimens can thus be considered representative of field conditions.

For the rectangular specimens, the minimum load was set at 1 kip in order to maintain the ram in compression during cycling. Maximum load applied on the specimens corresponded either to an HS20 load or to an overload of 55% as compared with the HS-20 standard on the bridge. The loads obtained corresponded to 35% and 53%, respectively, of yield in the reinforcing bars.

The test program is summarized in Table 4.5. For the first and second cycled beams in the MB series, cyclic loads between 1 kip and 8 kips (4.5 to 35.6 kN) were applied corresponding to a stress range of 35% of yield in the rebars. The first beam was subjected to 10,000 cycles; the second was subjected to 1,000,000 cycles. At this level, the bars were not expected to reach their fatigue limit (Figure 2.10).

For the third beam of the MB series, the maximum load was increased to 12.5 kips (55.6 kN) to reach 53% of yielding, corresponding to an overload of approximately 55% on the pan-joist bridge as compared to the HS-20 standard. At this stress level the rebars were expected to reach their fatigue life around 1,000,000 cycles. The beam was subjected to 1,000,000 cycles.

In a similar way, the maximum load for the first beam of the SK series was 12 kips (53.4 kN), and was 17 kips (75.6 kN) for the second.

Because of the excellent overall behavior of the strengthened beams, the last beam was subjected to a post-yielding fatigue test to investigate the mode of

failure under extreme fatigue conditions. The last beam was cycled between 1 and 33 kips (4.5 and 147 kN).

4.5.3 Test program

Tests were conducted at ambient room temperature. Table 4.5 shows details of the static and repeated loading program. The following nomenclature was used to label the specimens:

- SERIES NAME-Number of cycles-Minimum load/Maximum load in kips
- MB: Master Builders wet lay-up system
- SK: Sika pultruded plate system.

Initially, the test specimens were loaded statically to the maximum fatigue load before starting the application of the repeated load sequence. The fatigue loading was interrupted at intervals to subject the beams to a static loading and monitor the change in the static response. Static loading was applied in steps of 3 kips in order to take acoustic emission measurements.

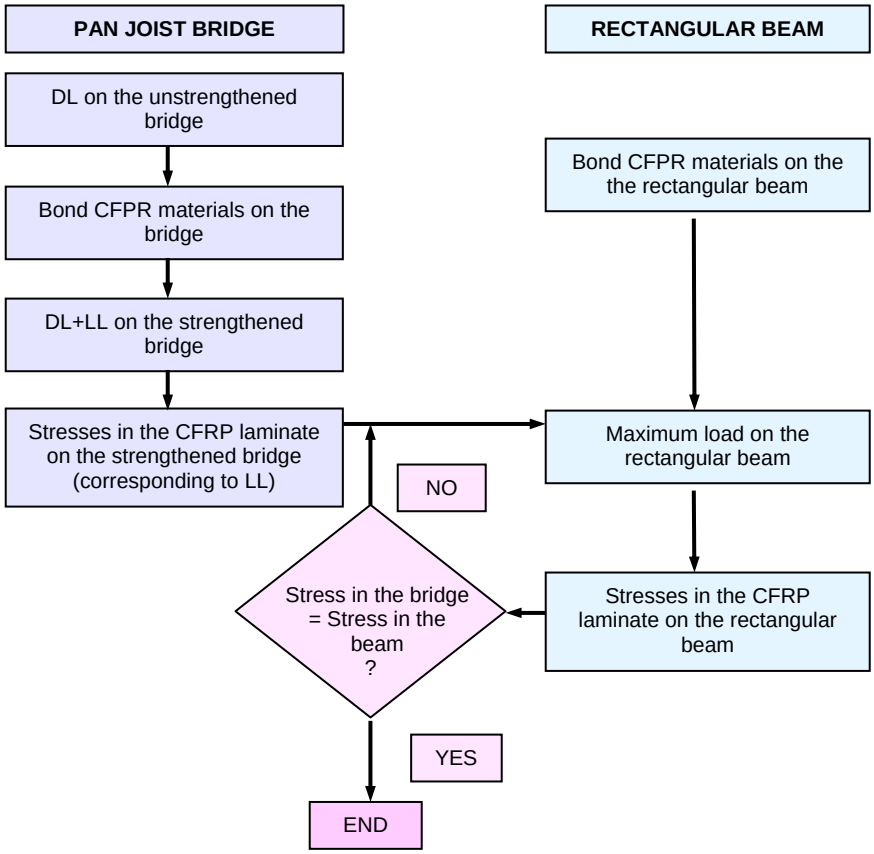

Figure 4.13: Iterative process to compute the load on the test specimens
(DL: Dead Load, LL: Live Load)

Table 4.5.a: Test program, Imperial units.

SPECIMEN	CROSS-SECTION [inxin]	NUMBER OF CYCLES	CYCLING LOAD [kips]		MAXIMUM LOAD [% of ultimate capacity]	STRESS RANGE IN REBARS [ksi]	MAX STRESS IN REBARS [% of yield]	DESCRIPTION
			MIN	MAX				
UN14	8x14	1	-	-		-	-	Unstrengthened control specimen subjected to static loading
MB-1	8x14	1	-	-		-	-	Control specimen strengthened using MB flexible sheets subjected to static loading
MB-e4-1/8	8x14	10^4	1	8	27%	22	35%	MB beam subjected to 10,000 cycles between 1 and 8 kips
MB-e6-1/8	8x14	10^6	1	8	27%	22	35%	MB beam subjected to 1 million cycles between 1 and 8 kips
MB-e6-1/12.5	8x14	10^6	1	12.5	42%	33	53%	MB beam subjected to 1 million cycles between 1 and 12.5 kips
UN16	8x16	1	-	-		-	-	Unstrengthened control specimen subjected to static loading
SK-1	8x16	1	-	-		-	-	Control specimen strengthened using SK pultruded plates subjected to static loading
SK-e6-1/12	8x16	10^6	1	12	30%	22	35%	SK beam subjected to 1 million cycles between 1 and 12 kips
SK-e6-1/17	8x16	10^6	1	17	40%	33	53%	SK beam subjected to 1 million cycles between 1 and 17 kips
SK-9000-1/33	8x16	9,000	1	33	83%	63	102%	SK beam subjected to cycling between 1 and 33 kips, fatigue failure after 9,000 cycles

Table 4.5.b: Test program, SI units.

SPECIMEN	CROSS-SECTION [cmxcm]	NUMBER OF CYCLES	CYCLING LOAD [KN]		MAXIMUM LOAD [% of ultimate capacity]	STRESS RANGE IN REBARS [MPa]	MAX STRESS IN REBARS [% of yield]	DESCRIPTION
			MIN	MAX				
UN14	20x36	1	-	-		-	-	Unstrengthened control specimen subjected to static loading
MB-1	20x36	1	-	-		-	-	Control specimen strengthened using MB flexible sheets subjected to static loading
MB-e4-1/8	20x36	10^4	4.5	35.6	27%	150	35	MB beam subjected to 10 000 cycles between 4.5 and 35.6 kN
MB-e6-1/8	20x36	10^6	4.5	35.6	27%	150	35	MB beam subjected to 1 million cycles between 4.5 and 35.6 kN
MB-e6-1/12.5	20x36	10^6	4.5	55.6	42%	227	53	MB beam subjected to 1 million cycles between 4.5 and 55.6 kN
UN16	20x41	1	-	-		-	-	Unstrengthened control specimen subjected to static loading
SK-1	20x41	1	-	-		-	-	Control specimen strengthened using SK pultruded plates subjected to static loading
SK-e6-1/12	20x41	10^6	4.5	53.4	30%	150	35	SK beam subjected to 1million cycles between 4.5 and 53.4 kN
SK-e6-1/17	20x41	10^6	4.5	75.6	40%	250	53	SK beam subjected to 1million cycles between 4.5 and 75.6 kN
SK-9000-1/33	20x41	9 000	4.5	147	83%	434	102	SK beam subjected to cycling between 4.5 and 147 kN, fatigue failure after 9 000 cycles

Chapter 5 Presentation and discussion of test results

5.1 Introduction

The experimental program reported herein discusses the influence of fatigue loading on the static behavior of rectangular R/C beams strengthened using CFRP materials.

Six specimens were subjected to fatigue loading with different stress ranges and number of cycles (Section 4.5.3). The specimens that survived the repeated load sequence were tested monotonically to failure. The cumulative damage in concrete, in the CFRP laminates, and at the bond interface are reported, as well as the overall deformation behavior. The post-cyclic static response and failure mode are compared with control specimens subjected to direct static loading.

For the specimen that failed under fatigue loading, damage propagation during cycling is analyzed closely and test data are compared with the literature in an S-N curve.

Finally, overall structural behavior of the test specimens is described quantitatively using deflection ductility, curvature ductility, and energy ductility indices.

5.2 Verification of data for test instruments

The experimental program is summarized in Table 4.5, Section 4.5.3. For each specimen, validity of data from the strain gages was checked using the horizontal forces and the internal moment equilibrium conditions. Internal forces were computed using the material properties presented in Section 4.1, and the internal moment was obtained for each data point. Horizontal equilibrium was within a maximum error of ±20%, and internal moment was in the range of ±20% from the applied moment.

Figure 5.1 shows the data verification for both the fatigue and the static loading tests for the specimen MB-e4-1/8. Measures appear to be more accurate at high load level (above 10 kips, 45 kN) even when the resistance of concrete in tension is considered in the material model. However, at low load level (under 5 kips, 22 kN), electric-resistance strain gages do not provide reliable data. After yield (24 kips, 107 kN), the internal moment deduced from the strain gages readings shows several plateaus corresponding to different load increments. This is thought to be due to permanent deformations in the strain gages at high load level. Thus, when the specimen is partially unloaded, the gage still indicates the same reading. When the specimen is loaded again, the strain increases with the load.

The same approach was used for each specimen. Readings from the strain gages are considered to present a satisfactory accuracy considering the models used to describe the materials, the precision with which the gages were placed and the dispersion of measurements in an inhomogeneous and cracked material such as reinforced concrete.

Moreover, the strain gages appeared to be affected by cycling, with readings being less and less accurate with increasing number of cycles. For the specimen MB-e6-1/8, the external gages on the CFRP sheet were damaged during cycling and

replaced prior to static loading up to failure. For the SK series, data collected from the strain gages fixed to the reinforcing bars were available up to 500,000 cycles for the beam SK-e6-1/12, 100,000 cycles for the beam SK-e6-1/17, and 10 cycles for the beam SK-9000-1/33, limiting the analysis for beams in the SK series. This is thought to be due to cyclic deterioration of the glue used to bond the gages. It is likely that the adhesive was not probably resistant to fatigue degradation.

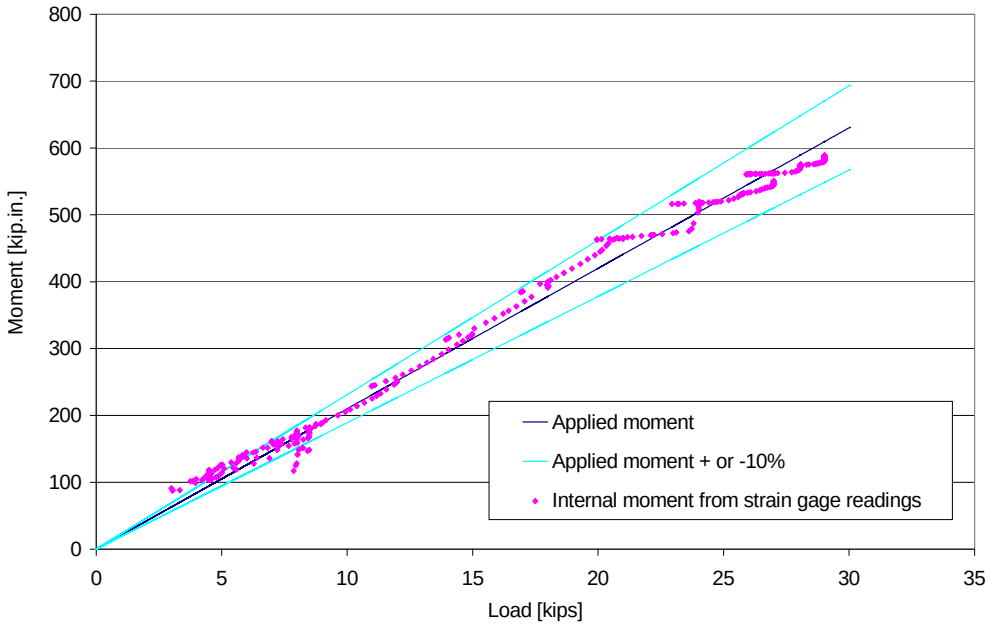

Figure 5.1: Strain gage data verification for the specimen MB-e4-1/8. Comparison of internal moment obtained from strain gage readings versus applied moment for both the fatigue and the static loading.

Linear potentiometers used to measure beams deflections have a precision of ±0.01 in. (±0.25 mm). During cycling, the linear potentiometers were pulled back from the specimen to avoid fatigue damage to the instruments. An additional error of ±0.01 in. (±0.25 mm) was possible due to repositioning of the instruments after each repeated sequence of loading.

5.3 Static behavior

5.3.1 Load-deflection response

Analysis of the static tests presented herein is limited to results relevant to the research objectives described in Section 1.3. An analysis of the complete static test program briefly described in Section 4.4 can be found in References [11] and [12].

Figure 5.2 shows the load-deflection response of strengthened and unstrengthened specimens subjected to monotonic loading to failure. The theoretical response curves are computed using the algorithm developed by Breña [12]. The theoretical model did not include tensile resistance of the concrete. The strengthened beams (MB-1 and SK-1) exhibit the typical behavior as described in Section 2.3.1. The initial stiffness of the strengthened specimens is essentially equal to the stiffness of the unstrengthened control beams before cracking. Post-cracking stiffness, yield load, and ultimate capacity are enhanced by the composite materials. The increase is more notable for the SK series beams due to the larger quantity of CFRP materials used to strengthen the specimens (Section 4.2.1).

Characteristics of the measured load-deflection response are compared in Table 5.1. In the MB series, the yield load was increased by 6%, and the ultimate

capacity was increased by 18%. In the SK series, the yield load and ultimate capacity were increased respectively by 34% and 62%.

Table 5.1: Load and deflection characteristics of specimens subjected to monotonic loading

	MB SERIES			SK SERIES		
CHARACTERISTICS	UN14	MB-1	Δ [%]	UN16	SK-1	Δ [%]
Yield load, kips, (kN)	22.6 (101)	24.0 (107)	+6 %	22.4 (100)	29.7 (132)	+34 %
Yield deflection, in., (mm)	0.33 (8.4)	0.34 (8.6)	+3 %	0.31 (7.9)	0.38 (9.7)	+23 %
Load at ultimate deflection of strengthened beam, kips, (kN)	25.4 (113)	30.0 (134)	+18 %	25.0 (111)	40.7 (181)	+62 %
Ultimate deflection in., (mm)	1.8 (46)	1.2 (31)	-36 %	2.3 (58)	0.84 (21)	-63 %

Δ: Variation

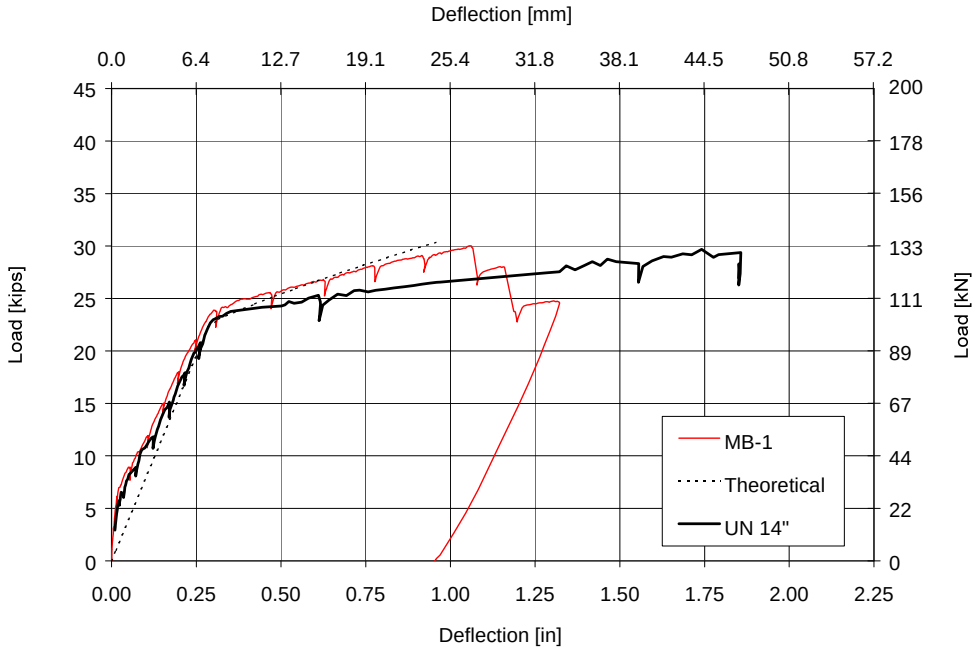

(a)

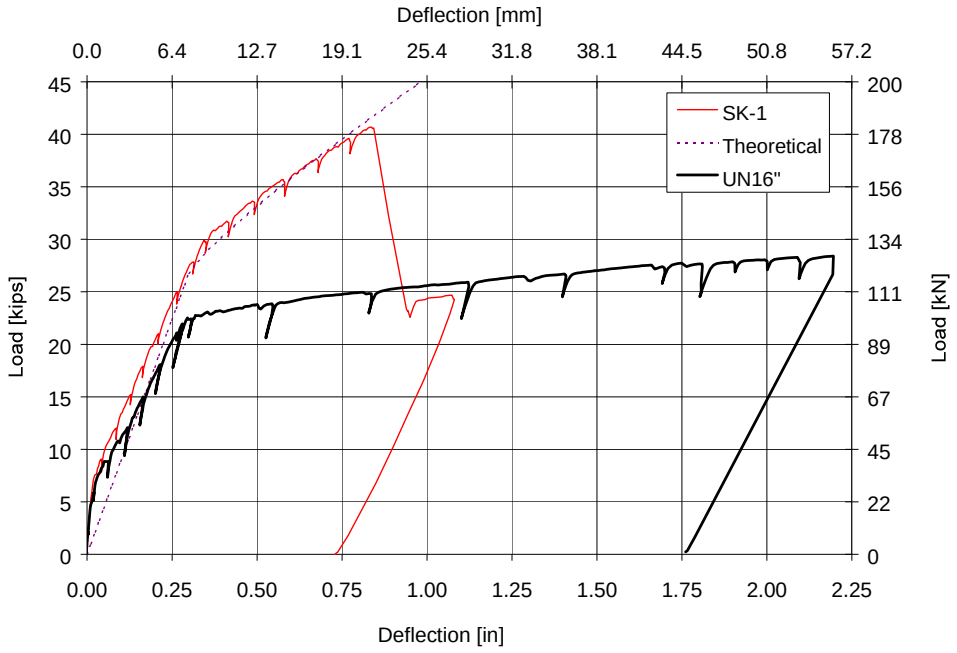

(b)

Figure 5.2: Comparison of load-deflection response of strengthened and unstrengthened specimens subjected to monotonic loading (a) MB series (b) SK series.

5.3.2 Moment-curvature response

The moment curvature response for the beams in the MB series (Figure 5.4) was obtained from the strain gage readings. The neutral axis position, x, and the curvature, ϕ, were computed assuming a linear distribution of strains over the depth of the section (Figure 5.3), using the following equations:

Neutral axis:

$$x = \frac{1.5.\left|\varepsilon_{S,SG}\right| - 12.5.\left|\varepsilon_{C,SG}\right|}{\left|\varepsilon_{S,SG}\right| - \left|\varepsilon_{C,SG}\right|} \qquad (5.1)$$

Maximum stain in concrete at top extreme fiber:

$$\varepsilon_{C,\max} = \frac{x.\left|\varepsilon_{C,SG}\right|}{x - 1.5} \qquad (5.2)$$

Curvature:

$$\phi = \frac{\left|\varepsilon_{C,\max}\right|}{x} \qquad (5.3)$$

Before yielding of the reinforcing steel, the strengthened specimen behaves as expected, following the theoretical curve. After yield, the curvature increases rapidly until it reaches 0.0015 rad/in., corresponding to the beginning of the strain hardening, as it can be observed for the unstrengthened specimen. When the ultimate moment is reached at 626 kips-in. (70.7 kN.m), the curvature reaches the maximum value of 0.0017 rad/in.

However, curvatures between 0.0005 and 0.0016 1/in. are not considered reliable because the neutral axis at this load level was very close to the concrete gage position at the top of the beam (Figure 5.4). The ultimate curvature, though, is considered to be reasonable (Section 5.2), and thus was used in the analysis of the structural ductility (Section 5.5.3).

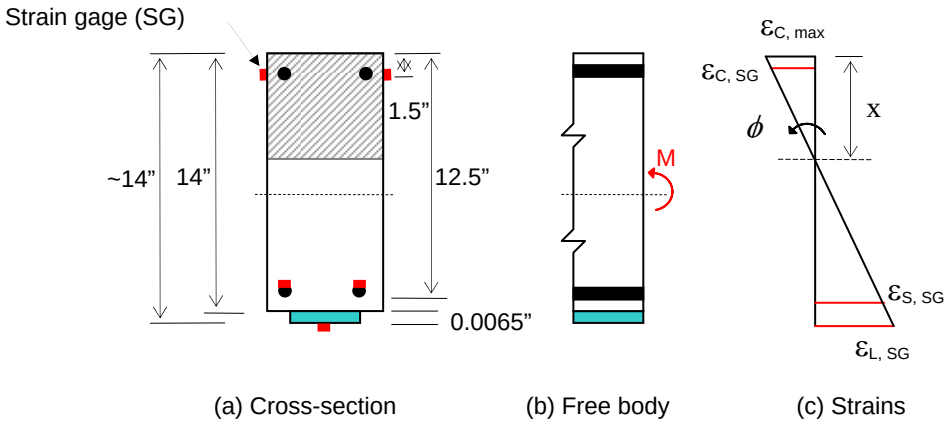

Figure 5.3 Computation of curvature from strain gage readings.

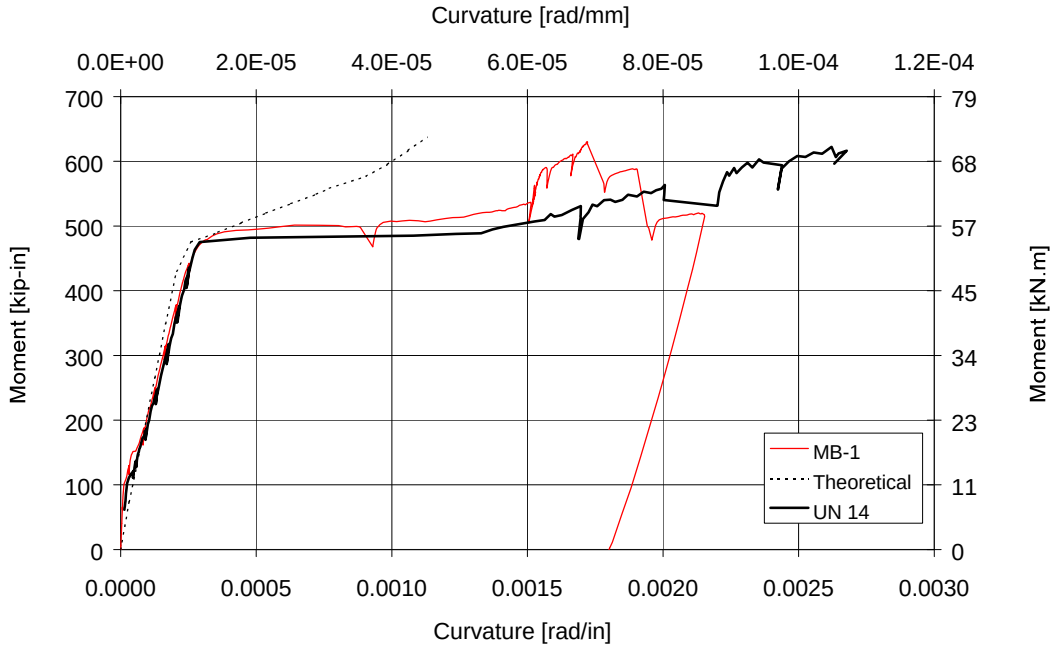

Figure 5.4: Comparison of moment-curvature response of strengthened and unstrengthened specimens in the MB series subjected to monotonic static loading

Strains over the section depth at midspan are displayed in Figure 5.5 for the MB series beams. Marks on the figures indicate the data points. At service load levels, up to 8 kips (35.6 kN), no significant difference can be observed between the unstrengthened and strengthened specimens. With increasing load, the action of the CFPR laminate reduces strains in the reinforcing steel indicating a transfer of stresses from the steel to the CFRP laminate. Strain in the steel for the strengthened beam represents approximately 80% of the strain in the steel for the unstrengthened specimen at yield load (24.0 kips, 107 kN), and only 68% at ultimate (30.0 kips, 134 kN).

The strain compatibility is evident up to yield of the reinforcing steel (24 kips, 107 kN). After yielding, strain in the CFRP laminate is less than would be expected assuming perfect bond of the composite to the concrete. The laminate is subjected to a large strain increase, and the no-slip composite action apparently cannot be maintained any longer.

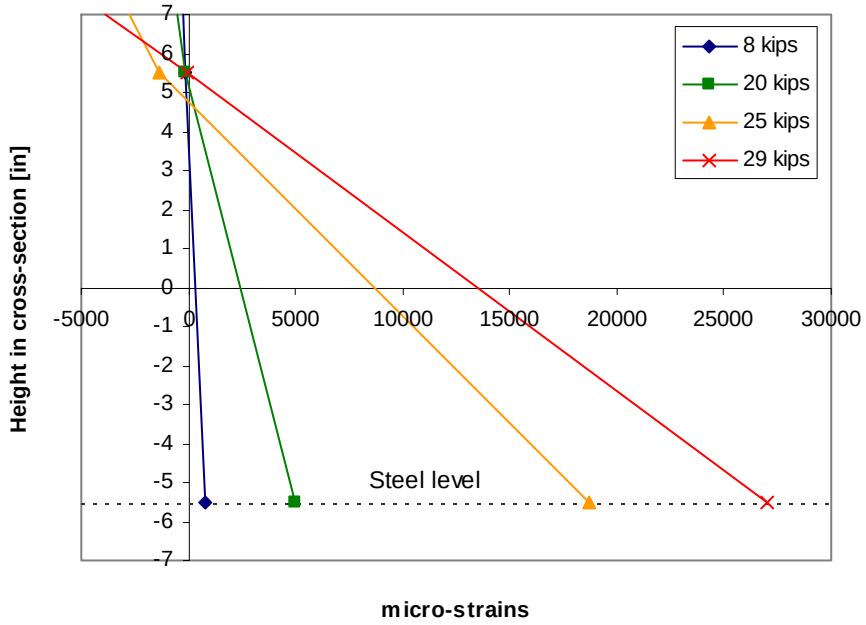

(a)

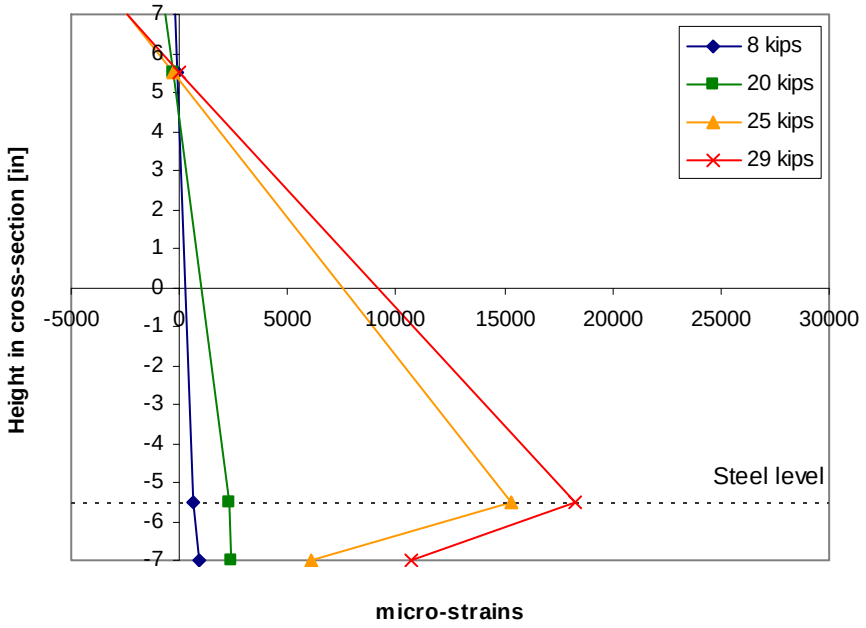

(b)

Figure 5.5: Strains over the section depth at midspan. Comparison between (a) unstrengthened and (b) strengthened beams subjected to monotonic static loading in the MB series.

The ultimate bending capacity of the beams is computed using the procedure proposed in Chapter 3 for the strengthened specimens, and conventional RC strength theory for the unstrengthened specimens. According to the test results, the design model proposed in Chapter 3 provides approximately the same precision as classical RC theory. Details of the hand computations are presented in the Appendix B, and the results are summarized in Table 5.2.

The good correlation between the calculated and measured ultimate capacities validates the proposed design procedure. A maximum error of -7.1% between measured and theoretical values is observed for the beam SK-1 as compared with +6.7% for the unstrengthened specimens.

For the beam SK-1, the ultimate elongation of the CFRP plate was assumed equal to 1.0% with respect to the ultimate elongation in the epoxy adhesive (Section 4.1.4). However, the maximum strain observed before debonding in the CFRP was 0.62%, which explains why the calculated flexural capacity of the beam SK-1 was overestimated by assuming perfect bond to failure (Section 3.2). The failure of the specimen SK-1 revealed a delamination of concrete at the bond interface (Section 5.3.3). This observation points out that, for design purpose, further verifications are needed such as the verification of the shear stresses at the bond interface (Section 3.2).

Table 5.2: Comparison between calculated and measured flexural capacities of test specimens.

SPECIMEN	CALCULATED FLEXURAL CAPACITY		MEASURED FLEXURAL CAPACITY		Δ	MAXIMUM STRAIN IN CFRP LAMINATE [%]	
	[kip.in.]	[kN.m]	[kip.in.]	[kN.m]	[%]	ASSUMED	MEASURED
UN14*	445	50.3	475	53.7	+6.7%	-	-
UN16*	519	58.6	538	61.0	+3.7%	-	-
MB-1	613	69	618	70	+2.8%	1.5%	1.19%
SK-1	1051	119	976	110	-7.1%	1.0%	0.62%

* The strain hardening was not taken into account.

Δ: Variation

5.3.3 Failure mode

The two RC control beams failed in a ductile manner with crushing of concrete in the compression zone following yielding of the reinforcing steel.

Beam MB-1 failed by progressive rupture of the longitudinal CFRP sheet. The laminate first started to debond at the north end of the beam at 28 kips (125 kN), and pulled off the first, then the second strap. The laminate ruptured at midspan over half its width, leading to a progressive drop off of the load before complete failure of the laminate (Figure 5.2.a, and Figure 5.6.c). The straps at the end of the beam showed evidence of splitting of the longitudinal laminate, exhibiting large cracks parallel to the fiber direction. This observation confirms the measured strains over the section depth at midspan, showing a partial loss of composite action after yielding. The maximum strain measured in the laminate was 1.19%.

Beam SK-1 failed by sudden debonding of the pultruded plate, with a substantial drop in load capacity at the time of failure (Figure 5.2.b). The plates started to debond in the maximum moment region at 36 kips (160 kN). The four straps at the south end of the beam partially dedonded sequentially, leading to failure by peeling-off of the laminate at the south end. Concrete wedges, formed by primary flexural cracks and diagonal cracks, became loose at the bottom face of the beam, and concrete pieces were pulled off from the surface at the south end of the plate. The maximum strain in the plates was 0.62 %, which was much lower than the ultimate elongation of 1.9% reported by the manufacturer, and lower than the ultimate elongation of 1.0% for the epoxy adhesive.

The crack patterns (Figure 5.6 and Figure 5.7) show a significant reduction in the number of cracks and a decrease in the average crack width in both series compared with the unstrengthened specimens.

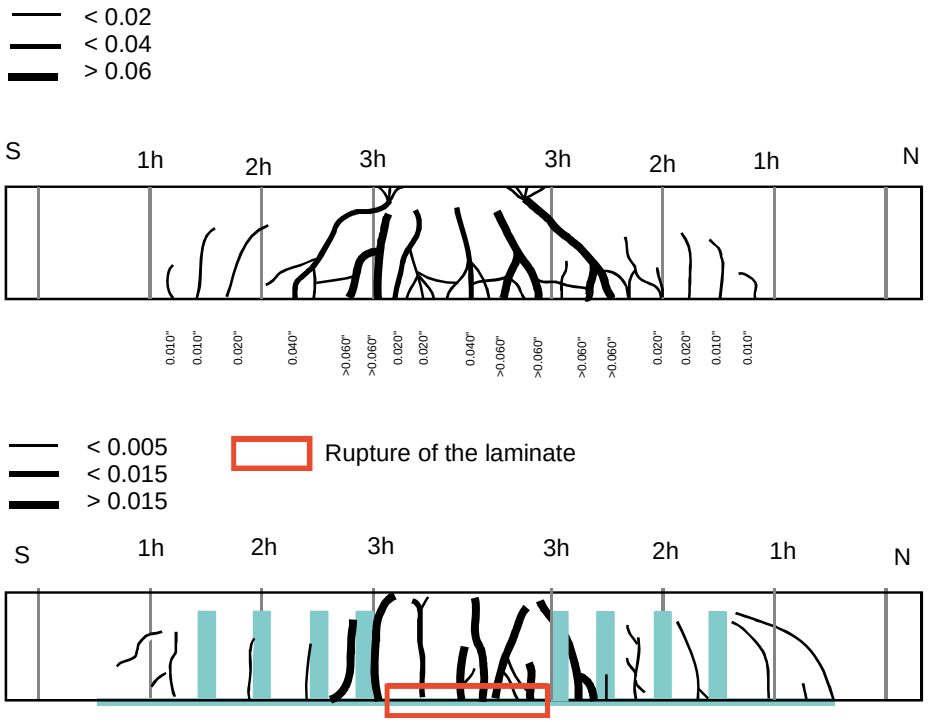

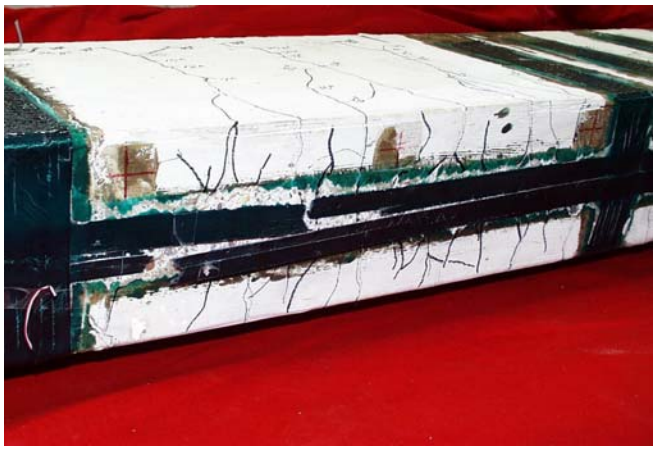

Figure 5.6: Crack pattern after failure of specimens from the MB series subjected to monotonic static loading (a) Unstrengthened UN14 (b) Strengthened MB-1 (c) Photograph of the rupture of the longitudinal CFRP sheet.

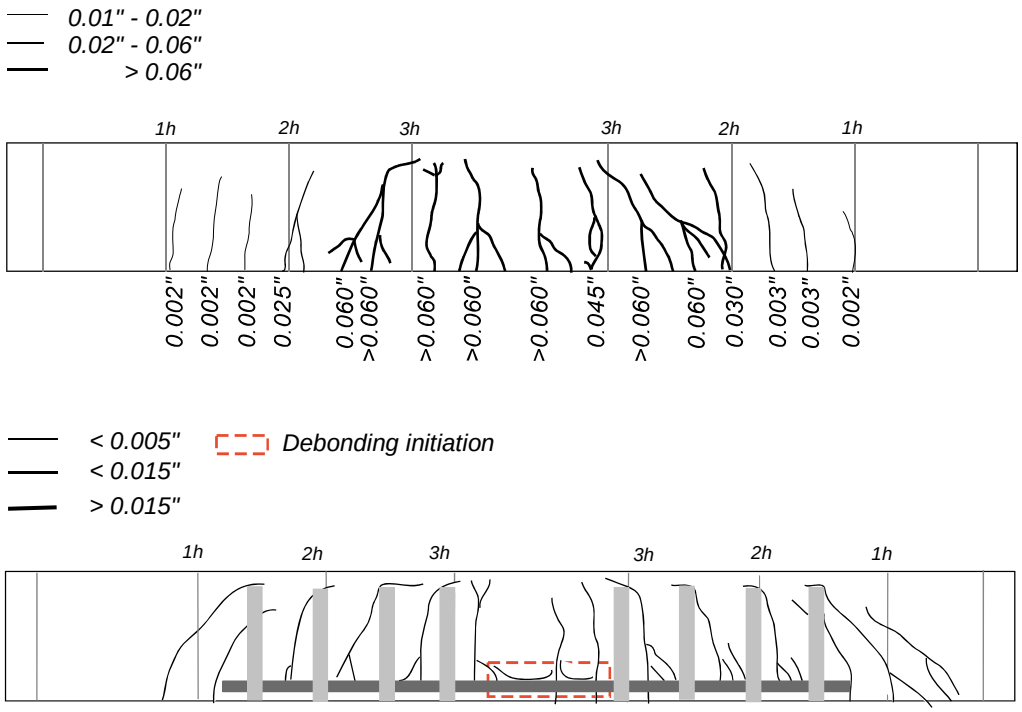

Figure 5.7: Crack pattern after failure of specimens from the SK series subjected to monotonic static loading (a) Unstrengthened, (b) Strengthened

5.4 Behavior during cyclic loading

5.4.1 Damage propagation

As for RC members (Section 2.2.2), beams strengthened using CFRP materials exhibit a progression of cracking when subjected to fatigue loading. Before the end of the repeated sequence of loading, new cracks appeared, cracks increase in length, and the width of the main flexural cracks increased. The same type of cracking pattern was observed within beams of the same series subjected to cyclic loading, with the exception of beam SK-9000-1/33, which is discussed in Section 5.4.3.

Bond of the CFRP laminate showed no evidence of damage during cycling when the members were subjected to a stress range corresponding to service load levels, which was 8 kips (35.6 kN) for the MB series and 12 kips (53.4 kN) for the SK series. Under higher load level, premature debonding was observed (Figure 5.6). Starting from the main flexural cracks, several thin diagonal cracks propagated toward the laminate. Depending on the load level, the debonding zone could stay localized (MB-e6-1/12.5 and SK-e6-1/17) or propagate along the laminate leading to failure (SK-9000-1/33, Section 5.3.3). The above observations are summarized in Table 5.3.

Figure 5.8.b shows the initiation of debonding of the longitudinal pultruded plate in the shear span for the beam SK-e6-1/17. The main crack formed after the first static cycle and grew in the direction of the transverse anchorage. Cracking progressed from the main crack toward the laminate forming a delta pattern after 100,000 cycles (mark 17^{III}), and initiated debonding after 250,000 cycles (mark 17^{IV}).

Table 5.3: Evolution of debonding during cycling

SPECIMEN	PEAK LOAD		STRESS RANGE IN REBARS		OBSERVED DAMAGE IN THE LAMINATE
	[kips]	[kN]	[ksi]	[MPa]	
MB-e4-1/8	8	35.6	22	152	No evidence of damage at the bond interface
MB-e6-1/8	8	35.6	22	152	No evidence of damage at the bond interface
SK-e6-1/12	12	53.4	22	152	No evidence of damage at the bond interface
MB-e6-1/12.5	12.5	55.6	33	228	Debonding initiation at 5 locations, no propagation
SK-e6-1/17	17	75.6	33	228	Debonding initiation at 9 locations, no propagation
SK-9000-1/33	33	147	63	434	Progression of debonding leading to failure

(a) (b)

Figure 5.8: Initiation of debonding of the longitudinal laminate during cycling

(a) Beam MB-e6-1/12.5: Local debonding after 125,000 cycles at the location of the crack initiator

(b) Beam SK-e6-1/17: Debonding initiation after 250,000 cycles: cracks spread as they reached the CFRP plate

5.4.2 Deformation behavior

All specimens exhibited a gradual increase in deflections during cyclic loading along with a decrease in the average stiffness (Figure 5.9 and Figure 5.10). The evolution of deflections at peak load during cycling is compared with deflections of respective control specimens subjected to monotonic static loading tests (Figure 5.11). At the end of the repeated loading sequence, the deflection was up to 150% of that of the control specimen at the same load level.

Damage induced by the repeated load sequence for all specimens is summarized in Table 5.4. Both deflections and static stiffness are affected by cycling. Residual deflections after 1,000,000 cycles may represent up to 12% of the maximum deflection, leading to a reduction in post-cyclic deformation capacity.

Tests carried out by Barnes and Mays [6] demonstrated that strengthened members exhibit a gradual increase in deflections during cycling, followed by a sudden increase just before failure. In the present series of tests, no sudden increase in deflections was observed, even for the specimen SK-e6-1/33 that failed under fatigue loading. Moreover, comparing the deflection at rupture of specimen SK-9000-1/33 with the other specimens in the SK series, it appears that the specimen exhibited much smaller deflections at failure as compared with the other specimens in the SK series (Table 5.4 and Figure 5.10.b).

Table 5.4: Damage due to the repeated load sequence.

CHARACTERISTICS	MB SERIES			SK SERIES		
	MB-e4-1/8	MB-e6-1/8	MB-e6-1/125	SK-e6-1/12	SK-e6-1/17	SK-9000-1/33
Residual deflection after cycling [in]	0.019	0.054	0.067	0.051	0.11	NA
Ultimate deflection [in]	1.06	1.07	0.85	0.77	0.95	0.62*
Deflection ratio [%]	2%	5%	8%	7%	12%	NA
Residual curvature after cycling [in^{-1}]	1.9×10^{-5}	2.6×10^{-5}	3.6×10^{-5}	NA	NA	NA
Ultimate curvature [in^{-1}]	1.7×10^{-3}	1.3×10^{-3}	1.5×10^{-3}	NA	NA	NA
Curvature ratio [%]	1%	2%	2.5%	NA	NA	NA
Stiffness at first cycle [kips/in]	185	118	146	273	150	92
Stiffness after cycling [kips/in]	163	109	129	234	115	89*
Stiffness ratio [%]	-12%	-9%	-9%	-17%	-30%	-4%

The initial static stiffness was computed using the unloading branch. Residual deformations after cycling are for the unloaded specimens. NA: non available. *Failure during fatigue loading

Shahawy and Beitelman [45] reported on the behavior of post-strengthened members, which were previously subjected to fatigue loading for 150,000 cycles (Section 4.5.2), and noted that the stiffness after strengthening remained relatively constant during cycling up to just before failure. In the present tests, all specimens demonstrated a reduction in stiffness of approximately 10% (Table 5.4) over that which was observed during the initial static cycle, the larger part occurring during the first 100,000 cycles.

Thus, the decrease in stiffness is thought to be due to the evolution of concrete damage. As cracking progressed, the width of the cracks increased,

leading to an increase in strains in the longitudinal CFRP laminate and in the reinforcing steel. A steady increase of strain in the CFRP pultruded plates of the beam SK-e6-1/17 during cycling (Figure 5.12) indicates a transfer of stress from the steel to the CFRP laminate as cracking in the beam progressed. The CFRP laminate, working at a higher stress level, compensates for the concrete damage and helps to maintain a relatively constant stiffness after 100,000 cycles. The same observations, made for the other specimens, are presented in the Appendix C.

Furthermore, strains from the two-instrumented sections displayed for the beam SK-9000-1/33 (Figure 5.13) demonstrate the same rate of increase, indicating no stress-redistribution with time along the CFRP plates. Barnes and Mays [6] reached the same conclusion.

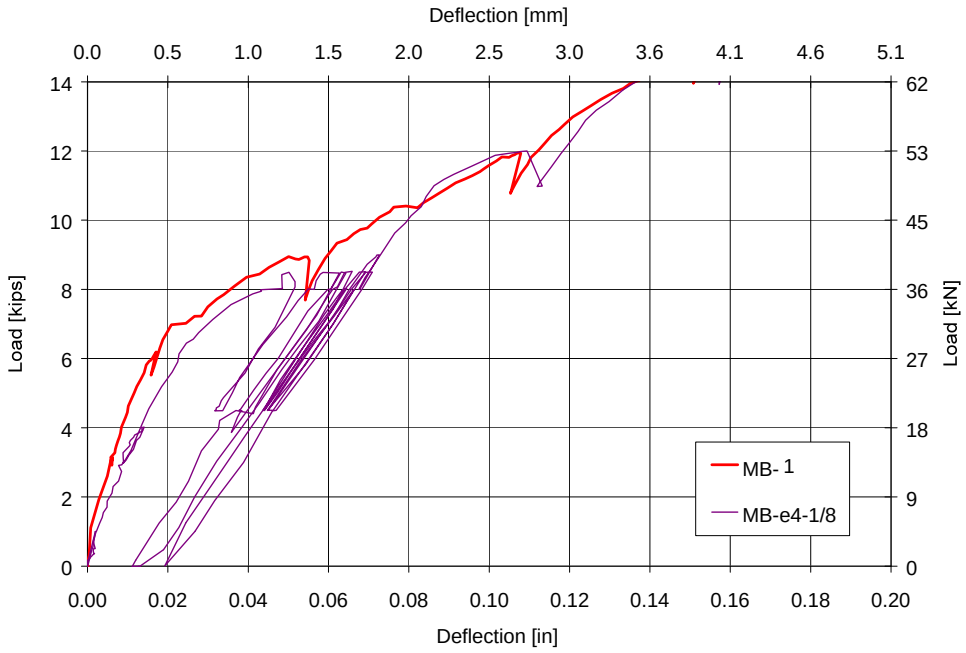

(a)

Figure 5.9: Load-deflection response during cycling for the MB series

(a) MB-e4-1/8 (b) MB-e6-1/8 (c) MB-e6-1/12.5

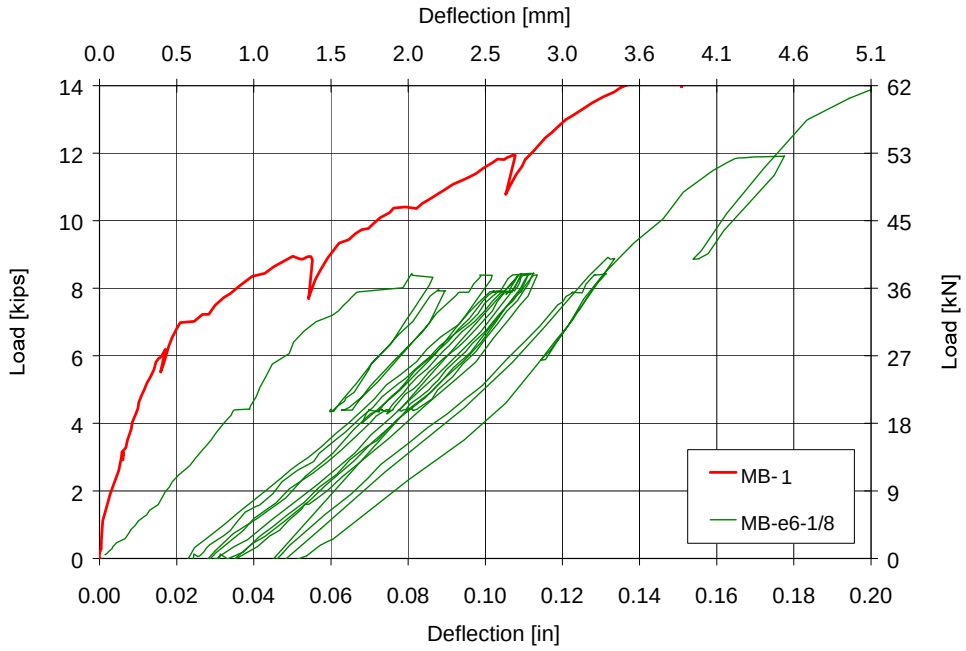

(b)

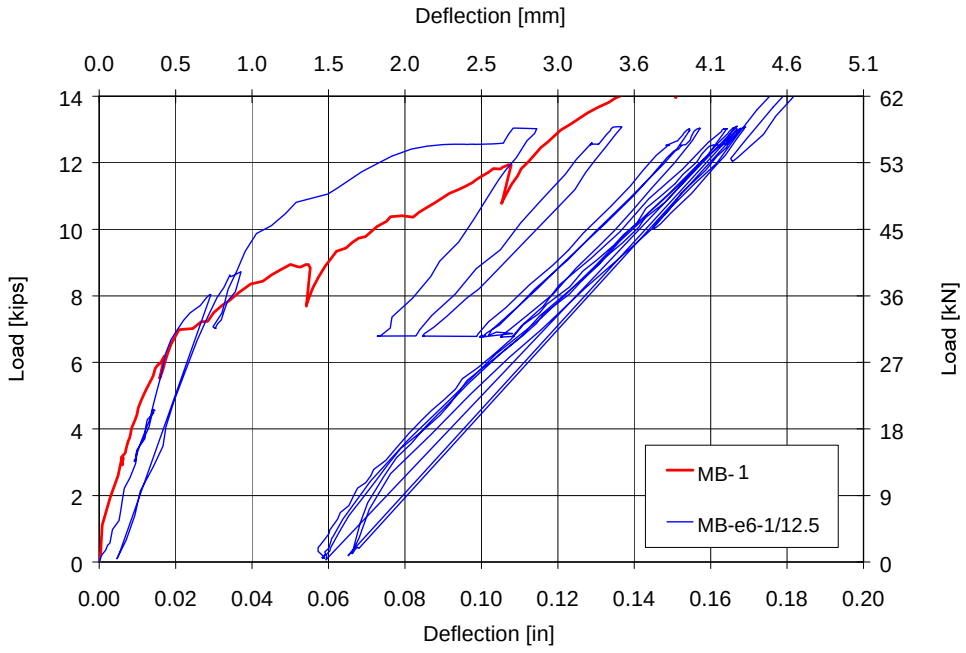

(c)

Figure 5.9: Load-deflection response during cycling for the MB series

(a) MB-e4-1/8 (b) MB-e6-1/8 (c) MB-e6-1/12.5

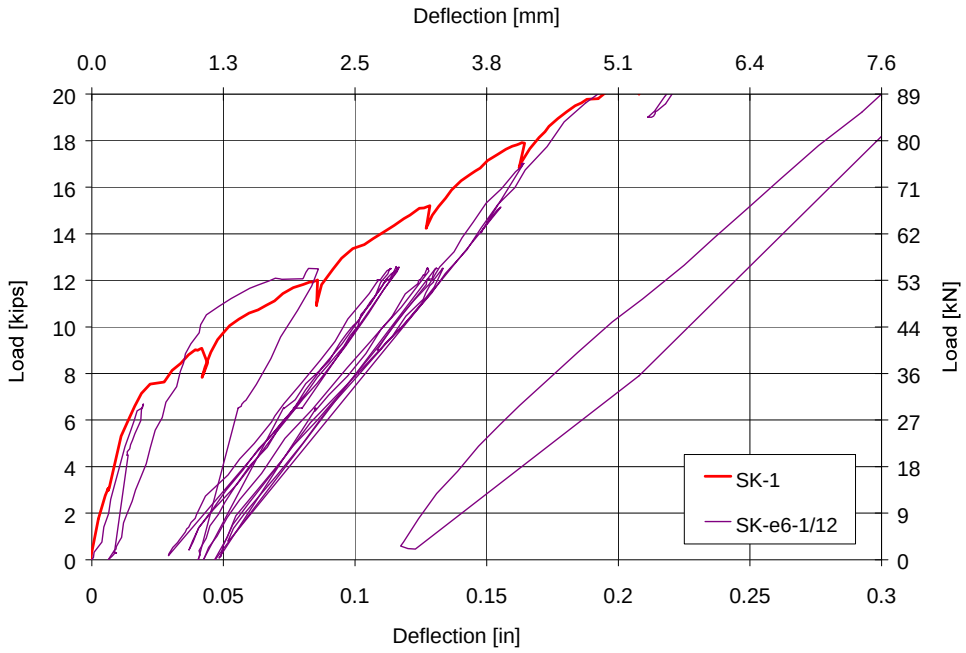

(a)

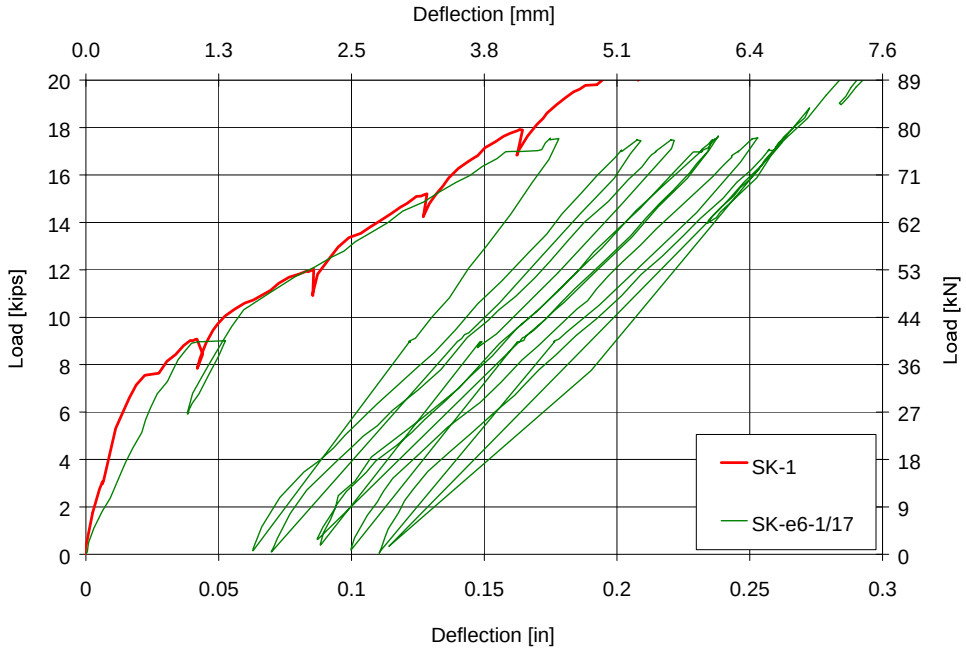

(b)

Figure 5.10: Load-deflection response during cycling for the SK series

(a) SK-e6-1/12 (b) SK-e6-1/17 (c) SK-9000-1/33 displayed on a different scale.

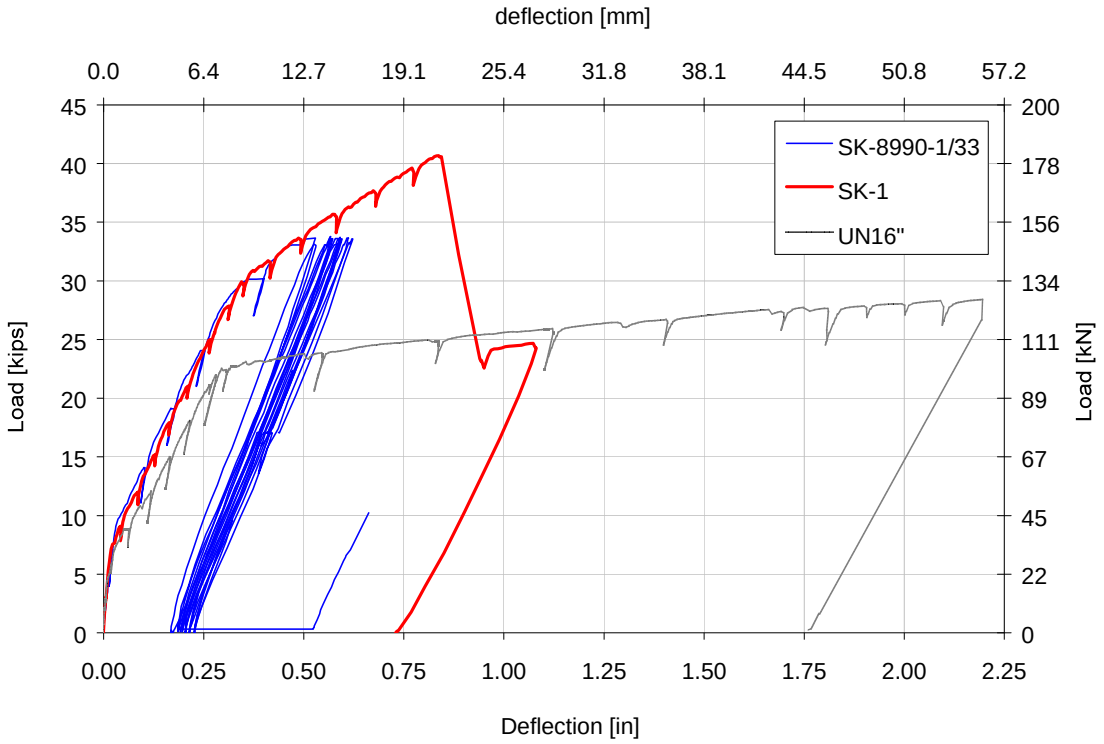

(c)

Figure 5.10: Load-deflection response during cycling for the SK series (a) SK-e6-1/12 (b) SK-e6-1/17 (c) SK-9000-1/33 displayed on a different scale

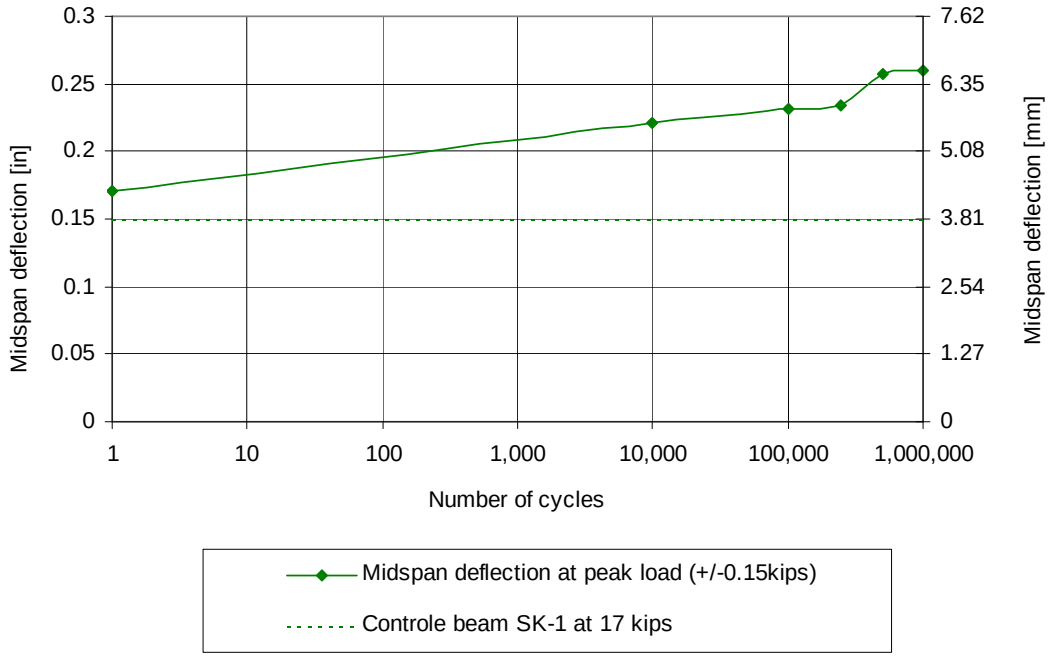

Figure 5.11: Evolution of maximum deflections during cycling for the beam SK-e6-1/17.

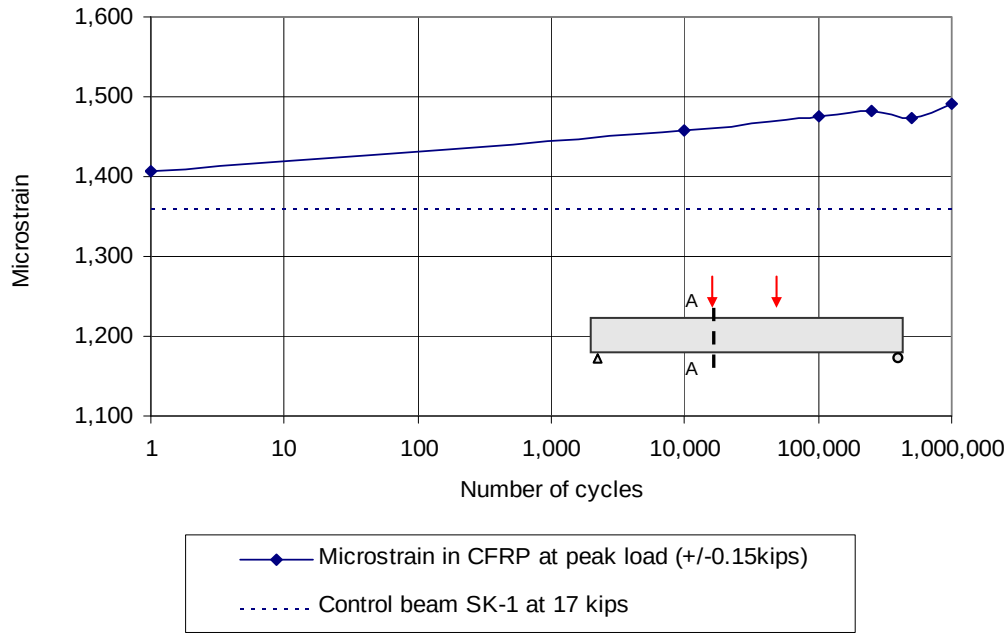

Figure 5.12: Evolution of strains in the CFRP plate at section A-A during cycling for the beam SK-e6-1/17 (Section A-A: see Figure 4.4).

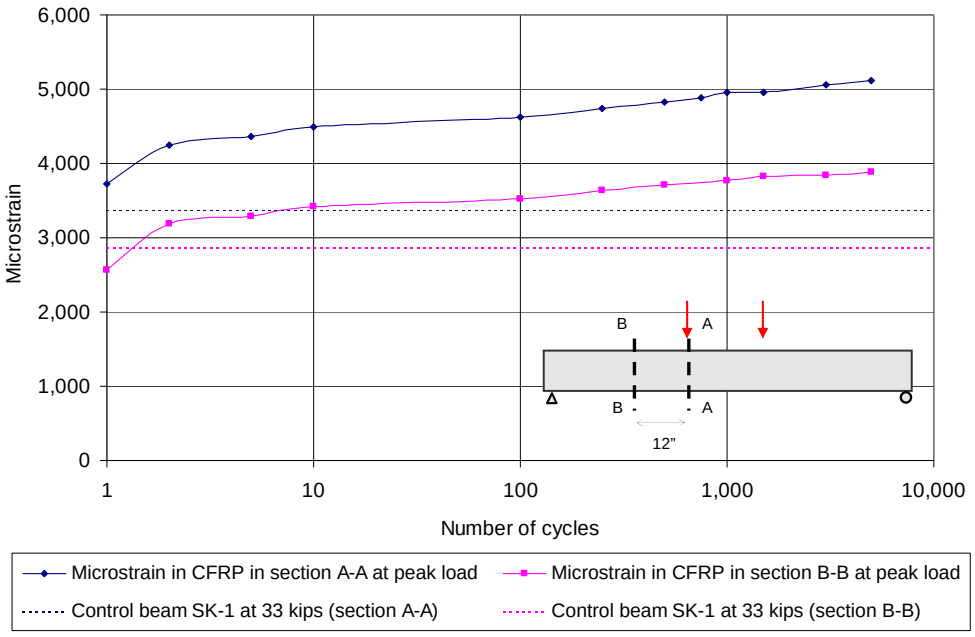

Figure 5.13: Comparison between the evolutions of the strains in the CFRP plates in sections A-A and B-B at peak load (33 kips) during cycling for the beam SK-9000-1/33. (Sections A-A and B-B: see Figure 4.4)

5.4.3 Failure under fatigue loading

Beam SK-9000-1/33 was subjected to cycling between 1 kip and 33 kips (4.5 kN and 147 kN) and failed under after 9,000 cycles. The maximum load corresponds to stresses in the reinforcing steel above yield. The crack pattern is shown after 1, 5,000, and 9,000 cycles (Figure 5.14).

After the first cycle, the beam was already severely damaged, exhibiting two cracks at midspan with width larger than 0.02 in. (0.5 mm) and five debonding initiation zones along each plate. Debonding first progressed between the main flexural cracks, then spread from the maximum moment region toward the north end of the plate. Shear cracks crossing transverse straps forced partial debonding of the

anchorage at the south end of the beam, without affecting the overall behavior. The progression of a flexural-shear crack under a strap is shown in Figure 5.15.b.

The debonding reached the end of the plate after 5,000 cycles, and it was totally debonded over half its length after 8,800 cycles but still maintained in place by the transverse anchorages. Anchorages at the north end failed by rupture of the fibers (Figure 5.15.c), leading to complete failure of the strengthening system (Figures 5.15.a and c).

Examination of the CFRP plates and concrete surfaces demonstrated a typical failure by delamination of the concrete below the reinforcing bars: a layer of concrete, approximately 1/10 in. thick (2 to 3 mm), stayed attached to the plate along the whole length. A four inch-piece of concrete, formed by the main flexural crack and diagonal cracks at the bottom face and on the side of the beam, was pulled off from the surface, exposing the reinforcing bars at midspan (Figure 5.15.d).

Examination of the reinforcing bars after failure revealed no sign of fatigue fracture in the steel.

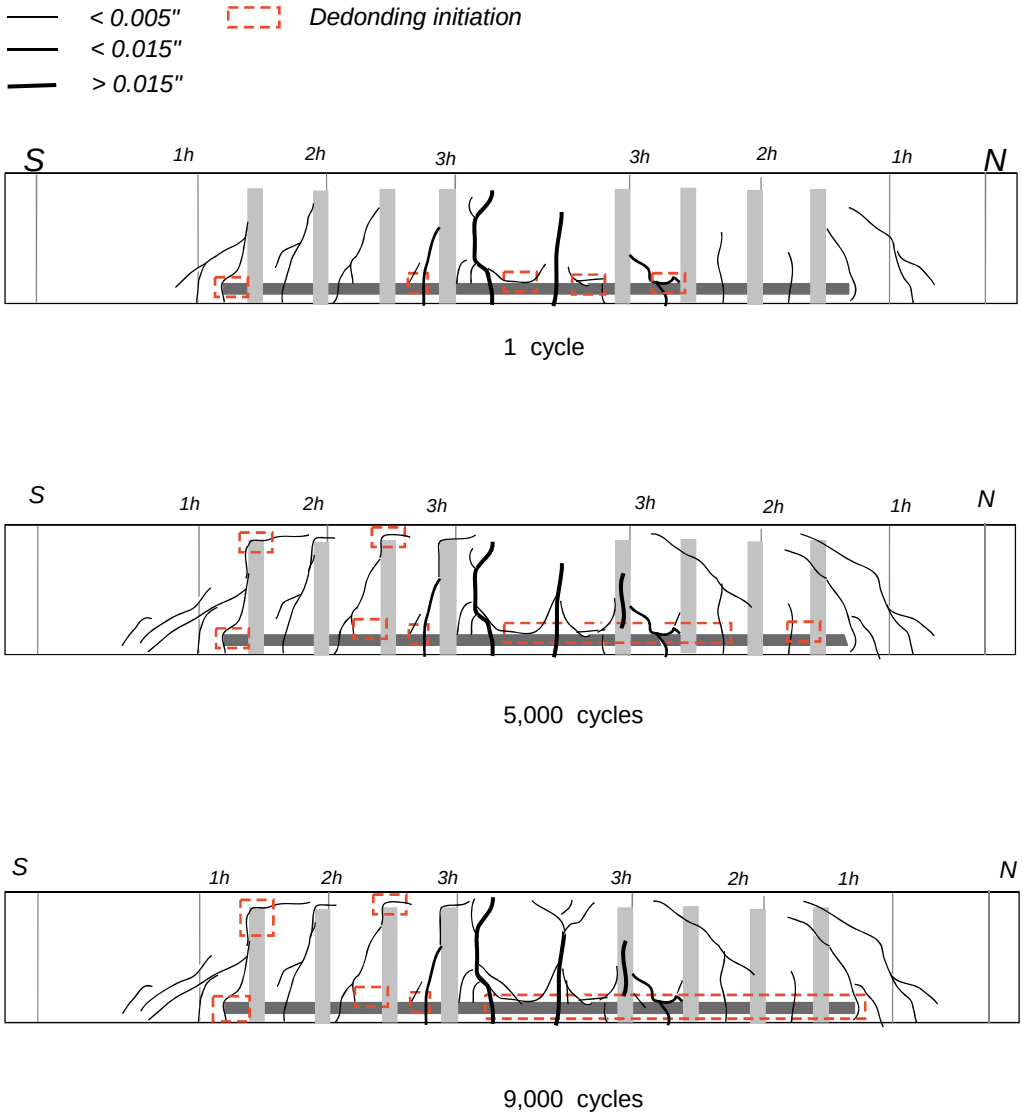

Figure 5.14: Evolution of the crack pattern during cycling for the beam SK-9000-1/33.

Figure 5.15.a: Debonding of the CFRP pultruded plate at midspan

Figure 5.15.b: Debonding propagation and progression of cracking under transverse strap

Figure 5.15.c: Debonding of the north end of the longitudinal plate and rupture of the transverse anchorage

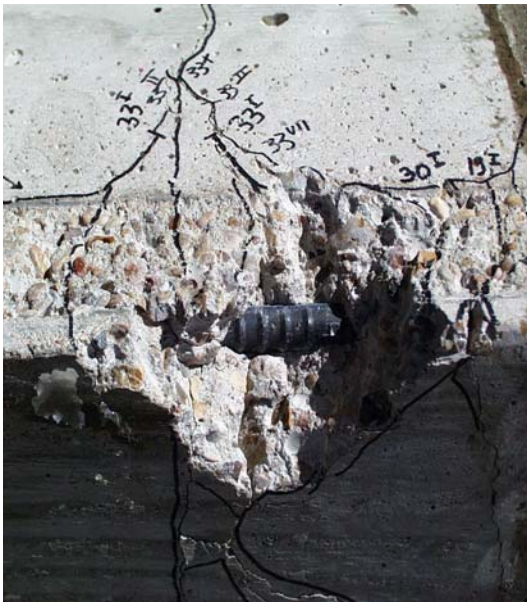

Figure 5.15.d: Spreading of cracking forming a delta pattern at midspan and concrete cover pulled off by the laminate

Figure 5.15: Fatigue failure of the beam SK-9000-1/33

Data obtained for the specimen SK-9000-1/33 strengthened using a pultruded CFRP plate system are compared with the research results reviewed in Section 2.3.4 in the S-N curve presented in Figure 5.16. Testing is still ongoing at the time of writing at the Phil M. Ferguson Structural Engineering Laboratory. Another specimen, strengthened using the same arrangement of CFRP plates and sheet as for the SK series, failed under fatigue loading after 55,000 cycles at a stress range of 56 ksi (385 MPa). The complete analysis of this last test can be found in Reference [12] and the result is reported in Figure 5.16.

As for the strengthened beams tested by Barnes and Mays [6], the test result corresponds approximately to the design curve proposed by Mallet [34] for reinforced concrete beams. However, test results for strengthened beams seem to present a shallower decrease of fatigue resistance with increasing number of cycles as compared with RC beams, indicating an improvement of the fatigue endurance due to strengthening.

As compared with the curve for reinforcing steel bars tested in air, usually assumed for RC design, the fatigue life of strengthened beams, including the specimen SK-9000-1/33, appears to be enhanced.

Results obtained at EMPA do not appear to fit well with the other data. However, the beam subjected to a stress range of 131 MPa (19.0 ksi) was placed in harsh environment that could have affected its fatigue life. On the other hand, the beam subjected to a stress range of 386 MPa (56.0 ksi) appears to have performed exceedingly well. However, fatigue data may contain significant scatter (see Figure 2.10 for instance).

Data for the two other beams in the SK series that did not fail under repeated loading are also displayed in Figure 5.16. According to the assumed fatigue life of the reinforcing bars (Figure 2.10), the specimen SK-e6-1/17 was probably close to reaching its fatigue endurance after 1 million cycles (Figure 5.16).

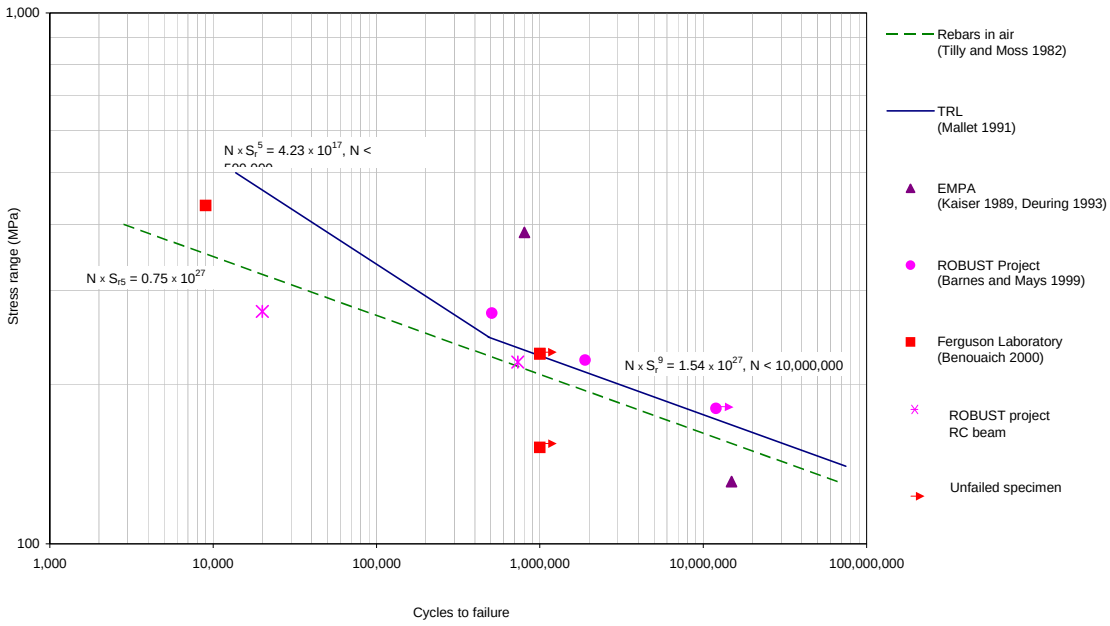

Figure 5.16: Comparison of the test results with the literature. Fatigue data for reinforcing steel bars, RC beams, and RC beams strengthened using externally bonded CFRP materials (SI units).

Sources: Tilly and Moss 1982 (*in* [6]), Mallet 1991 (*in* [6]), Kaiser 1989 (*in* [28]), Deuring 1993 (*in* [28]), Barnes and Mays 1999 [6].

5.5 Behavior under static loading after a repeated load sequence

5.5.1 Load response

Table 5.5 compares the load at yield and ultimate for all strengthened specimens, including those tested under static loading. The results demonstrate no significant influence of cycling on the yield load or on the ultimate capacity.

Table 5.5: Influence of cycling on static load response

SPECIMEN	YIELD LOAD		ULTIMATE CAPACITY	
	[kips]	[kN]	[kips]	[kN]
MB-1	23.8	105.9	30.0	133.5
MB-e4-1/8	24.0	106.8	30.0	133.5
MB-e6-1/8	24.0	106.8	29.9	133
MB-e6-1/12.5	23.8	105.9	29.5	131.2
SK-1	29.7	132.1	40.6	180.6
SK-e6-1/12	30.3	134.8	39.7	176.6
SK-e6-1/17	29.8	132.6	42.5	189.1
SK-9000-1/33	30.1	133.9	-	-

5.5.2 Deformation behavior

The load-deflection and moment-curvature responses are presented in Figures 5.17, 5.18, and 5.19. Deflections were measured with linear potentiometers, whereas curvatures were computed from gage readings. Curvatures for specimens in the SK series were not calculated due to a malfunction of strain gages on the reinforcing bars during cycling (Section 5.2)

The general tendency shows a reduction in deformation capacity at failure after a repeated loading sequence. Both deflections and curvatures are reduced at ultimate as compared with the specimen subjected to monotonic static loading. Deformations at cracking load level and yield load level seem not to be affected by cycling. For the moment-curvature response, the same discussion as for the static test can be made (Section 5.3.2). In order to give a quantitative basis to the above observations, the deformation capacity is evaluated in Sections 5.5.3 and 5.5.4 using structural ductility and energy ductility indices.

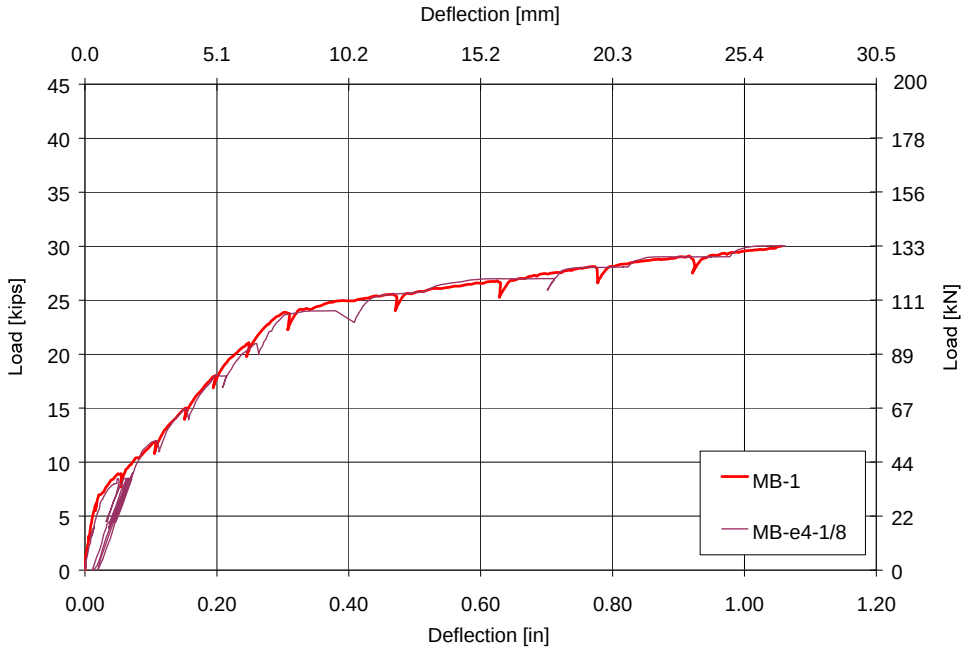

(a)

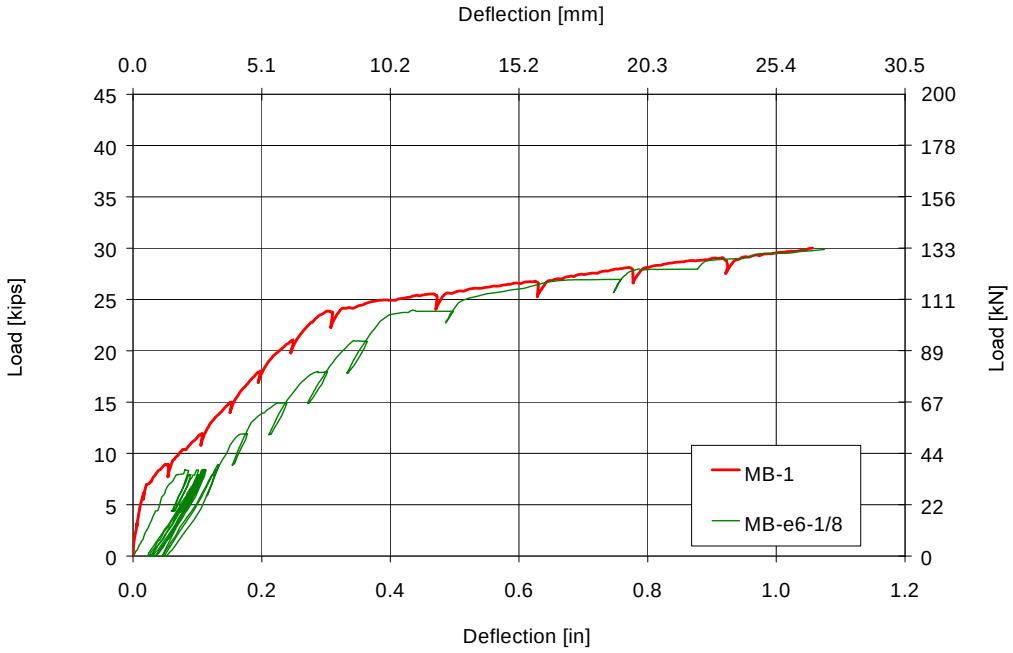

(b)

Figure 5.17: Load-deflection response, MB series (a) MB-e4-1/8 (b) MB-e6-1/8 (c) MB-e6-1/2.5

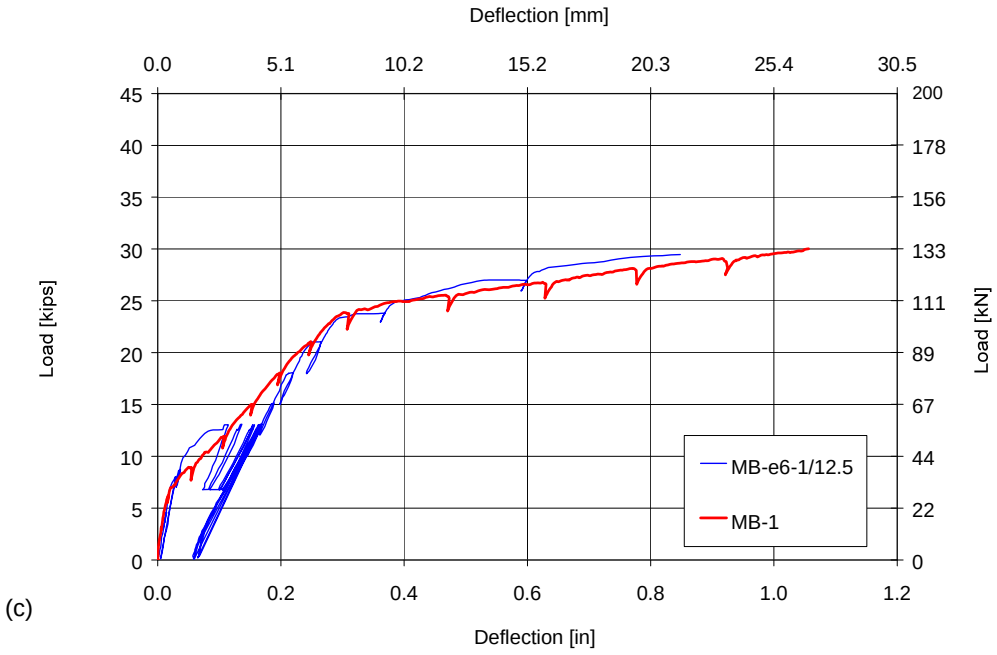

(c)

Figure 5.17: Load-deflection response, MB series (a) MB-e4-1/8 (b) MB-e6-1/8 (c) MB-e6-1/2.5

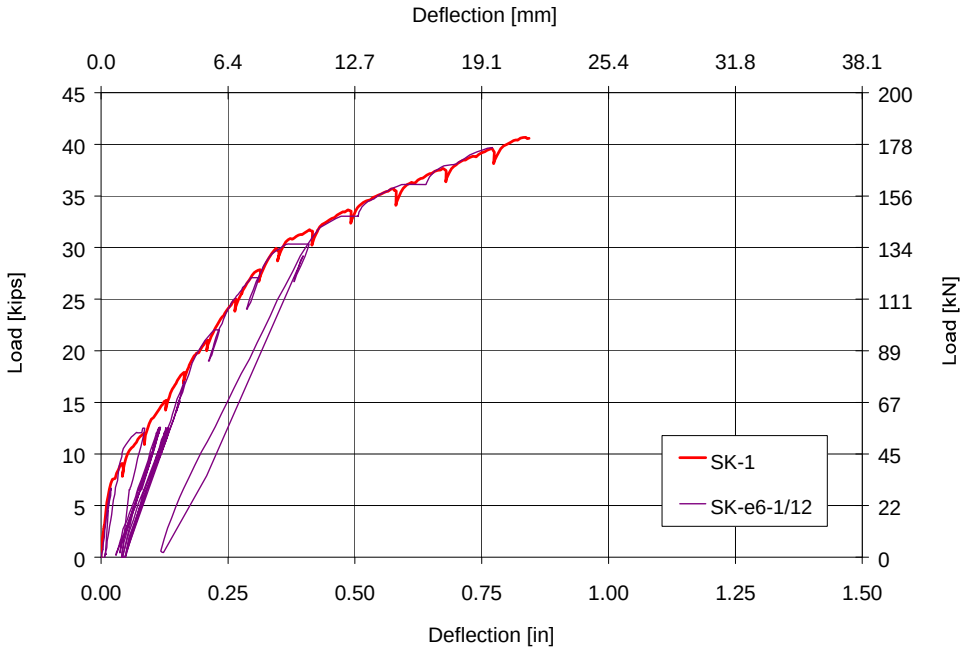

(a)

Figure 5.18: Load-deflection response, SK series (a) SK-e6-1/12 (b) SK-e6-1/17

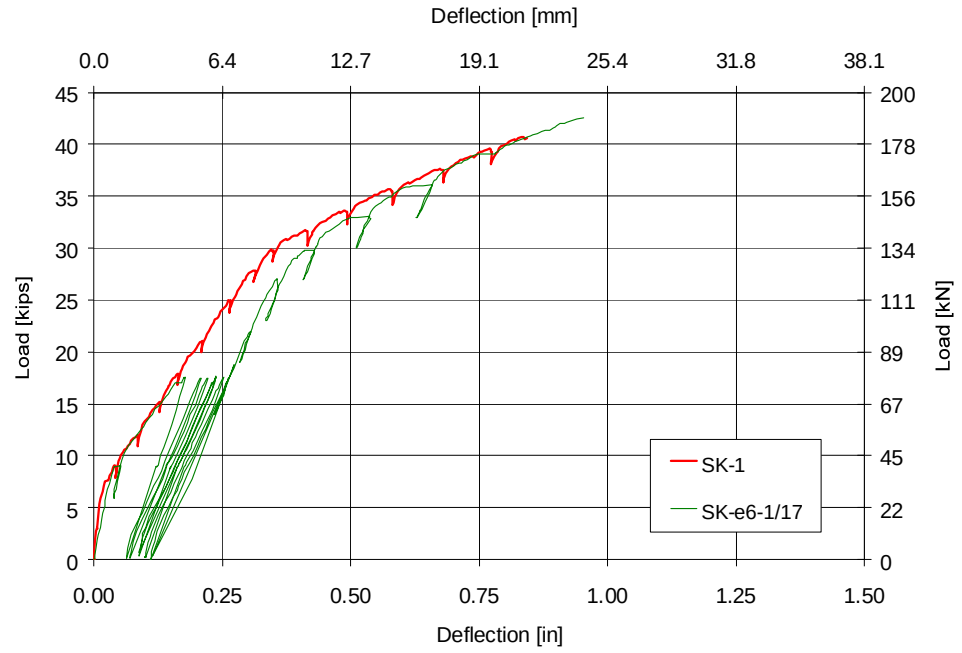

(b)

Figure 5.18: Load-deflection response, SK series (a) SK-e6-1/12 (b) SK-e6-1/17

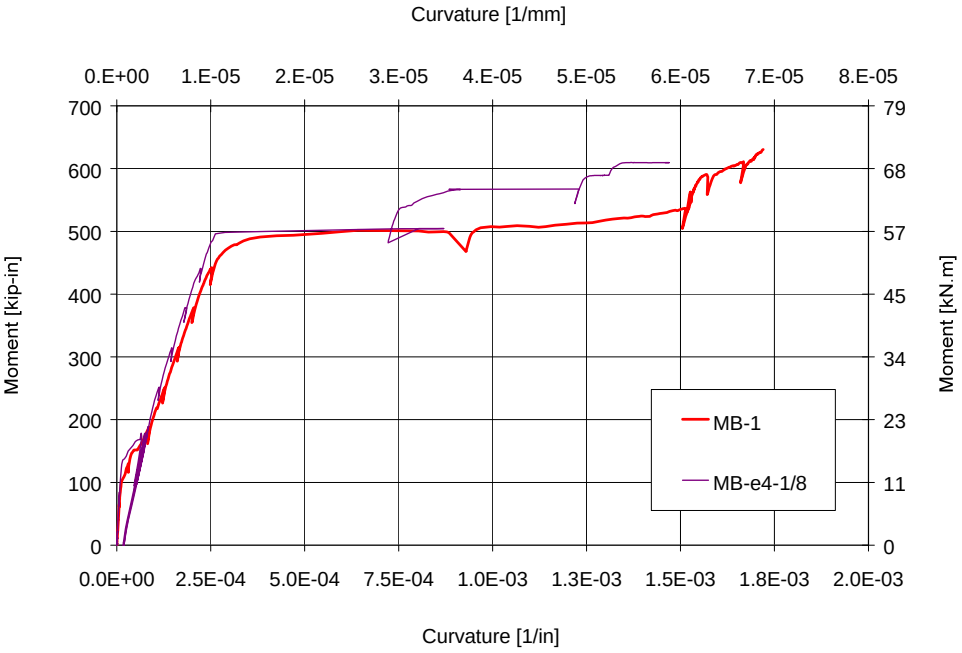

(a)

Figure 5.19: Moment-curvature response, MB series (a) MB-e4-1/8 (b) MB-e6-1/8 (c) MB-e6-1/2.5

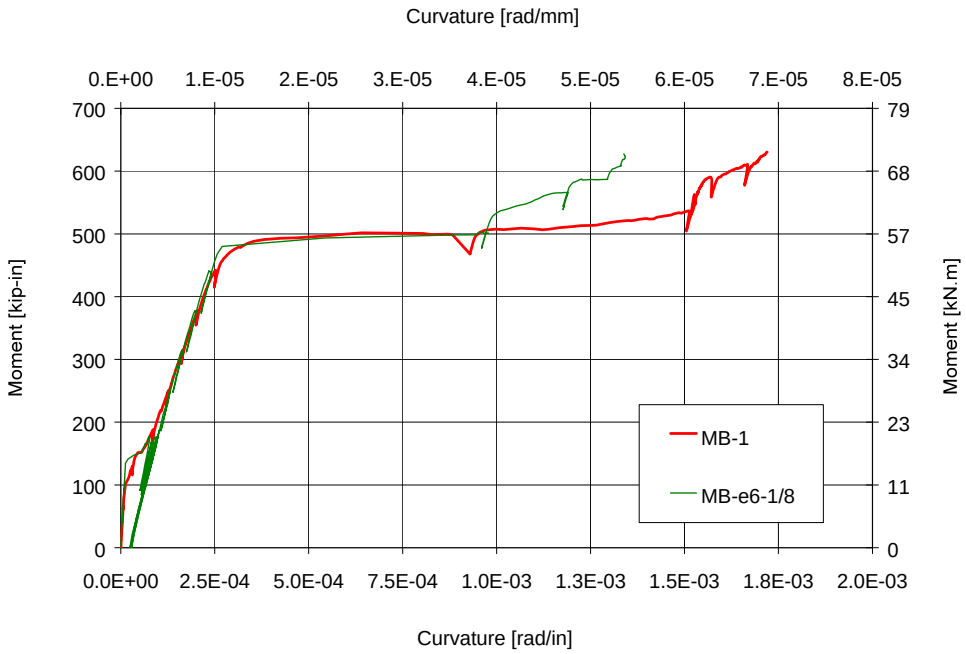

(b)

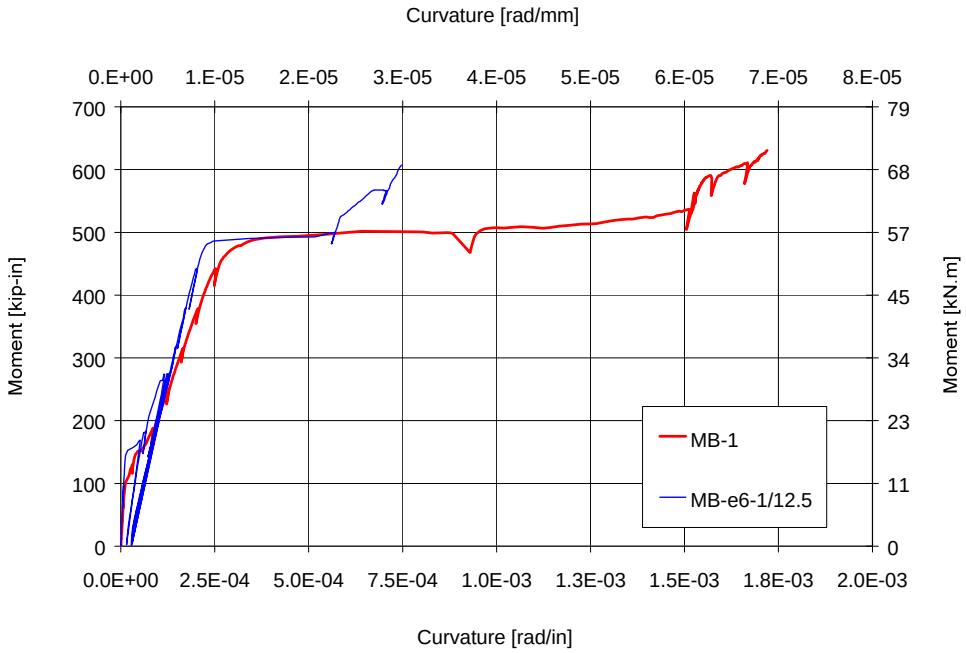

(c)

Figure 5.19: Moment-curvature response, MB series (a) MB-e4-1/8 (b) MB-e6-1/8 (c) MB-e6-1/2.5

The strains over the depth of the section at midspan are displayed in Figure 5.20 for the MB series. Cyclic loading does not seem to affect the composite action of the laminate before slip occurs: sections remain plane at the end of the repeated sequence of loading. As in the monotonic static test (Section 5.3) the assumptions of no-slip composite action of the CFRP laminate and strain compatibility were verified up to yield of the internal reinforcement. After yielding, the laminate exhibited a relatively quick slip to failure.

Cyclic loading affects furthermore the deformation capacity of the section, reducing strains in the reinforcing steel at ultimate by approximately 20% as compared to the strengthened specimen subjected to monotonic static loading. This represents a reduction of approximately 45% compared to the unstrengthened specimen (Figure 5.5).

The strain gage on the CFRP sheet of the beam MB-e6-1/8 was damaged during cycling and replaced prior to static loading. The dashed lines in the corresponding figure represent the corrected data assuming the same strain in the laminate as for beam MB-e4-1/8 subjected to the same cyclic load. Using the corrected data, the same conclusions can be deduced for this specimen as for the other specimens in the MB series.

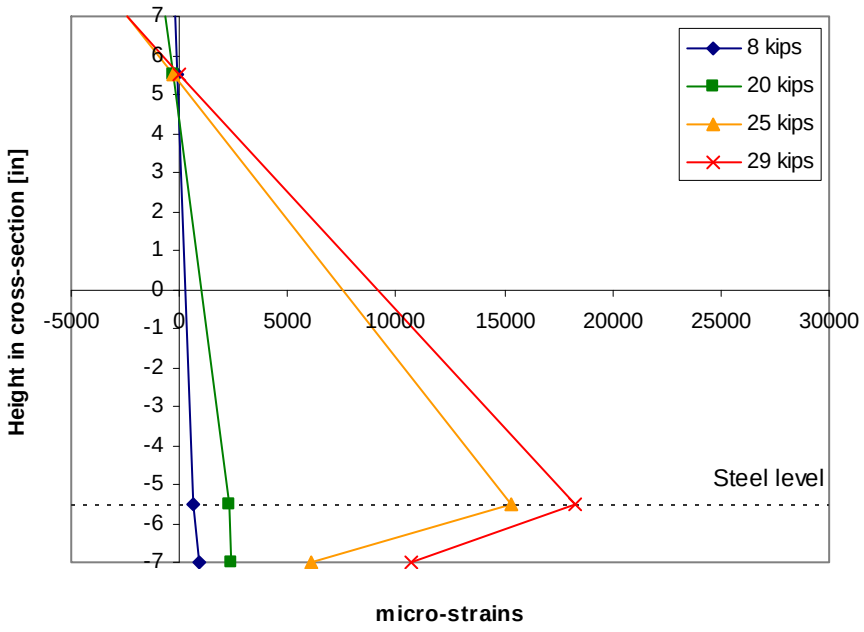

(a)

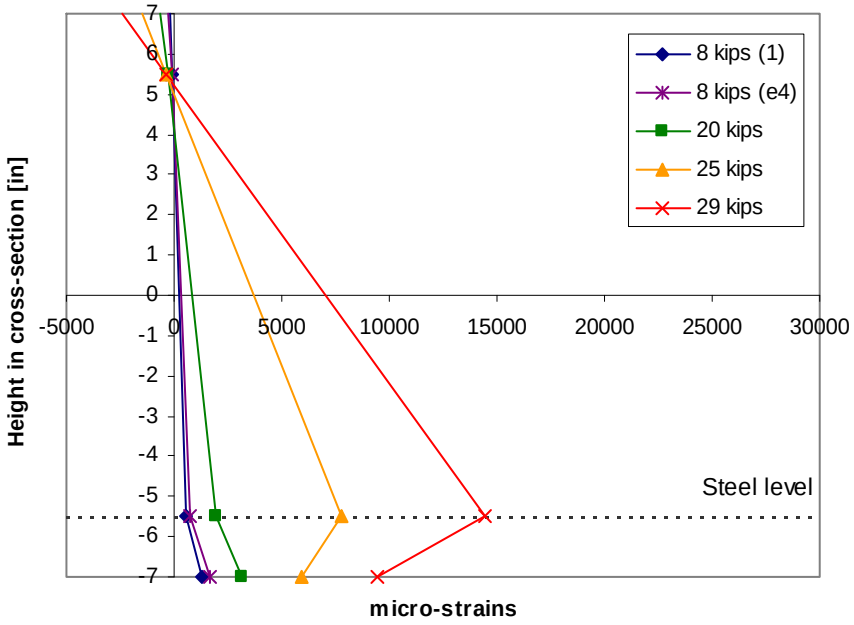

(b)

Figure 5.20: Strains over the section depth at midspan, comparison between beams subjected to cyclic loading and strengthened beam subjected to monotonic static loading in the MB series (a) MB-1 (b) MB-e4-1/8 (c) MB-e6-1/8 (d) MB-e6-1/12.5.

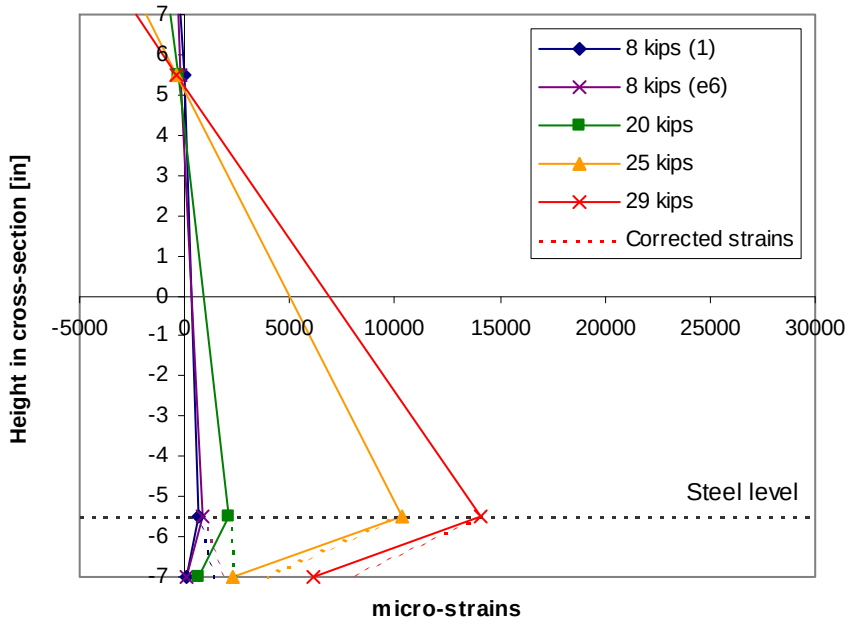

(c)

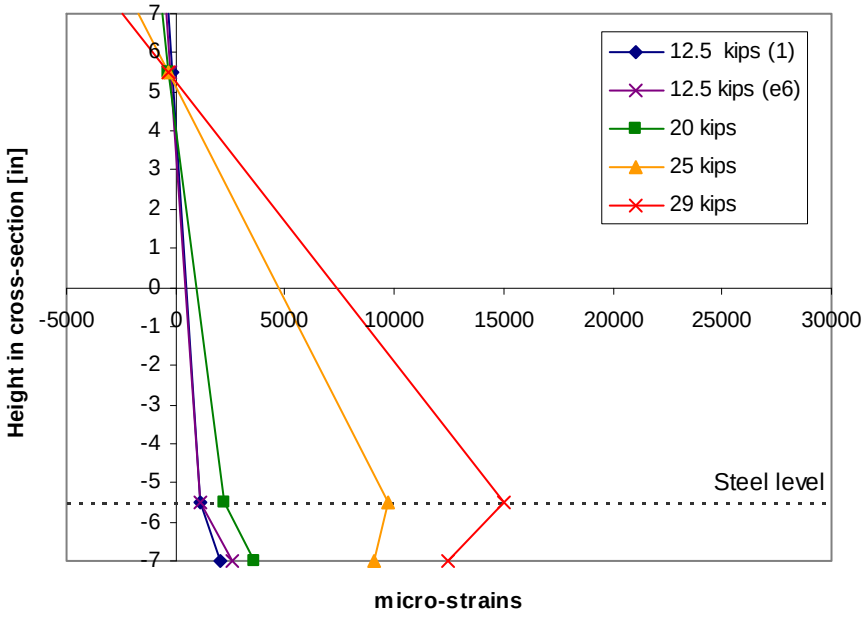

(d)

Figure 5.20: Strains across the section at midspan, comparison between beams subjected to cycling and strengthened beam subjected to direct static loading in the MB series (a) MB-1 (b) MB-e4-1/8 (c) MB-e6-1/8 (d) MB-e6-1/12.5.

5.5.3 Structural ductility

Even though the increase in load capacity constitutes the primary purpose of strengthening, the deformation capacity of the member is another important factor to be considered. An evaluation of the overall structural behavior can be assessed using structural ductility indices, namely, deflection ductility (Equation 5.4) and curvature ductility (Equation 5.5):

Deflection ductility: $$\mu_{\Delta} = \frac{\Delta_u}{\Delta_y} \quad (5.4)$$

Curvature ductility: $$\mu_{\phi} = \frac{\phi_u}{\phi_y} \quad (5.5)$$

where Δ_u is the midspan deflection at ultimate load, Δ_y the midspan deflection at yield load, ϕ_u the curvature in the constant moment region at ultimate load, and ϕ_y the curvature in the constant moment region at yield load.

Calculated ductility indices for each specimen are shown in Figure 5.21 and Figure 5.22. The increase in load capacity of the strengthened specimens is accompanied by a substantial reduction of structural ductility as compared to the unstrengthened control specimen.

For the specimen subjected to static loading, the deflection ductility indices are reduced by 38% and 67% respectively in the MB and SK series, and the curvature ductility shows a reduction of 73% in the MB series as compared with the unstrengthened control specimens. These results compare well with those obtained for RC beams and strengthened beams with transverse anchorage subjected to static loading described by Spadea *et al*. [48].

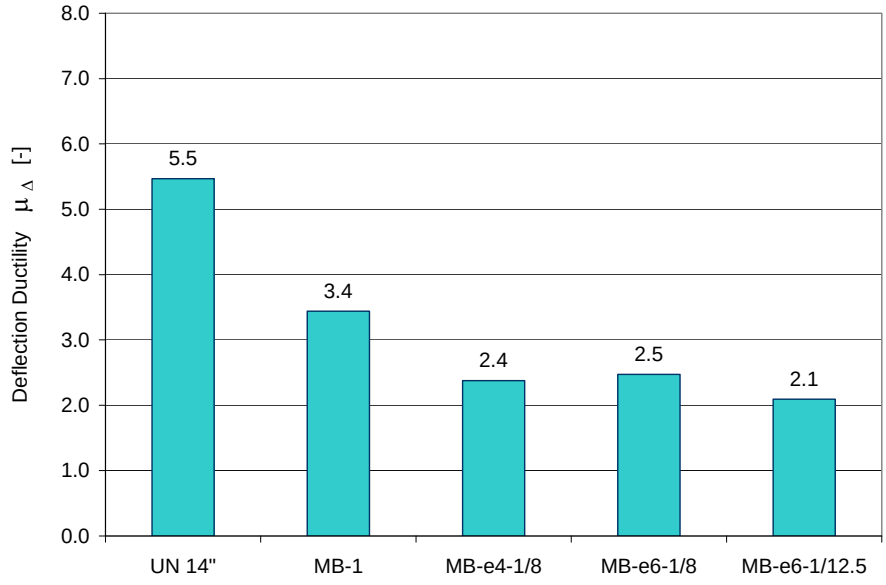

(a)

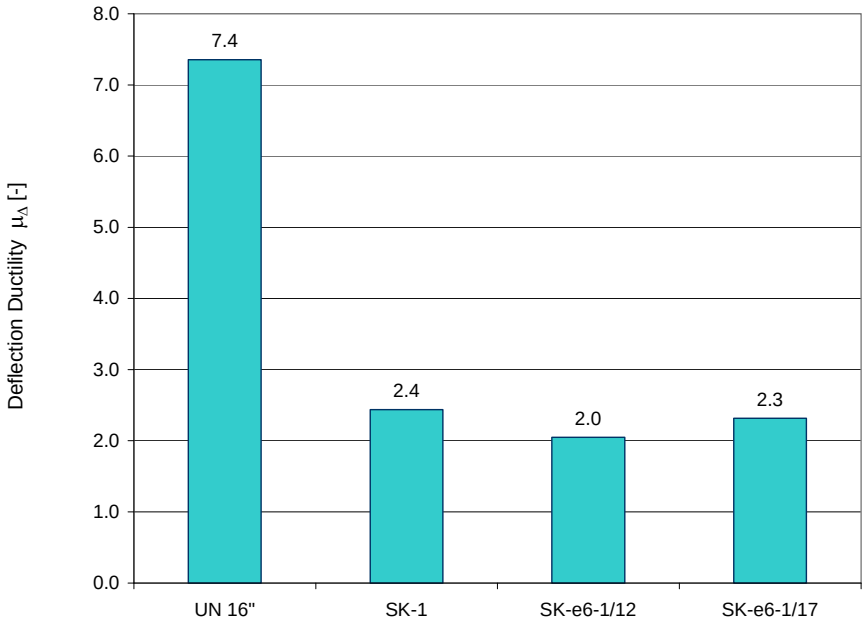

(b)

Figure 5.21: Structural ductility: Deflection ductility indices (a) MB series (b) SK series.

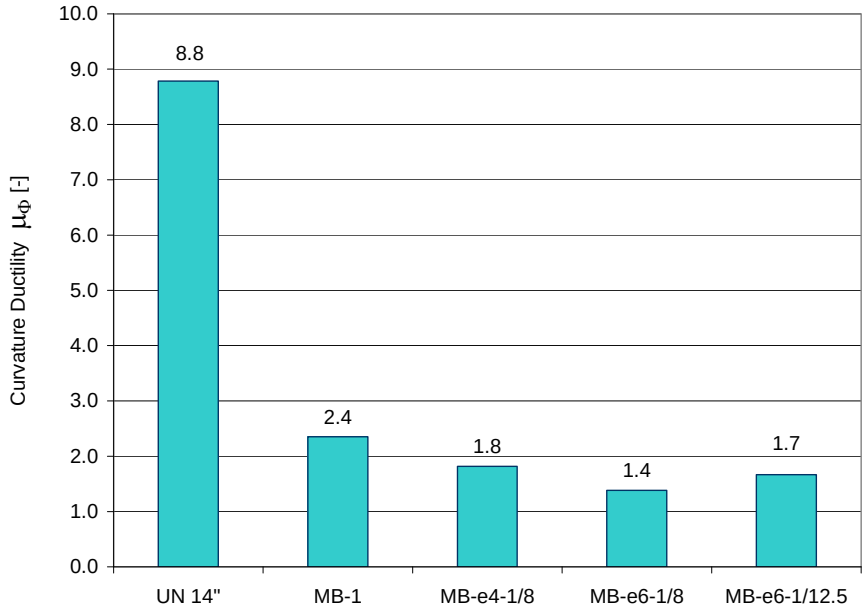

Figure 5.22: Structural ductility: Curvature ductility indices, MB series.

The influence of the repeated loading sequence is shown in Table 5.6. The cycled specimens in both series demonstrate a further decrease in ductility on the order of 25-35% for the deflection ductility and up to 50% for the curvature ductility as compared with the strengthened beam subjected to monotonic static loading. Thus both the pultruded plate system and the wet lay-up system exhibit a comparable reduction in structural ductility.

However, though the structural ductility indices show a substantial decrease for the specimens subjected to cycling, no obvious trend can be deduced from the test results on the influence of the number of cycles or on the influence of the stress range during cycling.

The specimen SK-e6-1/17 performed exceedingly well during the test, exhibiting an ultimate capacity even higher than that of the beam subjected to direct

static loading (Figure 5.18.b). This explains why the deflection ductility of this specimen is close to the value obtained for the control beam SK-1. This result can be considered as part of the unavoidable dispersion related to testing and application procedure.

Table 5.6: Structural ductility: Deflection ductility and curvature ductility

SPECIMEN	DEFLECTION DUCTILITY			CURVATURE DUCTILITY		
	Δ_{max} [in]	μ_{Δ}	Ratio μ_{Δ}	Φ_{max} [1/in]	μ_{Φ}	Ratio μ_{Φ}
MB-1	1.32	3.4	**1.0**	2.1×10^{-3}	2.4	**1.0**
MB-e4-1/8	1.06	2.4	**0.71**	1.46×10^{-3}	1.8	**0.66**
MB-e6-1/8	1.07	2.5	**0.74**	1.32×10^{-3}	1.4	**0.48**
MB-e6-1/12.5	0.85	2.1	**0.62**	7.95×10^{-4}	1.7	**0.48**
SK-1	1.08	2.4	**1.0**	NA	NA	NA
SK-e6-1/12	0.77	2.0	**0.83**	NA	NA	NA
SK-e6-1/17	0.95	2.3	**0.96**	NA	NA	NA
SK-9000-1/33	0.91	NA	NA	NA	NA	NA

Ratios compare ductility of the strengthened beams subjected to fatigue loading with the control specimen subjected to monotonic static loading.

Δ_{max} : Maximum deflection Φ_{max} : Maximum curvature

μ_{Δ} : Deflection ductility index μ_{Φ} : Curvature ductility index

5.5.4 Energy ductility

The energy ductility (Equation 5.6, and Figure 5.23) is another way to evaluate structural ductility taking into account the global load-deflection response:

Energy ductility: $$\mu_E = \frac{E_{tot}}{E_{0.75Pu}} \qquad (5.6)$$

where E_{tot} is the total area under the load deflection-curve up to failure corresponding to the total energy of deformation, and $E_{0.75Pu}$ is the area under the load-deflection curve up to 75% of the ultimate load corresponding to the elastic energy [48]. The definition of the elastic energy at 75% of the ultimate capacity was adopted because it corresponds approximately to the load at which the reinforcing steel yields in the control unstrengthened specimen (Figure 5.2).

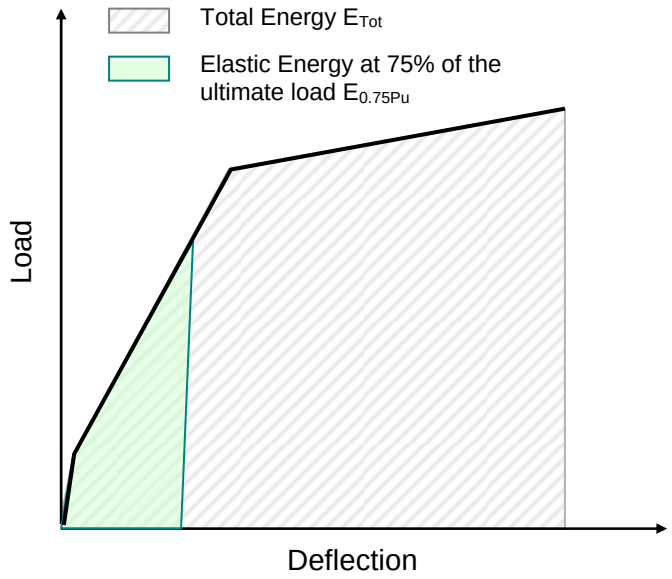

Figure 5.23: Definition of energy ductility, Spadea *et al.* [48].

Because all the strengthened specimens reached approximately the same maximum load, the total energy of deformation presented in Figure 5.24 provides an indication of the deformation capacity of the beam. However it does not give a description of the structural behavior. The total energy of the strengthened beams subjected to static loading represents 45 to 55% of the energy of the unstrengthened specimens.

Cycling also affected the total energy. In the MB series, the total energy is reduced with increasing number of cycles and increasing peak load during cycling. In the SK series, the total energy decreases with number of cycles except specimen SK-e6-1/17 which showed no reduction as compared to specimen SK-e6-1/12. This specimen performed remarkably well during the test, demonstrating an ultimate capacity and a total energy of deformation even higher than that of the beam subjected to direct static loading (Figure 5.18.b). This result is indicative of the scatter related to testing and the application procedure for the CFRP materials.

The energy ductility indices are summarized in Figure 5.25. The energy ductility is reduced considerably when using CFRP materials to strengthen the beam. For specimen MB-1, the energy ductility index of the strengthened beam represents approximately 55% of the index for the unstrengthened beam, whereas this ratio drops off to 30% for specimen SK-1. This analysis is thus consistent with the more ductile failure mode observed for the beam MB-1 (Section 5.3.3).

In the two series, the energy ductility does not appear to be reduced by the repeated sequence of loading. In the SK series, the energy ductility indices obtained for the two specimens subjected to cycling are equal to the energy ductility of the control specimen. For the MB series, a slight decrease on the order of 5 to 17% is observed. However, no obvious trend can be obtained from the test results for either the influence of the number of cycles or the stress range during cycling.

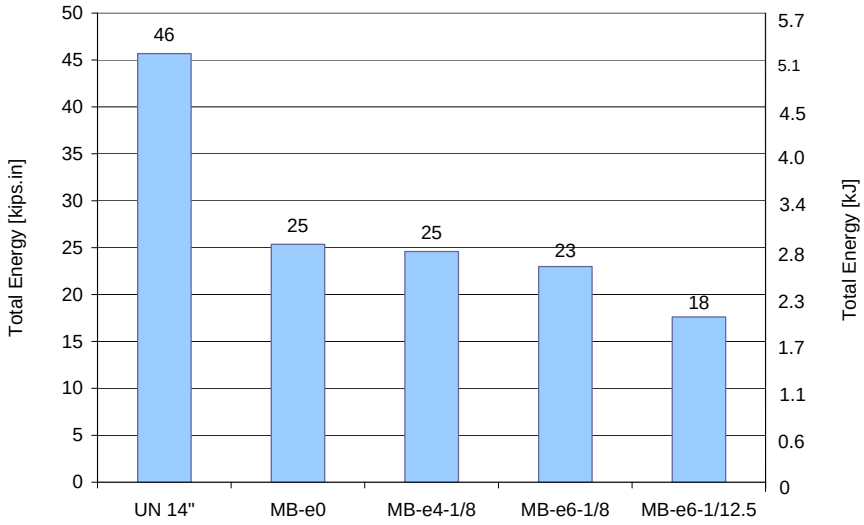

(a)

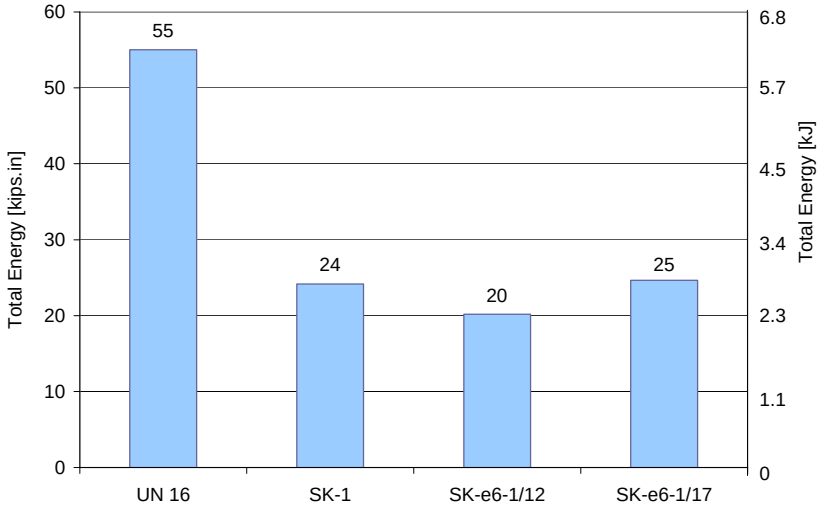

(b)

Figure 5.24: Total energy of deformation (a) MB series (b) SK series.

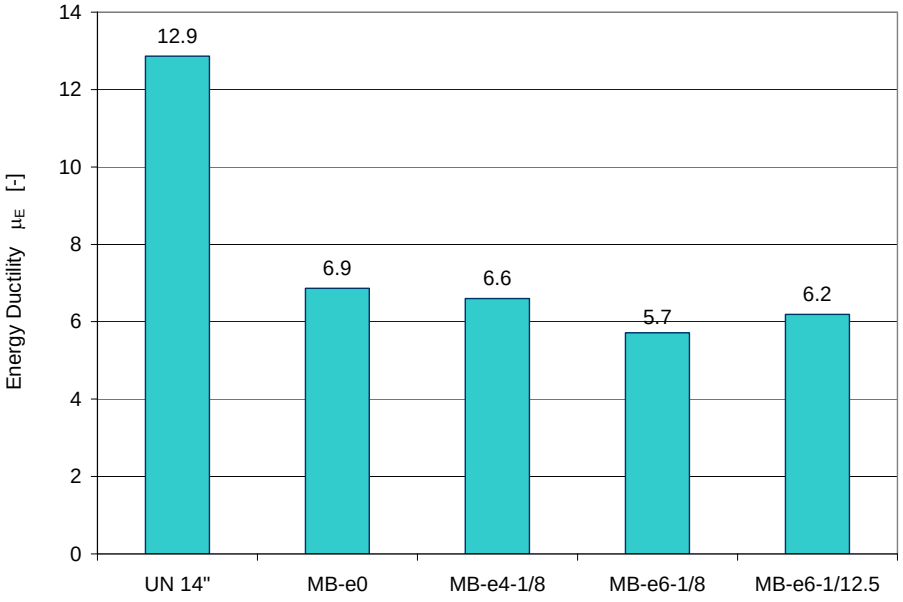

(a)

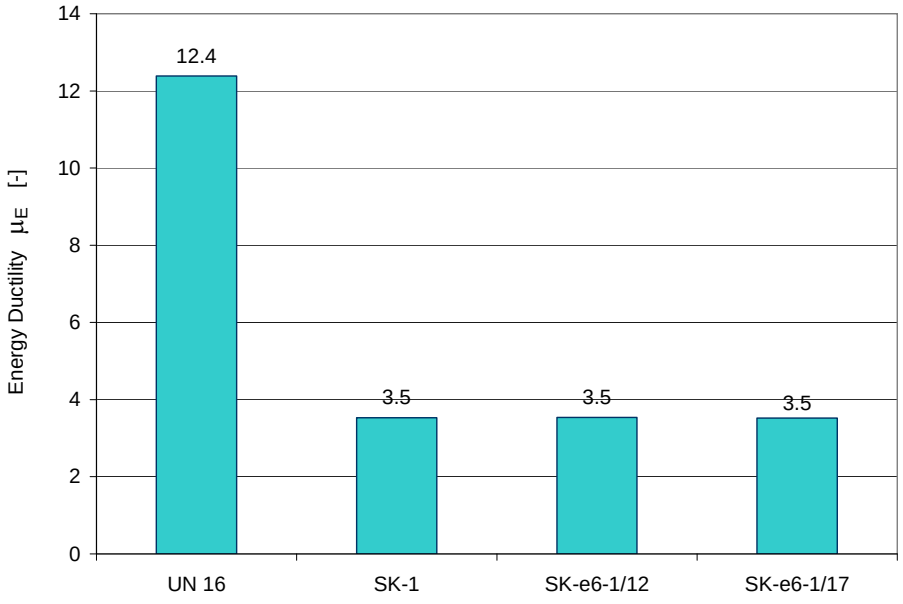

(b)

Figure 5.25: Structural ductility: Energy ductility indices (a) MB series (b) SK series

Table 5.7: Energy ductility

SPECIMEN	ENERGY DUCTILITY		
	E_{tot} [kips.in]	μ_E	μ_E(fatigue) /μ_E(static)
MB-1	25	6.9	**1.0**
MB-e4-1/8	25	6.6	**0.95**
MB-e6-1/8	23	5.7	**0.83**
MB-e6-1/12.5	18	6.2	**0.94**
SK-1	24	3.5	**1.0**
SK-e6-1/12	20	3.5	**1.0**
SK-e6-1/17	25	3.5	**1.0**
SK-9000-1/33	NA	NA	NA

Ratio compares the energy ductility of the strengthened beams subjected to fatigue loading with the control specimen subjected to monotonic static loading.

E_{tot} : Total energy of deformation

μ_E : Energy ductility index

NA: Not available

Spadea *et al.* [48] noted that the definition of energy ductility proposed in Equation 5.6 would need further examination. In order to investigate other ways to assess energy ductility, another definition proposed by Jeong [29] was also used in the analysis (Equation 5.7 and Figure 5.24).

Energy ductility: $$\mu_E = \frac{1}{2}\left(\frac{E_{tot}}{E_{el}} + 1\right) \qquad (5.7)$$

where E_{tot} and E_{el} are respectively the total energy of deformation and elastic energy of deformation at ultimate load, defined in Figure 5.26.

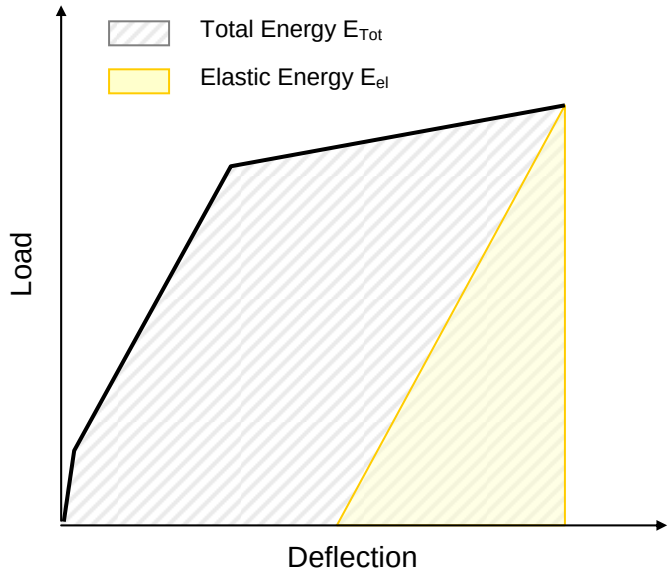

Figure 5.26: Definition of the energy ductility, Jeong [29].

The definition of energy ductility in Equation 5.7 was intended to be used to describe structural ductility of concrete beams prestressed using FRP tendons; the total energy and elastic energy being computed on the basis of the stress-strain response of the FRP tendon.

When applied to the test specimens, the results obtained showed random variations. This could be explained by the fundamentally different behavior of the two types of structures. Actually, concrete beams prestressed using FRP tendons exhibit large deformations at rupture and have an elastic energy of deformation at ultimate load in the neighborhood of the total energy. In the case of RC beams strengthened using externally bonded CFRP materials, the elastic energy at ultimate load is relatively small as compared to the total energy. Therefore, small variations in stiffness or ultimate load may greatly affect the energy ductility index as defined by Equation 5.7.

On the basis of the limited number of tests in this study, it appears that the definition of energy ductility as defined by Equation 5.7 is not appropriate to describe the behavior of RC beams strengthened using externally bonded CFRP materials.

5.5.5 Failure mode

The overall failure mode observed for the specimens subjected to cyclic loading in the SK series (with the exception of beam SK-9000-1/33) is similar to that for the monotonically loaded specimens (Section 5.3.3). Failure occurred by debonding of the plate at midspan (Figure 5.29), and strains in the CFRP plate reached the same elongation (0.62 to 0.65%). The crack patterns (Figure 5.27) showed an increase in damage due to cyclic loading when compared with the monotonically loaded tests as described in Section 5.3.3.

For the specimen SK-e6-1/12, debonding occurred sequentially on one side of the beam, then on the other. As a result, at the time of failure, the beam was subjected to a moment in the transverse direction that forced the cracks all the way to the top of the beam. After failure, cracks had penetrated half the width of the beam.

Compared to the control-strengthened specimen, beams subjected to cycling in the MB series demonstrated a totally different mode of failure. In this case, failure was initiated by debonding of the longitudinal sheet in the shear span. Debonding propagated suddenly, pulling off the straps and leading to complete failure of the strengthening system (Figure 30.a and c). Examination of the laminate surface (Figure 5.30.b) shows rupture in the bond interface between the epoxy and concrete: few pieces of concrete were pulled off along the laminate, and the concrete surface under the laminate was still relatively smooth (Section 2.3.2, Figure 2.13, mode 7).

Closer analysis of the beam soffits revealed that debonding was actually due to an uneven concrete surface resulting from a high spot on the form where the specimens were cast. The primary failure mode thus corresponds to the mode 5.b as described in Section 2.3.2 and Figure 2.13. The rupture of the bond interface being was a secondary failure.

The concrete surface at midspan (Figure 5.30.a) shows the evolution of cracking in the shape of a delta in the vincity of the laminate. Concrete wedges, formed by primary flexural cracks and diagonal cracks at the bottom face of the beam, pulled off from the surface.

Moreover, in both series, the CFRP transverse anchorage straps seem to act as external shear reinforcement. In the shear span, cracks due to flexure-shear interaction grew toward the load point at 45°. When reaching a transverse strap,

the cracks changed their initial direction and followed the direction of the carbon fibers (Figure 5.31).

In every case, rupture of the strengthening system was preceded well in advance by loud cracking noises in the concrete and in the composite material.

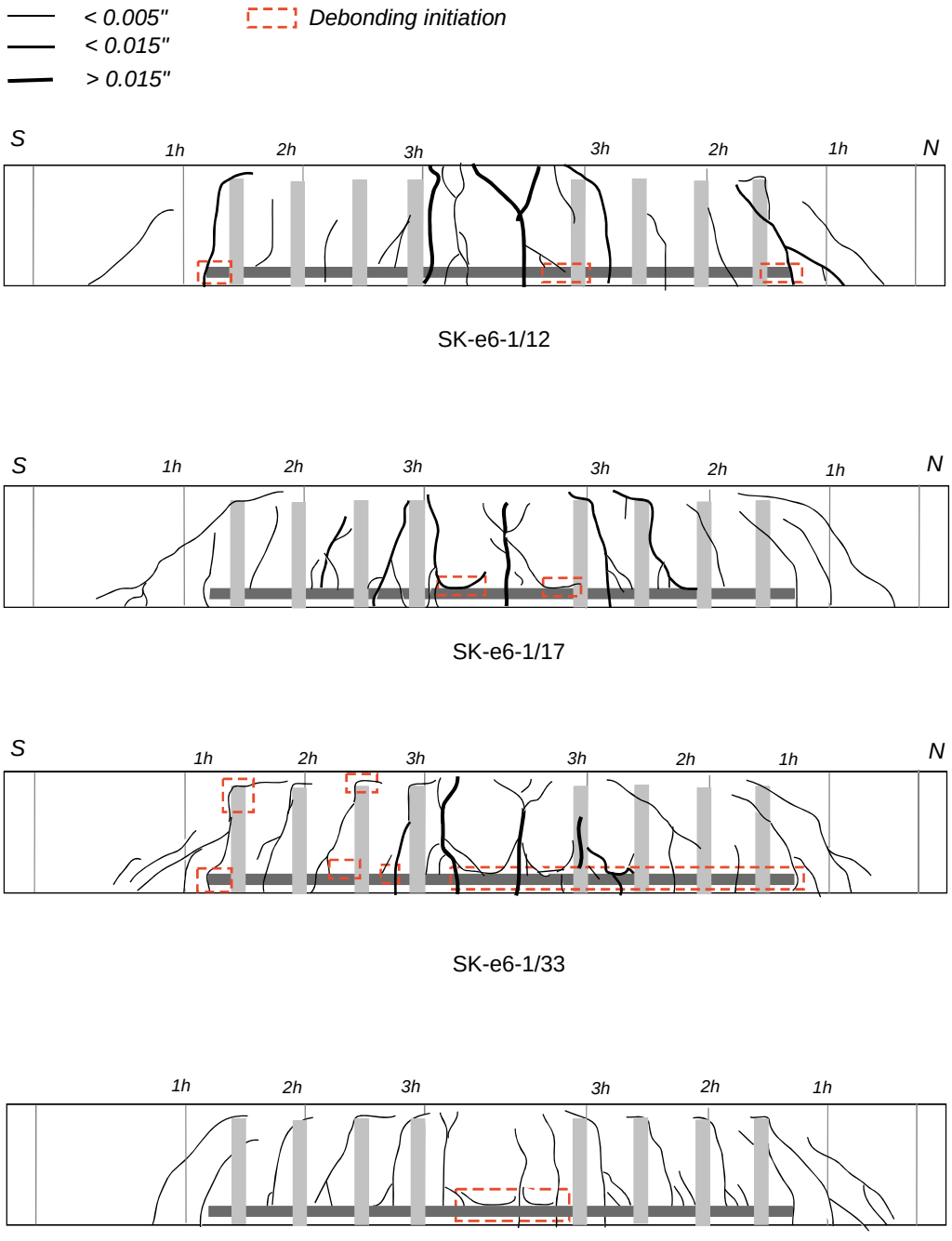

Figure 5.27: Crack pattern, SK series

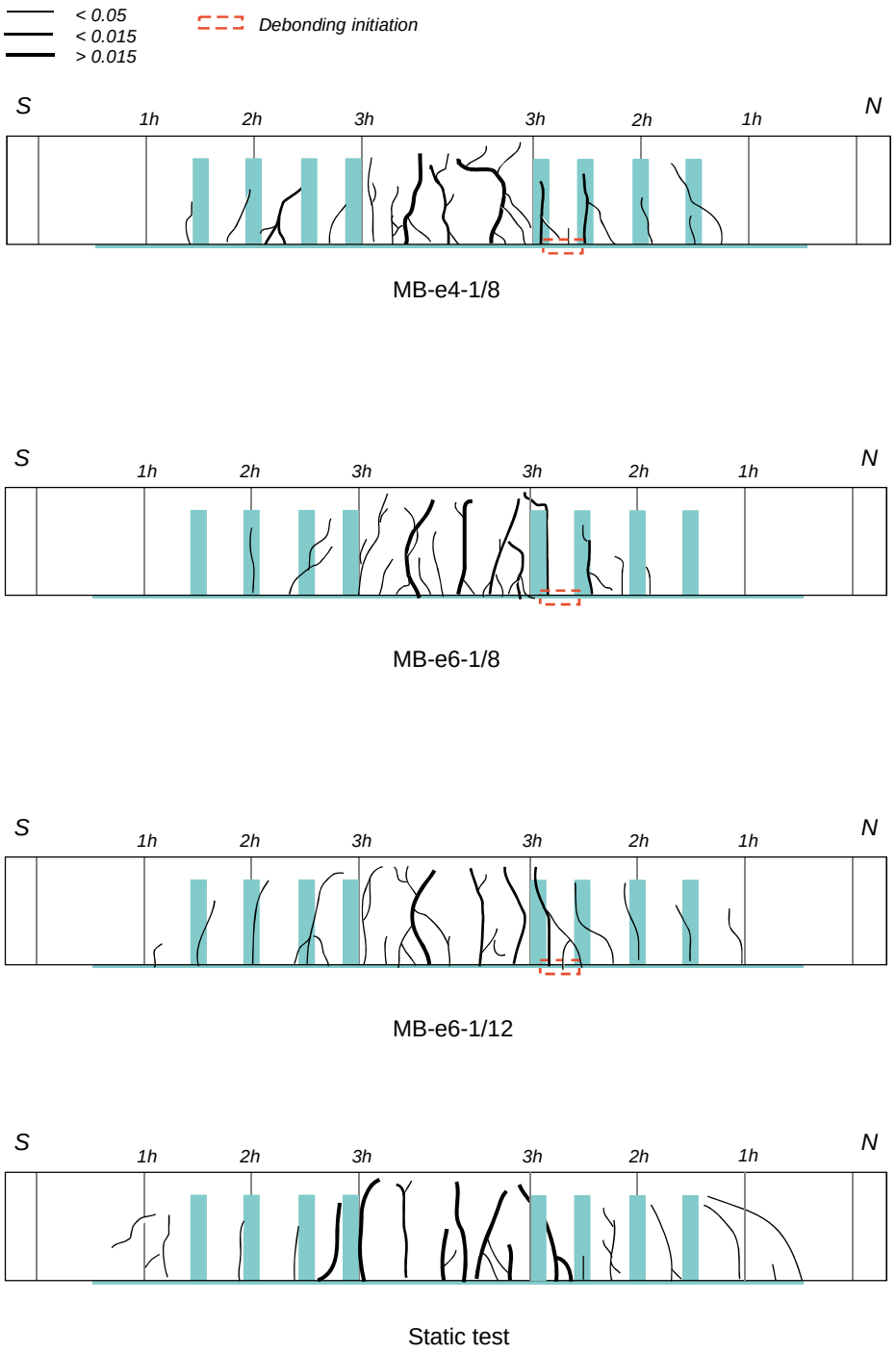

Figure 5.28: Crack pattern, MB series

Figure 5.29.a: Debonding at midspan (SK-e6-1/17)

Figure 5.29.b: Debonding at midspan (SK-e6-1/12)

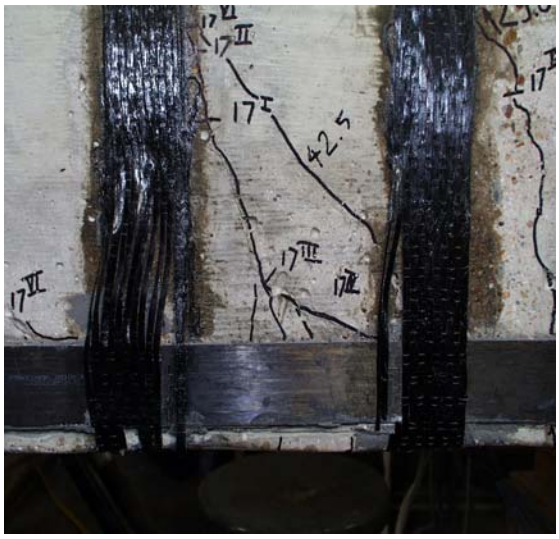

Figure 5.29.c: Progression of cracking in debonding zone; effect of anchorage on crack direction; slipping of plate at rupture (SK-e6-1/17)

Figure 5.29.d: Plate-concrete interface: delamination of concrete (SK-e6-1/17)

Figure 5.29: Failure mode of beams SK-e6-1/17and SK-e6-1/12 under static loading after cycling.

Figure 5.30.a: Debonding and slipping of longitudinal sheet initiated between the 2nd and 3rd strap; propagation of debonding along beam.

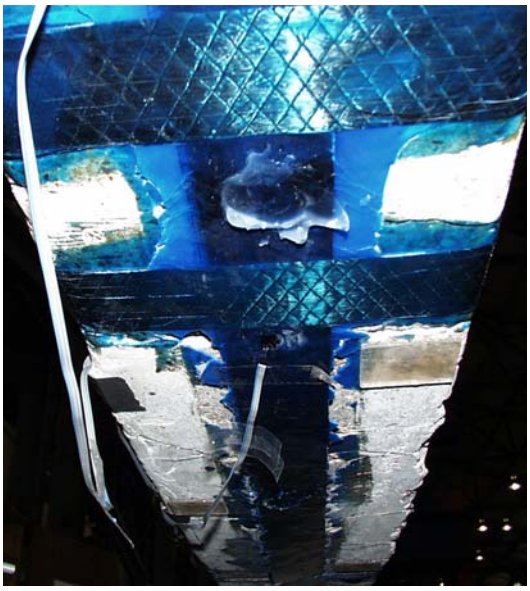

Figure 5.30.b: Debonding of longitudinal sheet (zoom Figure 5.30.a)

Figure 5.30.c: Sheet-concrete interface; concrete wedges pulled off at rupture; cracking in debonding initiation zone; few concrete pieces attached along the laminate

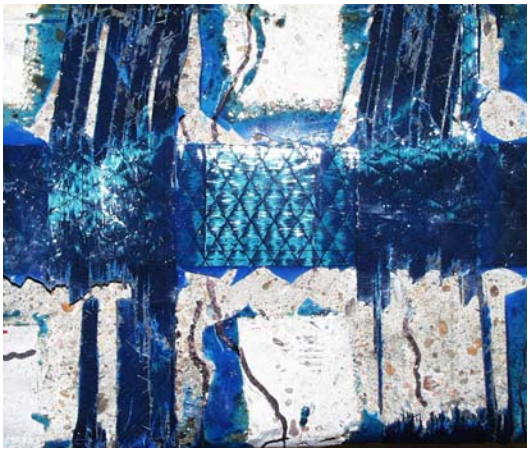

Figure 5.30.d: Transverse anchorage pulled off by debonding and slipping of longitudinal sheet; smooth concrete surface under longitudinal laminate

Figure 5.30: Failure mode of the specimen MB-e4-1/8 under static loading after cycling.

(a) (b)

Figure 5.31: Progression of flexural-shear cracks under transverse straps, beam MB-e6-1/8

(a) Crack during cycling (b) Inspection after rupture

5.6 Summary

The static response of the rectangular R/C test specimens strengthened using externally bonded CFRP materials was characterized by a large increase in load capacity along with a substantial decrease in deformation capacity. The different structural ductility indices used to quantify the reserve of plastic deformation, showed a drop off on the order of 40 to 70% as compared with the unstrengthened RC specimens. The failure mode was mainly governed either by debonding or by rupture of the longitudinal CFRP laminate.

During cycling, strengthened specimens exhibited a steady increase in deformations along with a loss of static stiffness. Under service-load conditions,

corresponding to stress ranges of either 33 or 53% of the reinforcing steel yield stress, damage at the bond interface initiated by local defects did not show evidence of propagation. In contrast, cycling with a stress range around yield of the reinforcing steel severely altered the concrete-adhesive interface. As a result, failure of the strengthening system occurred by sudden debonding of the laminate before reaching the fatigue limit of the reinforcing bars.

The post-cyclic static response demonstrated that the load capacity was not apparently affected by cycling. However, the deformations at ultimate appeared to be reduced. Structural ductility indices used to evaluate plastic deformations showed a decrease on the order of 25-50% as compared with the control strengthened beams tested monotonically to failure, indicating a reduction of the deformation capacity due to cycling. However, on the basis of the limited number of tests performed in the experimental program, no conclusion can be made with respect to either the particular influence of stress range under service-load conditions, or the number of cycles.

Another evaluation of structural ductility using an energy approach showed contrasting results. Specimens strengthened using the wet lay-up system demonstrated a decrease in the energy ductility on the order of 5-17%, whereas specimens strengthened using the pultruded plate system did not seem to be affected by the repeated load sequence. Therefore, no obvious trend can be deduced from the test results using energy ductility.

CHAPTER 5 PRESENTATION AND DISCUSSION OF TEST RESULTS 81

Chapter 6 Conclusions

Advanced composite materials applied for strengthening and rehabilitation of civil structures have been tested in laboratories for fifteen years. Research on reinforced concrete elements strengthened using externally bonded Fiber Reinforced Polymer (FRP) materials have demonstrated that the technique enhances both flexural and shear capacities, and provides a more uniform distribution of cracks. Several field applications of this strengthening method have been reported and designers are presently considering the use of FRP composites as an option to strengthen existing structures. However, current design practice is mainly based on experimental studies and no consensus-based design guideline or code are yet available.

Ongoing research to promote further knowledge in this field includes development of efficient anchorage of the FRP material to the concrete element, non-destructive evaluation of the bond interface, and assessment of long-term behavior, particularly under sustained loading, environmental exposure, and repeated loading.

The experimental program reported herein was intended to contribute to the knowledge on the response of reinforced concrete members strengthened using externally bonded Carbon FRP materials under fatigue loading. Previous static loading tests conducted at the Phil M. Ferguson Structural Engineering Laboratory identified optimal configurations of CFRP laminates providing a desired flexural strength increase. The fatigue program focused on damage propagation in the concrete and in the bond interface in order to assess the influence of repeated loading on post-cyclic static behavior.

A total of six specimens were tested under various stress ranges representative of service loading conditions and potential overloading. Monotonic static tests to failure were conducted on five specimens after they had undergone a repeated loading sequence to a maximum number of 1,000,000 cycles.

Increases in deflection and loss of initial static stiffness observed during cycling resulted in permanent deformation at the end of cyclic loading. This phenomenon can be attributed to damage accumulation and is consistent with the overall behavior of reinforced concrete structures. Therefore this does not necessarily reflect the influence of the CFRP composite materials bonded for strengthening. Moreover, under service-load conditions no visual evidence of damage propagation at the concrete-composite bond interface was observed.

Specimens that survived the repeated load sequence were tested statically to failure. The ultimate capacity was not apparently affected by the fatigue loading. However, ultimate deformations appeared to be reduced, as well as structural ductility, which was used to describe the reserve plastic deformation of the strengthened member.

On the other hand, the fatigue performance under high stress range, around the yield stress of the reinforcing steel, appeared to be controlled by the adhesive-concrete interface. At this load level, damage at the bond interface propagated rapidly and fatigue failure occurred by sudden debonding of the laminate.

Finally, the efficiency of the strengthening system is highly sensitive to workmanship and can be altered by any imperfection in the bond interface. Therefore, meticulous control of the application process and non-destructive evaluation of the strengthening system, such as infrared inspection, is required for a safe use of this technique.

Table 5.3: Evolution of debonding during cycling

SPECIMEN	PEAK LOAD		STRESS RANGE IN REBARS		OBSERVED DAMAGE IN THE LAMINATE
	[kips]	[kN]	[ksi]	[MPa]	
MB-e4-1/8	8	35.6	22	152	No evidence of damage at the bond interface
MB-e6-1/8	8	35.6	22	152	No evidence of damage at the bond interface
SK-e6-1/12	12	53.4	22	152	No evidence of damage at the bond interface
MB-e6-1/12.5	12.5	55.6	33	228	Debonding initiation at 5 locations, no propagation
SK-e6-1/17	17	75.6	33	228	Debonding initiation at 9 locations, no propagation
SK-9000-1/33	33	147	63	434	Progression of debonding leading to failure

(a) (b)

Figure 5.8: Initiation of debonding of the longitudinal laminate during cycling

(a) Beam MB-e6-1/12.5: Local debonding after 125,000 cycles at the location of the crack initiator

(b) Beam SK-e6-1/17: Debonding initiation after 250,000 cycles: cracks spread as they reached the CFRP plate

APPENDICES

Appendix A: Unit conversions

Table A.1: Conversion from Imperial to SI units

IMPERIAL / SI UNITS CONVERSION			
DIMENSION	**IMPERIAL UNITS**		**SI UNITS**
Weight	1 pound	1lb	0.454 kg
	1 ton (imperial ton)	1 ton	0.907 t
Density	1 pound per cubic foot	1 lb/cu ft	0.016
Length	1 inch	1 in.	25.4 mm
	1 foot	1 ft	0.305 m
Surface	1 square inch	1 sq in.	645 mm^2
	1 square foot	1 sq ft	0.0930 m^2
Volume	1 cubic foot	1 cu ft	0.0283 m^3
Force	1 pound force	1 lbf	4.45 N
	1 kilo pound force	1 kip	4.45 kN
Moment	1 pound force. foot	1 lb-ft	1.36 N.m
	1 kilo pound force. foot	1 kip-ft	1.36 kN.m
Stress	1 pound force per sq inch	1 psi or 1 lbf/sq in.	6.89 N/m^2
	1 kilo pound force per sq inch	1 kpsi	6.89 N/mm^2 or MPa

Table A.2: Conversion from SI units to Imperial units

SI UNITS / IMPERIAL CONVERSION			
DIMENSION	**SI UNITS**		**IMPERIAL UNITS**
Weight	1 kilogram	1 kg	1.83 lb
	1 ton (metric ton)	1 t	1.102 ton
Density	1 gram per cubic centimeter	1 g/cm^3	62.43 lb/cu ft
Length	1 meter	1 m	3.28 ft
	1 millimeter	1 mm	0.394 in.
Surface	1 square meter	1 m^2	10.76 sq ft
	1 square millimeter	1 mm^2	1.55x10-3 sq in.
Volume	1 cubic meter	1 m^3	35.3 cu ft
Force	1 Newton	1 N	0.225 lbf
	1 kilo Newton	1kN	0.225 kip or 0.1004 tonf
Moment	1 Newton. meter	1 Nm	0.738 lbf-ft
	1 kilo Newton. meter	1 kNm	0.738 kip-ft
Stress	1 Newton per sq meter	1 N/m^2	0.0209 lbf/sq ft
	1 Newton sq millimeter or 1Mega Pascal	1 N/mm^2 = 1 MN/m^2 or 1 MPa	145 lbf/sq in. or 0.145 ksi

Appendix B: Ultimate flexural capacity of test specimens

This Appendix presents the detail of the hand computation for the theoretical ultimate flexural capacity of the two types of beams tested.

Preliminary design

The preliminary design yields the maximum amount of composite that should be used to strengthen a RC rectangular beam in order to obtain a ductile mode of failure. The Equations used herein are developed in Chapter 3.

- **Preliminary design for the MB series:**

(3.1): $$x = \frac{0.0035}{0.0035 + 0.015} \times 14 = 2.65 in.$$

(3.4): $$t_{L,\max} = \frac{0.8 \times 2.65 \times 8 \times 5.5 - 0.62 \times 60}{505 \times 2} = 0.0055 in.$$

$$t_L \cong 0.8 \times t_{L,\max} = 40 mil \quad (> 13 mil)$$

- **Preliminary design for the MB series:**

(3.1): $$x = \frac{0.0035}{0.0035 + 0.010} \times 16 = 4.15 in.$$

(3.4): $$b_{L,\max} = \frac{0.8 \times 4.15 \times 8 \times 5.5 - 0.62 \times 60}{348 \times 0.00472} = 6.62 in.$$

$$b_L \cong 0.8 \times b_{L,\max} = 5.3 in. \quad (> 2 \times 2 in.)$$

According to the preliminary design, the amount of composite used to strengthen the test specimen should trigger a ductile mode of failure, assuming a perfect bond of the laminate to failure.

Ultimate flexural capacity

The procedure proposed in Section 3.3.2 to compute the ultimate bending moment requires the determination of the neutral axis using iterative process. The first iteration for the MB series is presented below, and Table B.1 summarizes the iterations necessary to obtain the position of the neutral axis, x, with sufficient precision for the two series:

- **First iteration, MB series:**

A first approximation of the position of the neutral axis is given by the preliminary design:

$$x^0 = 2.5in.$$

The corresponding strain in the extreme top fiber is given by Equation (3.16):

$$\varepsilon_C{}^0 = \frac{0.65 \times 0.015}{12.5} x_0$$

The stress-bloc coefficient is then obtained by Equation (3.10):

$$\chi_1{}^0 = \frac{3000 \times \varepsilon_C{}^0 - 2}{3000 \times \varepsilon_C{}^0} = 0.685$$

A new value of the neutral axis position can thus be deduced using Equation (3.17), leading to a new iteration:

$$x_1{}^1 = \frac{0.62 \times 60 + 2 \times 0.0013 \times 505}{\chi_1{}^0 \times 8 \times 5.5} = 1.669 \ \ in.$$

Table B.1: Position of the neutral axis (first part).

Step i	Parameter	MB series	SK series
i = 0	x^i [in.]	2.500	2.4
	ε_C^i	0.002120	0.001289
	χ_1^i	0.6854	0.5061
i = 1	x^i [in.]	1.6687	4.62 Replaced by: 3.5*
	ε_C^i	0.001394	0.20682
	χ_1^i	0.5100	0.6777
i = 2	x^i [in.]	2.2228	3.4512
	ε_C^i	0.001845	0.002030
	χ_1^i	0.6389	0.67160
i = 3	x^i [in.]	1.7900	3.482
	ε_C^i	0.001430	0.002054
	χ_1^i	0.5445	0.6755
i = 4	x^i [in.]	2.1007	23.46
	ε_C^i	0.0017213	0.002040
	χ_1^i	0.61374	0.6720

Table B.1: Position of the neutral axis (Second part).

Step i	Parameter	MB series	SK series
i = 5	x^i [in.]	1.8638	3.47
	$\varepsilon_C^{\,i}$	0.001497	-
	$\chi_1^{\,i}$	0.56184	-
i = 6	x^i [in.]	2.030 Replaced by 1.95*	-
	$\varepsilon_C^{\,i}$	0.001578	-
	$\chi_1^{\,i}$	0.5815	-
i = 7	x^i [in.]	1.967	-
	$\varepsilon_C^{\,i}$	0.001594	-
	$\chi_1^{\,i}$	0.5853	-
i = 8	x^i [in.]	1.95	-

*Average value between steps (i-1) and (i) in order to accelerate the convergence.

Results:

- MB series: $x = 1.95$ *in.*
- SK series: $x = 3.47$ *in.*

The stress bloc coefficient χ_2 is computed using Equation (3.13) for the MB series and (3.11) for the SK series:

- MB series: $\chi_2 = 0.363$
- SK series: $\chi_2 = 0.376$

Then the ultimate bending moment is deduced using Equation (3.18):

$$M_u = A_S f_{yS}(d - \chi_2 x) + A_L f_{Lu}(d_L - \chi_2 x) \qquad (3.18)$$

- **MB series:**

$$M_u. = 0.62 \times 60 \times (12.5 - 0.36 \times 1.95) + 2 \times 0.0013 \times 505 \times 14 - 0.36 \times 1.95$$

$$M_u. = 438 \ \ kips.in. + 175 \ \ kips.in$$

$$\underline{M_u = 613 \ \ kips.in}$$

- **SK series:**

For the SK series, Equation (3.18) is corrected because the maximal elongation in the laminate was assumed equal to 1.0%, whereas the ultimate elongation of the CFRP plate is 1.9%:

$$M_u = A_S f_{yS}(d - \chi_2 x) + A_L E_L \varepsilon_{L,\max}(d_L - \chi_2 x) \qquad (3.18.a)$$

$$M_u. = 0.62 \times 60 \times (14.5 - 0.376 \times 3.47)$$
$$+ 2 \times 2 \times 0.00472 \times 22{,}500 \times 0.01 \times (14.5 - 0.376 \times 3.47)$$

$$M_u. = 490 \ \ kip.in. + 626 \ \ kip.in$$

$$M_u = 1051 \ \ kip.in.$$

These results are discussed in Chapter 5, Section 5.2.2.

Appendix C: Test results

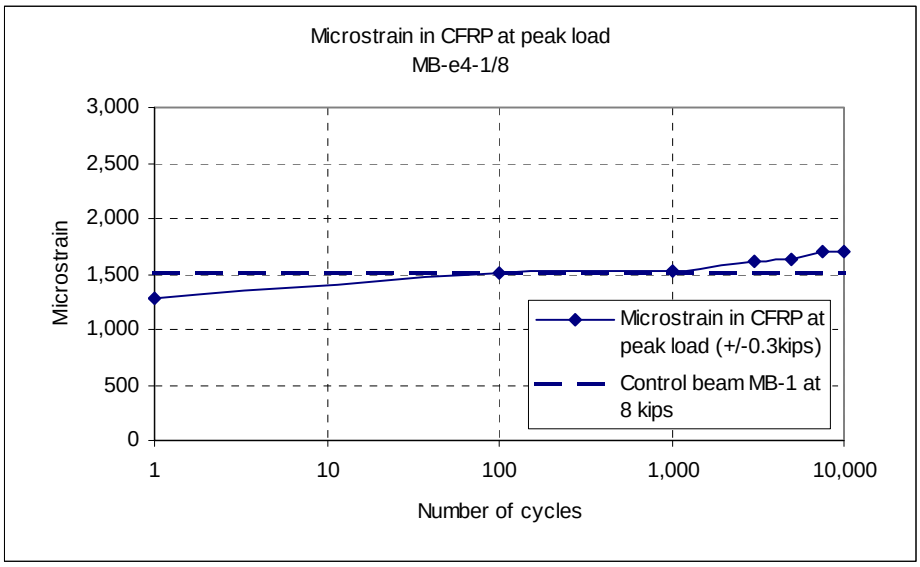

(a)

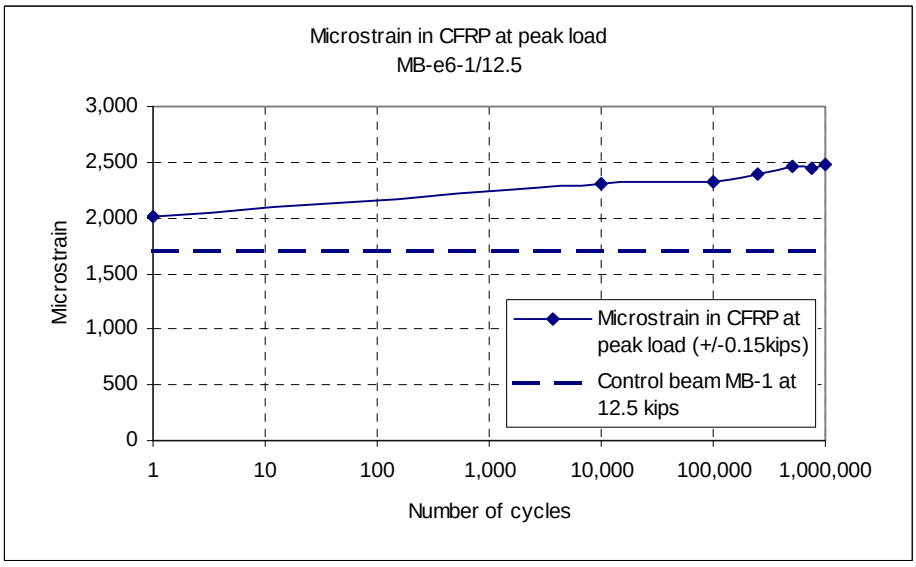

(b)

Figure C.1: Evolution of the strains in the CFRP plate in the section A-A during cycling for the MB series. (Section A-A: see Figure4.4).

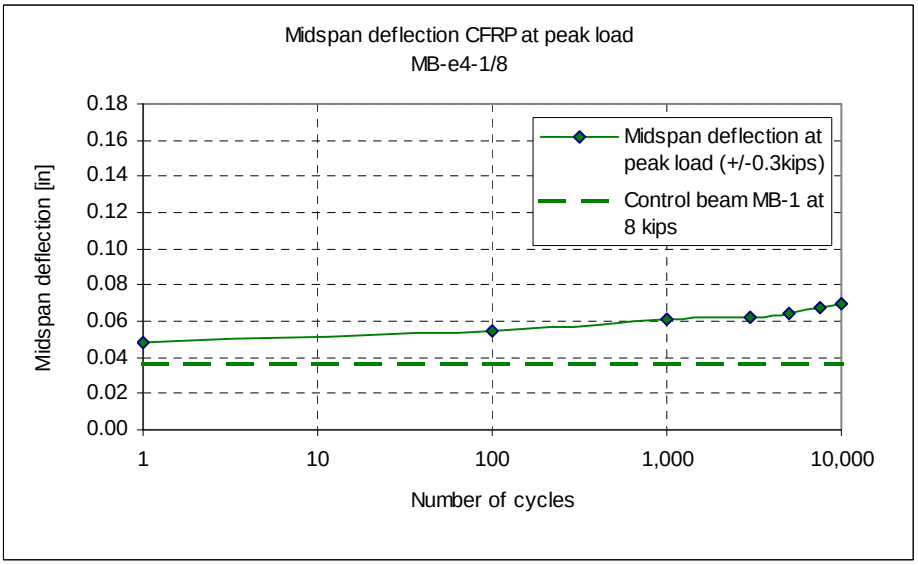

(a)

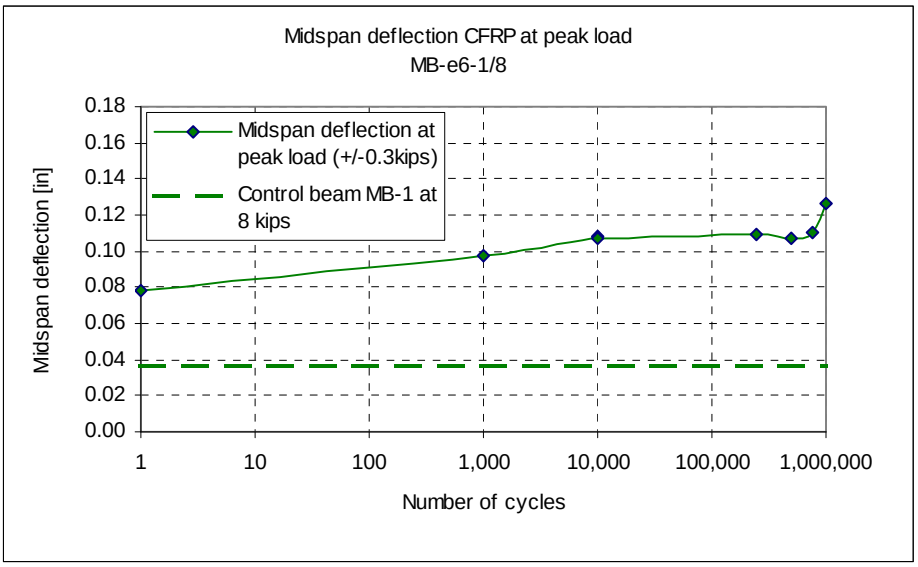

(b)

Figure C.2: Evolution of the deflection at midspan during cycling for the MB series.

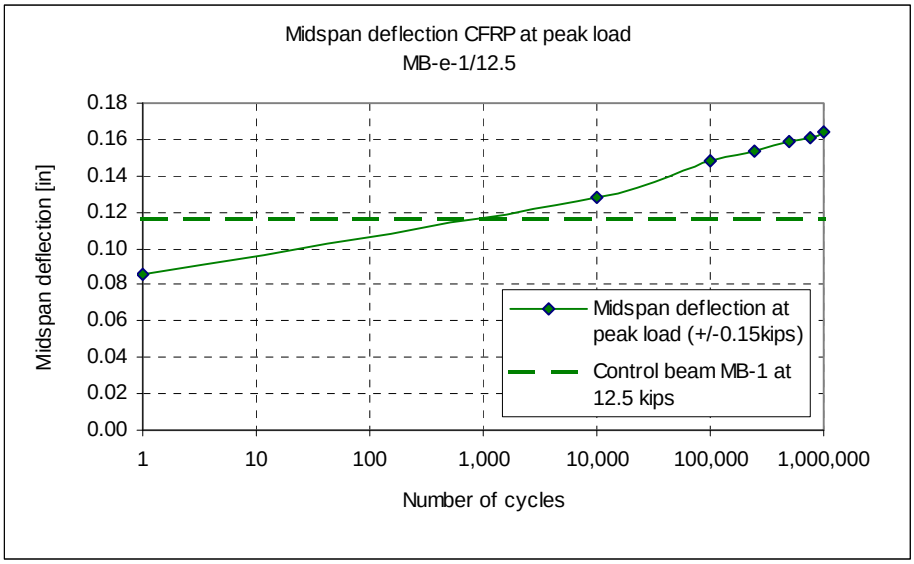

(c)

Figure C.2: Evolution of the deflection at midspan during cycling for the MB series.

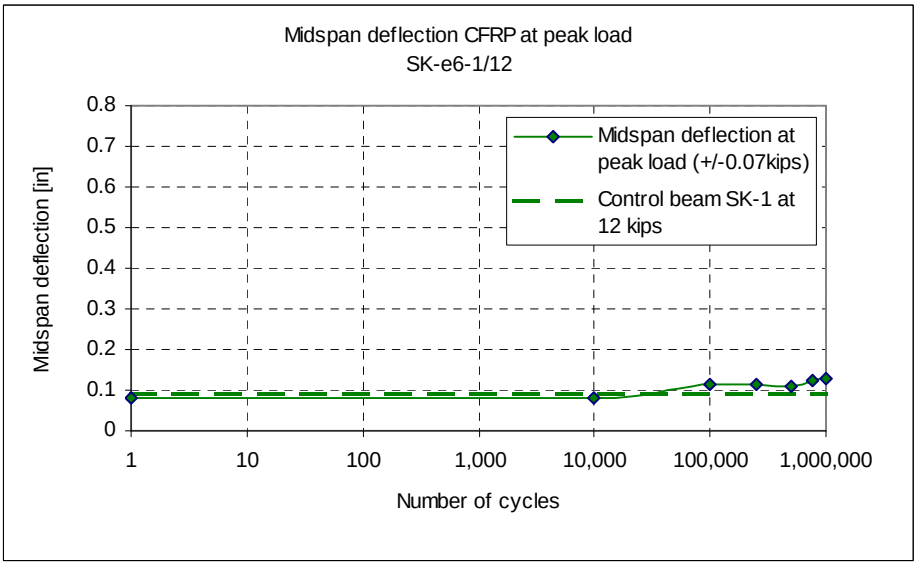

(a)

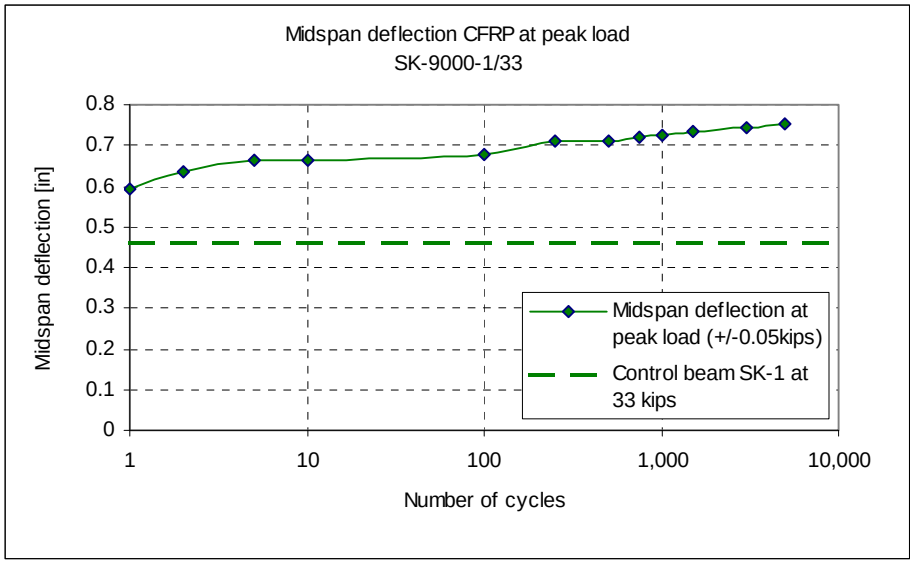

(b)

Figure C3: Evolution of the deflection at midspan during cycling for the SK series.

References

[1] ACI Bibliography No.3, " Fatigue of Concrete," Annotated, Prepared as part of the ACI Committee 215, Fatigue of Concrete, *American Concrete Institute*, Detroit, Michigan, USA, 1960.

[2] ACI Committee 215, "Consideration for Design of Concrete Structure Subjected to Fatigue Loading," (ACI 215R-74, revised 1992), *ACI manual of concrete practice*, American Concrete Institute, Detroit, Michigan, USA, 1993, pp. 215R-1 to 215R-24.

[3] ACI Committee 343, "Analysis and Design of Reinforced Concrete Bridges Structures," (ACI 343R-88), *ACI manual of concrete practice*, American Concrete Institute, Detroit, Michigan, USA, 1989, pp. 343R-1 to 343R-162.

[4] Arduini A., Di Tommaso A., Manfroni O., Nanni A., "Failure Mechanisms of Concrete Beams Reinforced with FRP Flexible Sheets," *Proceeding of Advanced Composite Materials in Bridges and Structures, M.M. El-Badry, Editor*, Canadian Society for Civil Engineering, Montreal, Quebec, Canada, 1996, pp.253-260.

[5] Ativitavas N., “The Use of Acoustic Emission to Inspect Composite Structures,” *The University of Texas at Austin, Ph.D. Thesis*, Austin, Texas, USA, forthcoming.

[6] Barnes R.A., Mays G.C., “Fatigue Performance of Concrete Beams Strengthened with CFRP Plates,” *Journal of Composites for Construction, Vol. 3, N° 2*, May 1999, pp.63-72.

[7] Batson R.G., Hyde J.H., “Mechanical Testing,” *Chapman and Hall*, Vol. II, London, U.K., 1922, pp. 231-236.

[8] Berry H.C., “Further Tests of Reinforced Concrete Beams under Oft-repeated Loading,” *Proceedings, ASTM*, Vol. 9, 1909, p.493.

[9] Berset J.-D., “Strengthening of Reinforced Concrete Beams for Shear Using FRP Composites,” *Massachusetts Institute of Technology, Master Thesis*, Cambridge, Massachusetts, USA, 1992.

[10] Berset J.-D., “Renforcement de Structures: Collage de Lamelles en Fibres de Carbone,” (Strenthening of Structures Using Externally Bonded Carbon Fiber Laminates) *Ingénieurs et Architectes Suisses*, N° 20, Switzerland, September 1995, pp. 384-390 (*in French*).

[11] Bramblett R., “Flexural Strengthening of Reinforced Concrete Beams Using Carbon Fiber Reinforced Composites,” *The University of Texas at Austin, Master Thesis*, Austin, Texas, USA, forthcoming 2000.

[12] Breña S., “Strengthening of Existing Concrete Bridges Using Carbon Fiber Reinforced Composites,” *The University of Texas at Austin, Ph.D. Thesis*, Austin, Texas, USA, forthcoming 2000.

[13] “Building Code Requirements for Structural Concrete (ACI 318-95) and Commentary (ACI 318R-95),” *American Concrete Institute,* 1995.

[14] Curtis P.T., “The Fatigue Behavior of Fibrous Composite Materials,” *Journal of Strain Analysis, Vol. 24, N°4,* 1989, pp.235-244.

[15] Demers C.E., “Fatigue Strength Degradation of E-glass FRP Composites and Carbon FRP Composites,” *Construction and Building Materials 12*, 1998, pp. 311-318.

[16] Dong-Il Chang, Wong-Kyu Chai, “A Study on the Fatigue Strength Behavior of Reinforced Concrete Structures,” *International Journal of Pressure, Vessel and Piping 40*, 1989, pp.51-75.

[17] Emmons P. H., Vaysburd A. M., Thomas J., “Strengthening Concrete Structures, Part I,” *Concrete International*, March 1998, pp.53-58.

[18] Emmons P. H., Vaysburd A. M., Thomas J., “Strengthening Concrete Structures, Part II,” *Concrete International*, April 1998, pp.56-60.

[19] FHWA, “The status of Nation’s Highway Bridge Replacement and Rehabilitation Program and National Bridge Inventory,” *Twelfth Report to the United States Congress*, US Department of Transportation, Federal Highway Administration, 1995.

[20] Frey F., “Materiaux Composites et Structures,” (Composite Materials and Structures) *Cours dispensé aux étudiants du 8ème semester de la section Génie Civil*, Ecole Polytechnique Fédérale de Lausanne, Département de Génie Civil, Laboratoire de Mécanique des Structures et Milieux Continus, Presses Polytechnique et Universitaires Romandes, Lausanne, Switzerland, 1997 (*in French*).

[21] Gardens H.N., Hollaway L.C., “An Experimental Study of the Influence of End Plate Anchorage of Carbon Fiber Composite Plates Used to Strengthened Reinforced Concrete Beams,” *Composite Structures 42*, 1998, pp. 175-188.

[22] Gardens H.N., Quantrill R.J., Hollaway L.C., Thorne A.M., and Parke G.A.R., “An Experimental Study of the Anchorage Length of Carbon Fiber Composites Plates Used to Strengthened Reinforced Concrete Beams,” *Construction building matter 12*, 1998, pp. 203-219.

[23] Heim K.E., ‘Einfluss haeufig wiederholter Belastungen auf die Rissbildung und Riss-Sicherheit von Eisenbeton balken,” (The Effect of Frequently Repeated Loading on the Formation of Cracks in Reinforced Concrete Beams on their Resistance to Cracking), *Mitteilungen, Institut fuer Beton und Eisenbeton, Technische Hochschule, Karlsruhe,* Published by Verlag Brechmer und Minuth, Breslau, 1930 (*in German*).

[24] Helgason T., J.M. Hanson, “Investigation of Design Factors Affecting Fatigue Strength of Reinforcing Bars – Statistical Analysis,” *Adeles Symposium: Fatigue of Concrete*, ACI, SP-41, 1974, pp.107-138.

[25] Hollaway L.C., “Polymer Composites for Civil and Structural Engineering,” Blackie Academic and professional, Glasgow, U.K., 1993.

[26] Hollaway L.C., Leeming M.B., ”Strengthening of Reinforced Concrete Structures Using externally-Bonded FRP Composites in Structural and Civil Engineering,” *CRC Press, Woodhead publishing limited*, Cambridge, England, 1999, 327 p.

[27] Inoue S., Nishibayashi S., Kuroda T.Omata F., “Deformation Characeristics, Static and Fatigue Strengths of Reinforced Concrete Beams Reinforced with Carbon Fiber Reinforced Plastic Plate,” *Transactions of the Japan Concrete Institute, Vol. 17*, 1995, pp. 149-156.

[28] Inoue S., Nishibayashi S., Yoshino A., Omata F., "Deformation Characeristics, Static and Fatigue Strengths of Reinforced Concrete Beams Reinforced with Carbon Fiber Reinforced Plastic Plate," *Transactions of the Japan Concrete Institute, Vol. 18*, 1996, pp. 143-150.

[29] Jeong S.M., "Evaluation of Ductility in Prestressed Concrete Beams Using FRP Tendons," *PhD Thesis, University of Michigan*, 1994.

[30] Kaiser H.P., "Strengthening of Reinforced Concrete with Epoxy-Bonded Carbon-Fiber Plastics," *Doctoral thesis, Diss. ETH No. 8918*, ETH Zurich, Switzerland, 1989 (*in German*).

[31] Leeming M.B., "Concrete in the Oceans Programme – Co-ordinating Report on the Whole Programme," *HMSO*, London, U.K., 1989.

[32] L'Hermite R., and Bresson J., "Béton Armé par Collage d'Armatures," (Concrete Strengthened Using Externally Bonded Steel Plates) *Colloque RILEM, UTI, Ed. Eyrolles* (1971), Vol. II, Paris, France, September 1967, pp. 175-203 (*in French*).

[33] MacGregor J. G., "Reinforced Concrete, Mechanics and Design," *Prentice Hall*, New Jersey, USA, Third Edition, 1998, 939 p.

[34] Mallet G., “Fatigue of Reinforced Concrete,” *HMSO*, London. U.K., 1991

[35] Master Builders, “MBrace® Composite Strengthening System Design Guide,” *Master Builders*, 1998.

[36] Meier U., ”Brückensanierungen mit Hochleistung-Faserverbundwerkstoffen,” (Bridge Retrofitting Using High Performance Composite Materials) *Material und Techni*, No.4, 1987, Switzerland, pp 125-128 *(in French and German).*

[37] Meier U., Deuring M., Meier H., Schwegker G., “ Strengthening of Structures with Advanced Composites,” reprint from *Alternative Materials For the Reinforcement and Prestressing of Concrete*, 1993, pp.153-171.

[38] Meier U., ”Strengthening of Existing Structures Using Carbon Fiber/Epoxy Composites,’ *Construction and Building Materials*, Vol9 N°6, 1995, pp. 341-351.

[39] Meier, U., “Composites for Structural Repair and Retrofitting,” *Proceeding of ICCI’96, Fiber Composite in Infrastructure*, 1996, pp. 1202-1216.

[40] Meier U., “Composite Materials in Bridge Repair,” *Applied Composite Materials*, paper in review in 1999, forthcoming 2000.

[41] Moss D.S., “Bending fatigue of high-yield reinforcing bars in concrete,” *TRRL Supplementary Rep. 748*, Transport and Road Research Laboratory, Crowthorne, U.K., 1982

[42] Muszynski L.C., Sierakowski R.L., “Fatigue Strength of Externally Reinforced Concrete Beams,” *Materials For the New Millennium, Proceedings of the Fourth Materials Engineering Conference*, Washington, D.C., November 10-14 1996, pp. 648-656.

[43] Nordby G.N., “Fatigue of Concrete – A Review of Research,” *ACI Journal*, August 1958, pp. 191-219.

[44] “Norme SIA 162, Ouvrages en Béton,” (Swiss Codes, Reinforced Concrete Structures) *SIA*, Zurich, Switzerland, 1993 (*in French and German*).

[45] Shahawy M., Beitelman T.H., “Static and Fatigue Performance of RC Beams Strengthened with CFRP Laminates,” *Journal of Composites for Construction, Vol. 125, N° 6,* June 1999, pp. 613-621.

[46] Shijie W., Ruixian Z., “Study of Fiber Composite Plates for Strengthening Reinforced Bridges,” *Proceedings 9th Int. Conf. Composite Materials*, Madrid, Spain, July 1993.

[47] Sika, “Sika CarboDur® Engineering Guideline for the Use of CarboDur® (CFRP) Laminates for Structural Strengthening of Concrete Structures,” *Sika Corporation*, 1997.

[48] Spadea G., Bencardino F., Swamy R.N., “Structural Behavior of Composite RC Beams with Externally Bonded CFRP,” *Journal of Composites for Construction*, August 1998, pp. 132-137.

[49] “Standard Specifications for Highway Bridges,” *AASHTO, sixteenth edition*, 1996.

[50] Talreja R., “Fatigue of Composite Materials: Damage Mechanisms and Fatigue Lifetime,” *Proceedings ICCM6*, London, U.K., 1987.

[51] Todeschini C.E., Bianchini A.C., Kesler C.E., “Behavior of Concrete Columns Reinforced with High Strength Steels,” *ACI Journal, Proceedings*, Vol. 61, No. 6, June 1964, p. 701-716.

[52] Treiber F., “Das Verhalten unter dem Einfluss dauernd ruhender und haeufig wiederholter Belastung,” (Behavior under the Static and Frequently Repeated Loads), *Dissertation at Karlsruhe under Probst*., 1934 (*in German*).

[53] Treiber F., “Das Verhalten von Eisenbeton-T-Balken unter dem Einfluss dauernd ruhender und haeufig wiederholter Belastung,” (Results of Tests on the Behavior of Reinforced Concrete T-beams under Static and Repeated Loading) *Bauingenieur*, Vol. 15, Berlin, Germany, March 1934, pp.131-133; No. 14, April 1934, pp. 178-182, (*in German*).

[54] Walter R., Mielbradt M., “Dimensionnement des Structures en Béton,” (Design of Reinforced Concrete Structures) *Traité de Génie Civil de l’Ecole Polytechnique Fédérale de Lausanne, Vol. 7*, Presses Polytechnique et Universitaires Romandes, Lausanne, Switzerland, 1990, 388 p. (*in French*).

Web Sites:

[55] EMPA – Swiss Federal Laboratories for Materials Testing and Research: http://www.empa.ch

[56] Master Builders: http://www.mbrace.com

[57] U.S. Department of Transportation, Federal Highway Administration: http://www.fhwa.dot.gov/bridge/britab.htm

[58] Sika: http://www.sikausa.com